I. DEPOLARIZED LIGHT SCATTERING STUDIES OF ROTATIONAL-TRANSLATIONAL COUPLING IN LIQUIDS COMPOSED OF SMALL ANISOTROPIC MOLECULES

II. INVESTIGATION OF THE COUPLING BETWEEN REORIENTATION AND LONGITUDINAL MODES IN THE BRILLOUIN SPECTRA OF LIQUIDS COMPOSED OF ANISOTROPIC MOLECULES

Thesis by

Byron Lance O'Steen

In partial fulfillment of the requirements

for the degree of

Doctor of Philosophy.

California Institute of Technology

Pasadena, California

1982

(Submitted September 10, 1981)

To my parents

ACKNOWLEDGMENTS

I would like to express my gratitude to Professor C.J. Pings for allowing me to freely pursue the work undertaken here.

I must also acknowledge the benefit of many helpful discussions with Dr. Claude Cohen and Gerry Fuller. As countless students before me, I am deeply indebted to Hollis Reamer for his valuable assistance and advice in the experimental work.

The experimental apparatus used in this study was purchased through a National Science Foundation equipment grant.

Finally, I want to thank Annie for her endless patience and encouragement during my final years at Caltech.

ABSTRACT

Part I

In an attempt to better understand the molecular interactions governing the behaviour of the coupling parameter R measured in light scattering experiments, the depolarized (I_{VH}) spectra for a series of liquids composed of small aromatic molecules, very similar in size and shape, have been measured. The molecules studied here were generally monosubstituted benzene and pyridine derivatives. All were found to exhibit the doublet structure indicative of dynamic coupling between molecular reorientation and shear modes, or more simply, rotational-translational coupling. The degree of this coupling is measured by a parameter R ($0 \leq R \leq 1$) which is often thought of as the fraction of the shear viscosity attributable to reorientational motion. From the depolarized spectra the coupling parameter R, collective reorientation frequency, and low frequency shear viscosity were determined.

The values of R were found to vary from 0.24 to 0.55 for the liquids studied here. This range is nearly as broad as that observed in all previous studies, which have included such diverse molecules as carbon disulfide, tri-phenyl phosphite, and the highly anisotropic liquid crystal MBBA. This suggests that size and shape considerations, or steric forces, are not the primary factor in determining the degree of rotational-translational coupling as measured by light scattering. If this is indeed the case then other non-steric interactions must be producing the observed variation in R. With this in mind, we have examined possible electrostatic interactions. A simple correlation with dipole moment was not found to exist. Instead it appears that the variation in R can only be understood by consideration of the detailed molecular charge distribution. This is determined to a large extent by resonance interactions with the aromatic ring which are

generally reflected in the change of dipole moment from the aliphatic compound (CH_3-R) to its aromatic analog (C_6H_5-R).

Based upon resonance structure arguments and our own experimental results, it is concluded that the anomolously large R values found for pyridine from the I_{HH} depolarized spectrum might well be correct and the more orthodox I_{VH} measurements in error. If this assertion is indeed correct, then the reliability of rotational-translational coupling measurements by I_{VH} depolarized light scattering must be considered questionable for weakly scattering molecules such as pyridine.

Part II

The coupling of reorientational motion to longitudinal modes was investigated by studying the Brillouin spectra of aniline and p-anisaldehyde over a wide range of scattering angles. The primary goal of these studies was to attempt to confirm the microscopic theory of orientational relaxation in the polarized spectrum. Theoretically it has been shown that for symmetric tops the coupling between longitudinal modes and reorientation in the polarized spectrum is identical to that between shear modes and reorientation in the depolarized spectrum. Thus the Brillouin scattering studies performed here also provide an internal check on the consistency of the 2-variable molecular theory for depolarized scattering and the corresponding theory of orientational relaxation in the Brillouin spectrum. Aniline and p-anisaldehyde were chosen for this investigation since their depolarized spectra at the temperature of interest are well described by the simple 2-variable molecular theory coupling shear modes to orientation. The collective reorientation frequency for both liquids could easily be varied in the low gigahertz range by operating at temperatures near the freezing point. Thus the effects of orientational relaxation in the propagation of

longitudinal waves (1 - 10 GHz) should be observable in an angular study of the Brillouin spectra. Moderate viscosites and large rotational-translational couplings also made these liquids attractive from an experimental standpoint since these quantities determine the relaxation strength.

Our results for attenuation and velocity of the longitudinal waves demonstrate that there is indeed relaxation in the shear viscosity as predicted by theory. However, shear relaxation in addition to that due to reorietational motion is indicated by the κ-dependence of the attenuation results. This stands as an apparent contradiction to the depolarized results which suggest that only orientational relaxation should be important under these conditions. Since the different relaxation effects cannot be unambiguously separated here, a detailed confirmation of orientational relaxation theory could not be obtained.

TABLE OF CONTENTS

LIST OF TABLES

LIST OF FIGURES

PART I

DEPOLARIZED LIGHT SCATTERING STUDIES OF ROTATIONAL-TRANSLATIONAL COUPLING IN LIQUIDS COMPOSED OF SMALL ANISOTROPIC MOLECULES

Chapter 1

INTRODUCTION

In the past decade laser light scattering has established itself as a powerful new spectroscopic probe for studying both static correlations and the dynamics of collective molecular motion in the liquid state. With the advent of the laser and concomitant detection techniques, a remarkable proliferation of both experimental and theoretical work has occurred in this field. One of the more recent areas of interest has been the study of collective reorientational motion of small anisotropic molecules in both neat liquids and solution. Of particular interest here is the coupling between reorientational motion and shear modes, or more simply, rotational-translational coupling. This coupling is manifested by fine structure in the depolarized or VH spectrum of light scattered by certain pure liquids. See figure 1 below.

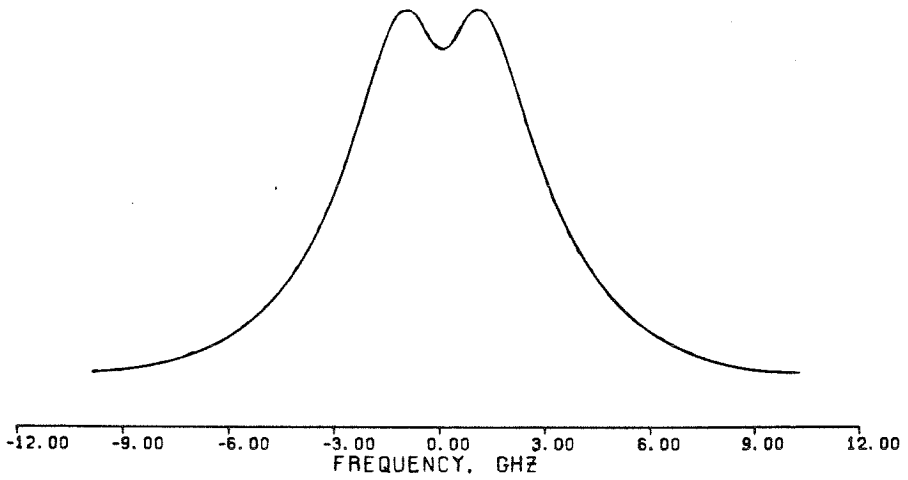

Figure 1. Schematic of depolarized spectrum with fine structure.

Early investigations of this fine structure were carried out by Stegeman and Stoicheff[1] and Starunov, et. al.[2]. They found what appeared to be a broad depolarized doublet with a minimum at the incident light frequency and peak separations of a few gigahertz. Later Stegeman and Stoicheff[3] undertook an extensive

study of 27 molecular liquids and found the doublet structure in 20 of these. They based the analysis of their spectra on the only theory available at the time, the hydrodynamic theory of Rytov[4]. This is basically a viscoelastic theory in which fluctuations in the local strain tensor are coupled to fluctuations in the dielectric tensor. It is well known that fluctuations in the local dielectric tensor are the direct source of scattered light. Rytov's theory is qualitatively correct, predicting a doublet structure arising from propagating shear waves. Stegeman and Stoicheff found good qualitative agreement between Rytov's theory and their experimental spectra but noted that an important theoretical relation among several of the parameters was not satisfied.

Rigorous molecular theories for the depolarized spectrum were first presented by both Anderson and Pecora[5] and Keyes and Kivelson [6]. The theory of Anderson and Pecora is based upon the projection operator technique of Mori[7] and Zwanzig[8] while Keyes and Kivelson's result is derived using linear response theory [9,10]. Both represent statistical mechanical approaches to "generalized hydrodynamics" and yield identical results for the depolarized spectrum. Keyes argues that the variable directly coupling to the dielectric tensor , or the "primary" variable, should be the polarizability density tensor and couples this to the transverse momentum density (shear modes). Anderson also presents a two variable theory but only requires that the primary variable be a tensor with the correct symmetry to couple with the transverse momentum density. Qualitatively the phenomenological theory of Rytov and the molecular theories are very similar. Both predict the observed doublet structure. However, it is in how the fine structure arises that the differences in the theories can be understood.

It has already been noted that the doublet structure in the Rytov theory arises from propagating shear waves. In molecular theories the fine structure is a result of "negative" coupling between non-propagating shear modes and

collective molecular reorientation. This produces an intensity dip at the center of a broad, unshifted Lorentzian arising from reorientational motion. The degree of this coupling depends on a parameter, R. It has been shown[11,12] that this parameter is determined in part by the dynamic coupling between shear stress and the angular momentum of the molecules.

$$R = \frac{|\int_0^\infty d\tau < \dot{\alpha}_{zx}(\tau)\sigma^*_{zx} >_Q|^2}{\nu_s \Gamma_{22} N_{11} N_{22}} \qquad (1.1)$$

In the above equation the bracketed quantity is the cross-correlation function of the time derivative of the zx component of the polarizability density tensor with the zx component of the microscopic stress tensor. The subscript Q indicates that the time dependence is modified by certain projection operators. This will be discussed fully in chapter 4. The denominator contains the kinematic shear viscosity, ν_s, the collective molecular reorientation frequency, Γ_{22}, and static auto-correlation functions of the transverse momentum, N_{11}, and polarizability density tensor, N_{22}. While well-defined, the coupling parameter R is not amenable to direct calculation. This is primarily due to the projected time dependence. R is often thought of as the fraction of the total shear viscosity arising from reorientational motion. No such quantity exists in the Rytov theory. In fact it can be shown that the Rytov result is a special case of the molecular theory with $R \equiv 1$ $(0 \leq R \leq 1)$[5] . This coupling parameter is probably the most important result of the molecular theories and is the central topic of almost all that follows.

A number of studies of the depolarized spectrum of pure liquids based upon molecular theory have been undertaken to date. Except for supercooled liquids, agreement has been very good[12,13,14]. Problems seem to arise for supercooled liquids,[13,15] and this is currently an active area of research[16,17,18]. However,

even well above the freezing point where agreement with theory is good, the behaviour of R is somewhat puzzling [19], and a systematic study attempting to probe its dependence upon different molecular parameters has yet to be undertaken. In table 1 the results of R measurements for 15 liquids are given. These represent all the results currently in the literature of which the author is aware and certainly reflect the temperature dependence and range of R values that have been observed to date. Note that the molecules signified with a (*) represent results published during the course of this investigation.

The most striking feature in table 1 is probably the lack of any significant temperature dependence. While this result might seem a little disturbing, and was certainly not expected initially, it has found some recent justification. By comparing molecular theory with de Gennes' phenomenological theory[28] for liquid crystals, Alms et.al.[20] have shown that R can be expressed as a ratio of viscosity parameters with similar temperature dependences. A more disturbing feature apparent in table 1 is the rather narrow range of R values that were initially observed. Prior to the very recent results for quinoline, nitrobenzene and trichlorobenzene, the range of R values seemed to be approximately 0.25 to 0.45 with most measurements indicating either 0.35 ± 0.03 or 0.43 ± 0.03 . Theoretically the coupling parameter, R, is only constrained to be between 0 and 1.0 . This range seems even more puzzling when one considers the wide variety of molecules presented in table 1. For example, the highly anisotropic liquid crystal p-methoxybenzylidene-(p-n-butyl)aniline (MBBA) has an R value identical to that of the oblate symmetric top pyridine. While nitrobenzene and quinoline* do appear to extend this range significantly, they must be considered anomalous and the question of the significance of such large R values arises. Perhaps some insight into these anomalous R's would lead to a better understanding of this

* Quinoline has been studied in our own lab and R was found to be 0.57 ± 0.02

Rotational-Translational Coupling Parameters				
Molecule	Temperature (°C)	R	Dipole[80] (debyes)	References for R
MBBA	150 170 190 230	0.34 0.36 0.37 0.37	-	20
p-Anisaldehyde	6.2 28.8 53.8 79.0	0.43 0.44 0.44 0.41	3.5	12
Pyridine	-55 to -10	0.35	2.2	21
Nitrobenzene*	0.5 19.5 40.0	0.55 0.56 0.57	4.25	22
Quinoline*	12.1 20.0 35.0	0.66 0.60 0.53	2.3	23
Carbon disulfide	-110 -98 -82	0.34 0.37 0.30	0.0	24
Benzonitrile	-10 0 10 20	0.35 0.36 0.38 0.37	4.14	25
Ethyl benzoate	-7.3 6.0 16.9 33.5	0.42 0.43 0.48 0.40	2.0	13
Acetophenone	-20 to 20	0.41	3.1	14
Trichlorobenzene*	17 30 50	0.24 0.15 0.22	0.0	26
Triphenylphosphite	-2.0 12.2 26.4 57.6 79.0	0.45 0.45 0.40 0.48 0.45	0.0	11
Salol	53.5 74.5 92.0 122.0	0.20 0.27 0.31 0.28	-	15
Tolane	60 to 130	0.4	0.0	19
n-Hexdecane	65	0.33	0.0	27
n-Docosane	110	0.38	0.0	27

TABLE 1. Rotational-translational coupling parameters, R, and dipole moments for liquids studied to date

understanding of this coupling parameter in general and thus help explain the narrow R range observed for so many liquids.

As has been previously mentioned, the coupling parameter has a rigorous molecular definition, but its complexity virtually precludes any direct calculation. However, one intuitively expects R to depend on some molecular parameters, e.g. geometrical anisotropy, molecular size, and dipole moment. There is certainly no reason to expect a near universal value for this parameter. One problem might be that the molecular theory has been developed for rigid, symmetric top molecules while most of the liquids actually studied are questionable approximations to these conditions. Of the molecules studied in table 1, only carbon disulfide and pyridine represent good approximations to rigid, symmetric tops. Another possible problem arises from the observation that the molecules studied to date may be too diverse in nature. The large differences in size and shape already noted should lead to considerably different steric or repulsive forces. Superimposed upon this variation is also a large change in dipole moment. Dipole moments vary from 0 debyes in the case of carbon disulfide, to 2.0 debyes for ethyl benzoate, to 4.25 debyes for nitrobenzene. This makes interpretation of the dependence of R upon different molecular parameters difficult and canceling effects might even be responsible for the narrow R range observed for most liquids.

Based upon the above discussion, we have undertaken a systematic study of several mono-substituted benzene and pyridine derivatives. Gierke[29,30] has considered the depolarized scattering from rigid, asymmetric molecules with C_{2V} symmetry and finds a spectrum with the same structure as in the symmetric top theory. R enters the asymmetric theory in a manner analogous to the symmetric top case but has a more complex definition due to the additional orientational variables needed to describe the scattering. The molecules used in the

present study should all represent good candidates for Gierke's asymmetric treatment, and thus we expect to see a spectrum with structure identical to that of a true symmetric top. Since these molecules all have approximately the same size and shape, differences in geometrical factors are expected to be unimportant. Thus changes in the coupling parameter should result primarily from differences in non-steric interactions. The depolarized spectra were obtained several times at a temperature which allowed for the best resolution of the fine structure. Measurements of R and collective reorientation frequency are reported. The low frequency shear viscosities were also obtained as fitted parameters and compared with their classically measured values. Temperature dependent studies of R were not attempted since a temperature dependence has never been observed.

Chapter 2

BASIC LIGHT SCATTERING THEORY

The basic light scattering experiment is illustrated in figure 2 below, where the scattering medium is assumed to be non-absorbing and non-conducting.

$$(\vec{n}_i, \vec{k}_i, \omega_i) \rightarrow (\vec{n}_f, \vec{k}_f, \omega_f)$$

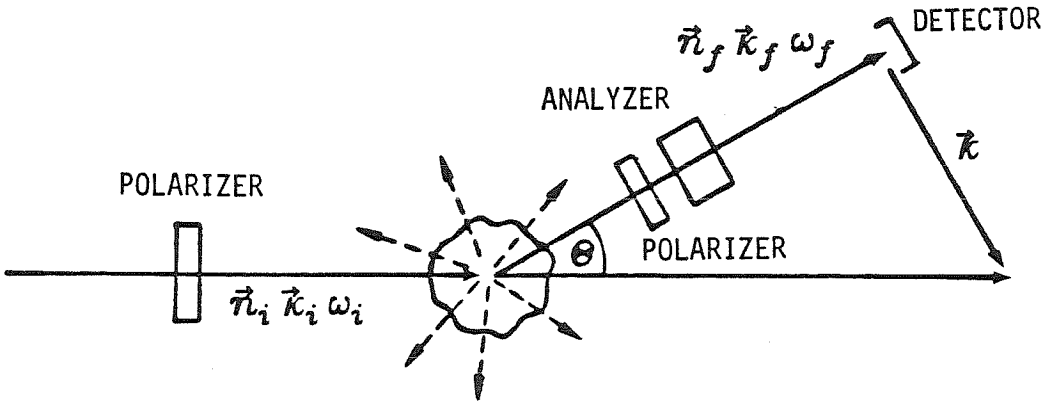

Figure 2. Schematic of basic light scattering experiment.

$\vec{n}_i, \vec{n}_f$ – polarization vector of incident, scattered light

$\vec{k}_i, \vec{k}_f$ – wave vector of incident, scattered light

$\vec{\kappa}$ – scattering wave vector

ω_i, ω_f – frequency of incident, scattered light

Θ – scattering angle

The scattering wave vector, $\vec{\kappa}$, is a measure of the momentum transfer and is given by

$$\vec{\kappa} = \vec{k}_f - \vec{k}_i \tag{2.1}$$

Assuming that the scattering is very nearly elastic, i.e. $\omega_i = \omega_f$, and using the law of cosines yields a Bragg condition for $\kappa = |\vec{\kappa}|$,

$$\kappa = 2\kappa_i \sin\frac{\Theta}{2} \tag{2.2}$$

Since κ_i is $o(10^5 \text{cm}^{-1})$, the momentum transfer is small, $o(10^{-3}\text{Å})$, and thus light

scattering is considered a probe of the low κ regime.

In a light scattering experiment the directly measureable quantities are the power spectral density, $I(\vec{\kappa},\omega)$, and the time auto-correlation function of the scattered electric field,

$$< E_s(\vec{\kappa},t)\ E_s^*(\vec{\kappa},0)> \ \equiv \ \lim_{T\to\infty}\frac{1}{T}\int_0^T d\tau\ E_s^*(\vec{\kappa},\tau)\ E_s(\vec{\kappa},\tau+t) \tag{2.3}$$

These are related as a Fourier transform pair by the Wiener-Khintchine theorem,

$$I(\vec{\kappa},\omega) = \frac{1}{2\pi}\int_{-\infty}^{\infty} dt < E_s(\vec{\kappa},t)\ E_s^*(\vec{\kappa},0)> \ e^{-i\omega t} \tag{2.4}$$

where: $\omega = \omega_f - \omega_i$

From a continuum point of view the scattered electric field at a distance R from the scattering volume can be related, via classical electromagnetic theory, to fluctuations in the local dielectric tensor, ε[31,32].

$$E_s(R,\vec{\kappa},t) \propto e^{i(\vec{k}_f R-\omega_i t)}\delta\varepsilon_{if}(\vec{\kappa},t) \tag{2.5}$$

where: $\delta\varepsilon_{if}(\vec{\kappa},t) = \vec{n}_f\cdot\delta\varepsilon(\vec{\kappa},t)\cdot\vec{n}_i$ (2.6a)

$$\delta\varepsilon(\vec{\kappa},t) = \int_v d\vec{r}\ e^{i\vec{\kappa}\vec{r}}\ \delta\varepsilon(\vec{r},t) \tag{2.6b}$$

$$\varepsilon(\vec{r},t) = \varepsilon_0 I + \delta\varepsilon(\vec{r},t) \tag{2.6c}$$

Thus the power spectral density in terms of dielectric fluctuations is given by

$$I_{if}(\vec{\kappa},\omega) \propto \int_{-\infty}^{\infty} dt < \delta\varepsilon_{if}^*(\vec{\kappa},0)\ \delta\varepsilon_{if}(\vec{\kappa},t)> e^{-i\omega t} \tag{2.7}$$

In order to proceed further, dynamical expressions for the $\delta\varepsilon_{if}(\vec{\kappa},t)$ must be found. Normally this involves expanding the dielectric fluctuations in terms of other fluctuating quantities whose time dependence can be calculated.

An expression for the scattered electric field can also be obtained from simple molecular considerations[33]. Consider a single molecule with an anisotropic polarizability tensor, $\alpha(t)$, in a lab-fixed frame. The incident light impinges upon the molecule inducing a time varying dipole which subsequently radiates an electric field proportional to $\alpha_{if}(t)e^{i\vec{\kappa}\cdot\vec{r}(t)}$. The term $\alpha_{if}(t)$ is the projection of α on the initial and final polarization directions

$$\alpha_{if}(t) = \vec{n}_i \cdot \alpha(t) \cdot \vec{n}_f \tag{2.8}$$

The scattered electric field at the detector is therefore proportional to the sum over all the scattered wavelets

$$E_s(\vec{\kappa},t) \propto \sum_j \alpha_{if}^j(t) e^{i\vec{\kappa}\cdot\vec{r}_j(t)} \tag{2.9}$$

where the sum is over only those molecules in the scattering volume. The term $\alpha_{if}^j(t)$ varies due to rotation and vibration, though only rotation will be considered here. The phase factor $e^{i\vec{\kappa}\cdot\vec{r}_j(t)}$ describes the translational motion of the molecule. Note that equation (1.8) is just the Fourier transform of the local polarizability density $\sum_j \alpha_{if}^j \, \delta(\vec{r} - \vec{r}_j(t))$.

In terms of the molecular polarizability, the power spectrum now becomes

$$I_{if}(\vec{\kappa},\omega) \propto \int_{-\infty}^{\infty} dt < \delta\alpha_{if}^*(\vec{\kappa},0) \, \delta\alpha_{if}(\vec{\kappa},t) > e^{-i\omega t} \tag{2.10}$$

where $\delta\alpha_{if}(\vec{\kappa},t)$ is given by equation (2.8). This expression for the scattered spectrum will certainly be an approximation since collisions will produce extremely short lived distortions in the electronic charge distribution which are not accounted for[34,35,36]. In general the α^j is not an isolated molecular polarizability but rather a renormalized or effective polarizability.

From the preceding discussion it is clear that any process which induces a fluctuation in the local dielectric tensor or alternatively the local polarizability density tensor will give rise to light scattering. The spectrum of scattered light will depend on the number of such processes involved, the dynamics of these processes, and the specific scattering geometry. It is important to realize that light scattering probes fluctuations characterized by wavelengths of $o(1000\text{Å})$. This can be seen from equation (2.2). Thus these fluctuations are produced by the cooperative motion of many molecules and should be seen in contradistinction to such single-particle probes as NMR, IR, and neutron scattering.

In the following chapters we shall be interested in both polarized and depolarized light scattering. A simple schematic of the basic scattering scattering geometry for each case is shown in figure 3 below.

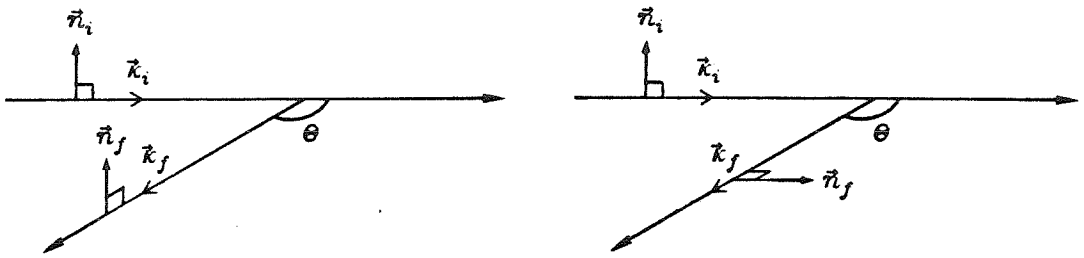

Figure 3. Polarized (a) and depolarized (b) scattering geometry.

Note the use of V and H to indicate polarization directions normal and parallel to the scattering plane. This is a common practice and negates the need to refer to a specific coordinate frame at this stage.

Chapter 3

EXPERIMENTAL

The construction of the light scattering spectrometer used here is similar to that of Chiao and Stoicheff[37]. A schematic of the spectrometer is shown in figure 4. The entire spectrometer excluding electronic components was assembled on a Newport Research Corporation vibration isolation table. The light source was a Spectra-Physics 3 watt argon ion laser. The laser was operated single mode at the 4880 Å line using an intra-cavity solid etalon. The temperature of the etalon was controlled to ± 0.005°C in order to prevent mode hopping. The maximum power level was approximately 700 mW under these conditions. A Spectra- Physics polarization rotator was attached to the front end of the laser in order to precisely set the orientation of the incident polarization vector. This polarization rotator provided phase retardation via a double Rhomb assembly with an extinction ratio of 10^3 and accuracy of rotation of ± 0.2°. The direction of polarization was determined by passing the incident beam through a microscope slide mounted perpendicular to the scattering plane and at its Brewster angle relative to the beam direction. The rotator was then turned until a minimum ocurred in the refracted beam intensity. This defined the vertical polarization of the incident beam with respect to the scattering plane. The horizontal orientation was obtained by 45° rotation of the rotator.

The direction of the incident beam was next carefully aligned using an Oriel laser beam aligner. This mirror assembly allowed for independent horizontal, vertical, and angular positioning of the beam. The standard aluminum coated mirrors on the beam aligner were replaced with high reflectivity dielectric coated mirrors (98% @ 4880Å) to minimize power losses. A Glans-Thompson polarizer (P_1) was then used to eliminate any undesired components of polarization (extinction ≥ 10^5), while a small aperature (A_1) was inserted to eliminate

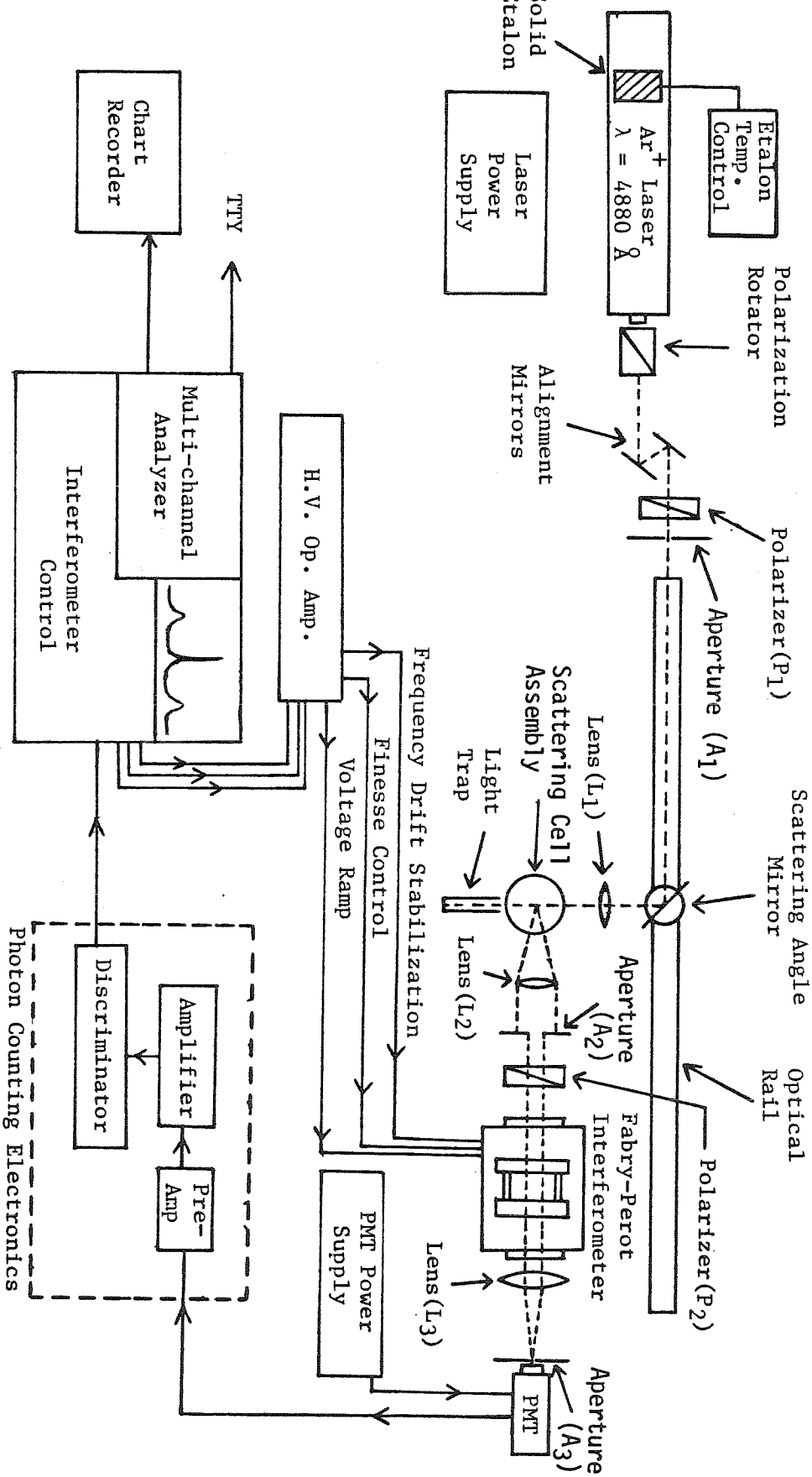

FIGURE 4 LIGHT SCATTERING SPECTROMETER

any spurious reflections. The beam was directed into the scattering cell using a mirror attached to a Gimbal mount which in turn was mounted on an Ardel precision rotation base. Calibration of the rotation base was accurate to 0.1°. This whole assembly was securely attached to a carrier base which could be moved to any point on a 5 foot optical rail. By simultaneously translating the carrier base and rotating the mirror, a scattering angle anywhere between 20° and 150° could easily be obtained. Since the optical rail was not of precision construction, the Gimbal mounting for the mirror was used to make very small correctional adjustments orthogonal to the scattering plane. In this way the incident beam was always assured of being in the scattering plane. The scattering angle was checked by triangulation at several angles and found to be in agreement with the rotation base reading to within 0.1°. This was about the accuracy of the rotation base calibration.

The incident beam was finally focused to the center of the scattering cell with a 13 cm focal length lens (L_1). The shortest distance between the scattering center and optical rail was approximately 19 cm . A schematic of the scattering cell assembly is shown in figure 5. The scattering cell assembly was mounted on a MicroInch microscope turntable. The focusing lens was also rigidly attached to this turntable at its focal length from the center of rotation. This lens was mounted in such a way as to allow for fine adjustment of both its position and orientation. The position of the scattering cell in the rotation plane of the turntable was adjusted by a pair of orthogonal translation stages so that the cell's axis of rotation coincided with the rotation axis of the turntable.

The sample cell itself was a C-105 Brice-Phoenix cylindrical call with flat entrance and exit windows. The cell dimensions were approximately 3.0 cm i.d. by 7.5 cm . The cell was inserted in a brass jacket for temperature control. The brass jacket rested on 3 small steel bearings to minimize heat transfer to the

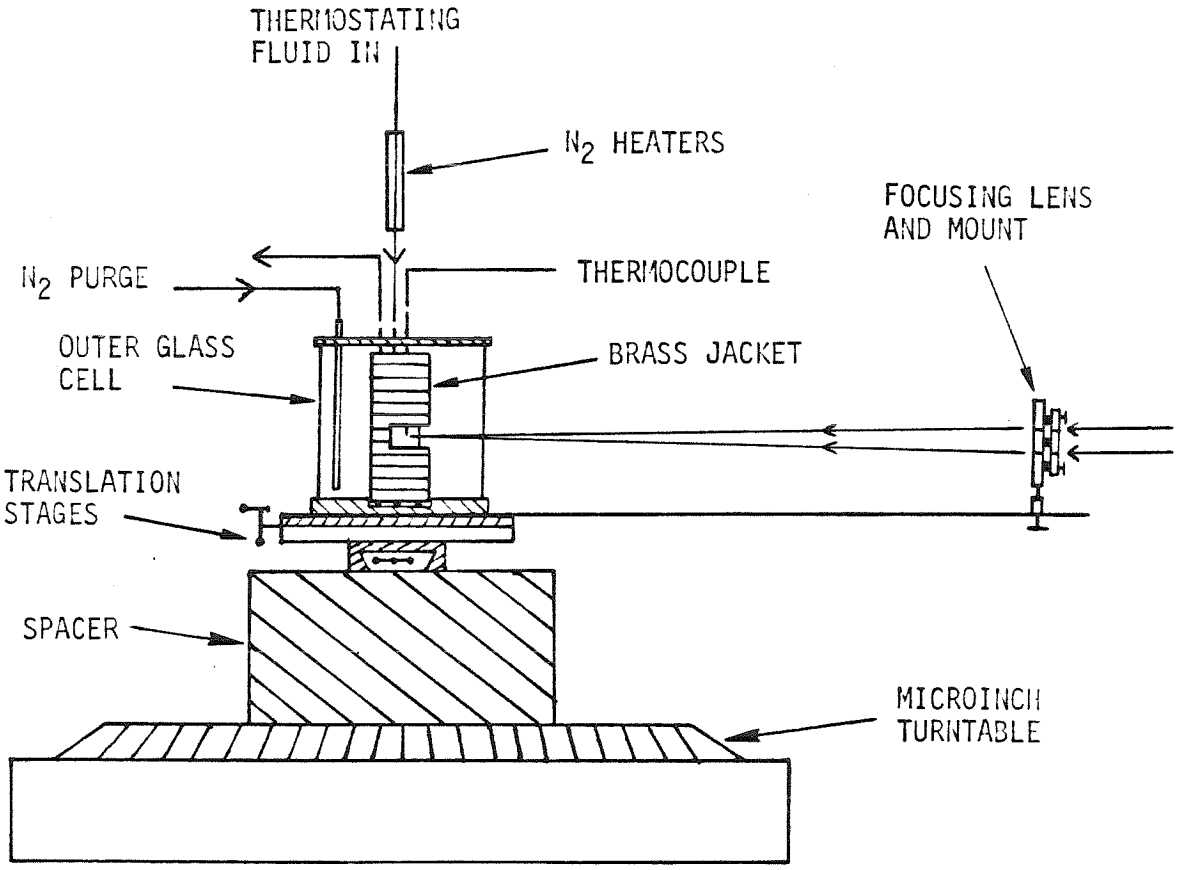

FIGURE 5 SCATTERING CELL ASSEMBLY

rest of the assembly. The cell and jacket were enclosed in a precision cut and polished cylindrical glass chamber. This chamber was slowly purged with dry nitrogen gas during the course of an experiment. This prevented condensation from forming on the cell at low temperatures and helped to minimize degradation of some of the liquids used.

Temperature control of the sample was achieved by one of two methods depending on the temperature desired. For temperatures above 8° C, water was circulated through the brass jacket from a constant temperature P.M. Thompson viscometer bath. The sample temperature was independently measured with a thermocouple inserted directly into the sample volume just above the incident light beam. The thermocouple was calibrated with a NBS certified platinum resistance thermometer. Fluctuations in the sample temperature were less than 0.05° C using water as the thermostating fluid. For temperatures below 8° C, dry nitrogen vapor was circulated through the brass jacket. Temperature control of the circulating N_2 was achieved by passing the cold vapor through a copper tube surrounded by a series of resistance heaters just before entering the jacket. The temperature of the N_2 gas was then measured with an in-line platinum resistance thermometer immediately downstream of the heaters. This temperature measurement was used for control purposes. With this system the sample temperature as measured by the thermocouple was constant to about ± 0.1° C during the course of an experiment.

The optical detection train was aligned so that it was parallel to the incident beam before it was directed into the scattering cell by the scattering angle mirror. The scattered light was collected by a 1.0 inch diameter achromatic collimating lens (L_2) situated at its focal length of 8.0 cm from the scattering center. The collecting lens, focusing lens and all mirrors were carefully glued into their respective mounting devices in order to prevent any stress induced

birefringence effects. This can be important for depolarized experiments on weakly scattering liquids. Since the collecting lens was at its focal length from the scattering center, the collected light was parallel after it passed through the lens. A variable iris diaphragm (A_2) immediately following the collecting lens determined the solid collection angle and thus the spread in measured wave vector, $\delta\kappa$, resulting from a finite collection angle. The minimum aperture diameter for the iris was approximately 3 mm . This produced a solid angle of 1.1×10^{-3} sr . The collection aperture is an important consideration in low angle polarized scattering since it can be a source of significant broadening in the Brillouin lines. For this reason all Brillouin spectra were collected using the 3 mm aperature size.

The polarization component of the scattered light to be analyzed was isolated using a Glans-Thompson polarizer. The intensity of this light was then frequency analyzed with a piezoelectric scanning Fabry-Perot interferometer. A discussion of this instrument's operation is given later. An optical interferometer is very sensitive to temperature variation of its environment. For this reason the interferometer's housing was heavily insulated and the entrance and exit light ports were fitted with anti-reflection coated optical flats. The lab temperature was also controlled to better than 0.1° C during the course of an experiment. The interferometer used here was a Burleigh RC-110. It was operated in a single pass mode with a typical scanning rate of 1 sweep/sec. The mirrors were 38 mm in diameter with a flatness of $\lambda/200$ and reflectivities of 98.5%. Typical operating finesse (resolving power) was approximately 90 and most spectra were obtained using a free spectral range of 25.85 GHz . The operation of the interferometer was completely controlled by its companion Burleigh DAS-1 unit (data acquisition system) and high voltage amplifiers. The DAS-1 allowed for continuous correction of frequency drift whether it resulted from the laser or the inter-

ferometer. Parallelness of the interferometer mirrors was also continuously maintained by the DAS-1 resulting in an optimum finesse.

Scattered light, after passing through the interferometer, was focused with a 25 cm focal length lens (L_3) onto a 100 micron aperture (A_3). The light was then detected by a high gain EMI 9789B photomultiplier tube (PMT). A narrow band interference filter for the 4880Å line was placed in front of the PMT to exclude any stray white light, Raman bands, etc. . No cooling of the PMT was attempted and the dark count rate was found to be about 3 counts/sec. The voltage for the PMT was supplied by a Fluke 415B power supply. Normal operating voltage was 1350 volts. The signal from the PMT was sent to a package of Canberra photon counting electronics for processing. The photon counting instrumentation consisted of a model 583 charge sensitive pre-amp, a model 6018 amplifier, and a 6031 discriminator. A maximum counting rate of 2×10^5 counts/sec was indicated in the manufacturer's specifications. However, for the work done here, counting rates were not allowed to exceed 8×10^4. All signal carrying coaxial cable was kept as short as possible and carefully terminated to avoid spurious reflections.

Pulses from the discriminator were accumulated in a 1024 channel multichannel analyzer (MCA) incorporated in the DAS-1. The contents of the MCA were continously displayed on a CRT screen. The channel address was synchronized to a digital voltage ramp which supplied the input signal for the high voltage operational amplifiers driving the interferometers piezoelectric crystals. Thus a simple linear relationship existed between frequency and channel address. Normally the scanning rate for the interferometer was 1 msec/channel. This allowed for good frequency stabilization of the interferometer by the DAS-1. The spectra took anywhere from 4 to 20 minutes to collect at this rate, depending on the strength of the scattering and aperture size. Output of the MCA was to a

chart recorder for a graphical record and to paper tape for computer analysis. The data analysis method will be discussed later.

The Fabry-Perot Interferometer

In polarized light scattering from a pure liquid, Brillouin line shifts from 1 to 15 Ghz and linewidths from 50 Mhz up to 1 Ghz are encountered. Depolarized spectra commonly exhibit linewidths from 500 Mhz to 50 Ghz. Linewidths and shifts in this frequency range are best analyzed with a Fabry-Perot interferometer. The theory and description of the Fabry-Perot interferometer can be found in detail in several texts[38,39]. What we present here is a simple discussion, and some of the more relevant definitions, pertaining to its operation.

The operation of a Fabry-Perot interferometer is based upon interference by multiple reflection. The interferometer basically consists of two plane dielectric mirrors held parallel to each other and separated by a distance d. The cavity medium has a refractive index of n_3. See figure 6.

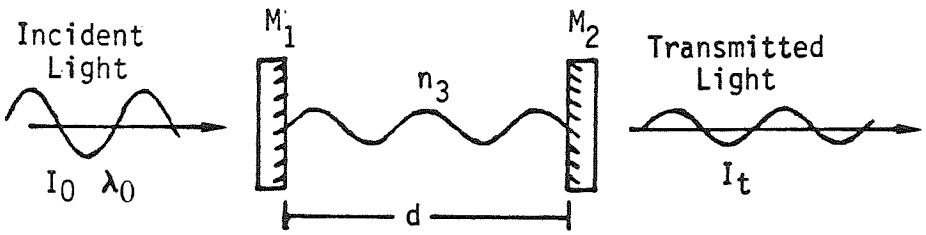

Figure 6. Schematic of a Fabry-Perot interferometer.

The degree of parallelness is extremely critical since deviations of only a few ten-thousandths of a degree can reduce the resolution noticeably. The inner surfaces of the mirrors are carefully ground and polished to a flatness of normally $\lambda/200$ or better. Dielectric coatings are then deposited to achieve reflectivities of greater than 98%. Usually light enters the cavity normal to the

mirrors and is reflected back and forth. The transmission coefficient, $T=\frac{I_t}{I_0}$, is given by the Airy formula

$$T=\frac{T_{max}}{1+F\sin^2\alpha} \tag{3.1}$$

where $F=\frac{T_{max}}{T_{min}}-1$ is called the contrast and depends on certain optical characteristics of the mirrors. The term α is given by

$$\alpha=\frac{2\pi n_3}{\lambda_o}d \tag{3.2}$$

Thus the condition for maximum transmission, T_{max}, is

$$d=\frac{m\lambda_o}{2n_3} \tag{3.3}$$

where m=0,1,2,...

A schematic of transmission versus frequency, ν, is shown in figure 7.

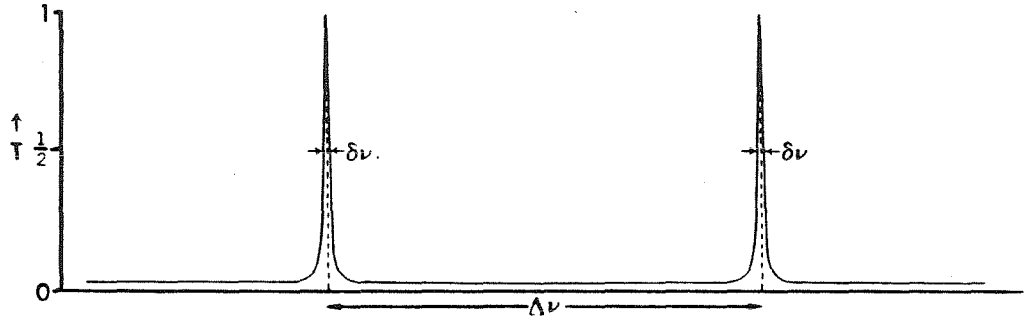

Figure 7. Transmission of an interferometer as a function of frequency.

Frequency scanning of the scattered light can be performed by varying d or n_3. Both techniques have been succesfully employed. By sealing the cavity and varying the pressure of the enclosed medium, n_3 can be changed in a predictable manner. The cavity length, d, can also be systematically changed by mounting one of the mirrors on piezoelectric crystals and then applying a known varying voltage to the crystals. The first method is inherently a slow scanning procedure but does not risk disturbing the mirror alignment. Scanning by the second

method can be done over a extremely wide range of rates, but gradual misalignment of the mirrors can be a problem. The interferometer used in the present studies employed piezoelectric scanning. This was essential since automatic interferometer control techniques are based on rapid scanning ability.

Note that as d is varied many transmission maxima can be observed corresponding to different values of the order, m. The spectral separation of adjacent transmission maxima is referred to as the free spectral range (FSR) and is given in frequency by

$$\Delta\nu = \frac{c}{2dn_3} \tag{3.4}$$

where c is the speed of light in vacuo. See figure 7. The ratio of the FSR to the instrumental linewidth, $\delta\nu$, is called the finesse and is indicative of the interferometer's resolving power. The overall finesse is determined by many factors including mirror reflectivity ($\frac{\pi}{2}F^{\frac{1}{2}}$), irregularites in the mirror's surface, mirror misalignment, absorption, etc. . With modern interferometers, finesses of over 100 can be achieved.

Data Analysis

The observed spectrum of scattered light obtained using an interferometer is not the true spectrum produced by the liquid. There are several instrumental effects which must be taken into account in order to obtain meaningful results[40,41,42]. These effects all produce significant line broadening and thus are most pronounced when measuring sharp linewidths and fine structure.

The first and most important source of line broadening results from the finite instrumental linewidth, $\delta\nu$. This simply means that the measuring "filter" is not perfect, but has a finite bandwidth. The fact that $\delta\nu$ is not zero is due to sur-

face imperfections, misalignment, etc. . If the instrument function, $I(\omega)$, is known and $S_A(\vec{\kappa},\omega)$ is the scattered spectrum being measured, then the broadened spectrum resulting from measuring with $I(\omega)$ will be

$$\bar{S}_A(\vec{\kappa},\omega) = \int_{-\infty}^{\infty} S_A(\vec{\kappa},\omega')\, I(\omega-\omega')d\omega' \qquad (3.5)$$

This is simply a convolution in frequency and is easily handled through the use of Fourier transform techniques. The instrument function can be obtained by observing the interferometer's response to a very narrow linewidth input. Probably the most obvious source of such an input signal is the direct laser light. However, for the results presented here, the instrument function was obtained by scattering light from high molecular weight polystyrene in solution. The polystyrene spectrum is a Lorentzian with a linewidth on the order of kilohertz. An instrument function was obtained before and after each experiment. However very little difference was ever noted in the lineshape. A typical instrument function is shown in figure 8. From the theoretical expression for the transmission coefficient in equation (3.1), it can easily be shown that near the peak the instrument function should be approximately Lorentzian in shape. A Lorentzian fit to the instrument lineshape is included in figure 8. As expected the fit is very good except for the near wings. The half-width at half-height (HWHH) from the fit was 142 Mhz, giving a finesse of 91. Lorentzian fitting of the instrument function was of course unnecessary since the actual discrete spectrum was used to correct for the convolution effect. However the convolution of two Lorentzians produces another Lortenzian with a HWHH equal to the sum of the HWHH's of the two initial Lorentzians. This fact was an important aid in the data analysis procedure.

Recall that the interferometer's condition for light transmission is $d=m\left[\frac{\lambda}{2}\right]$,

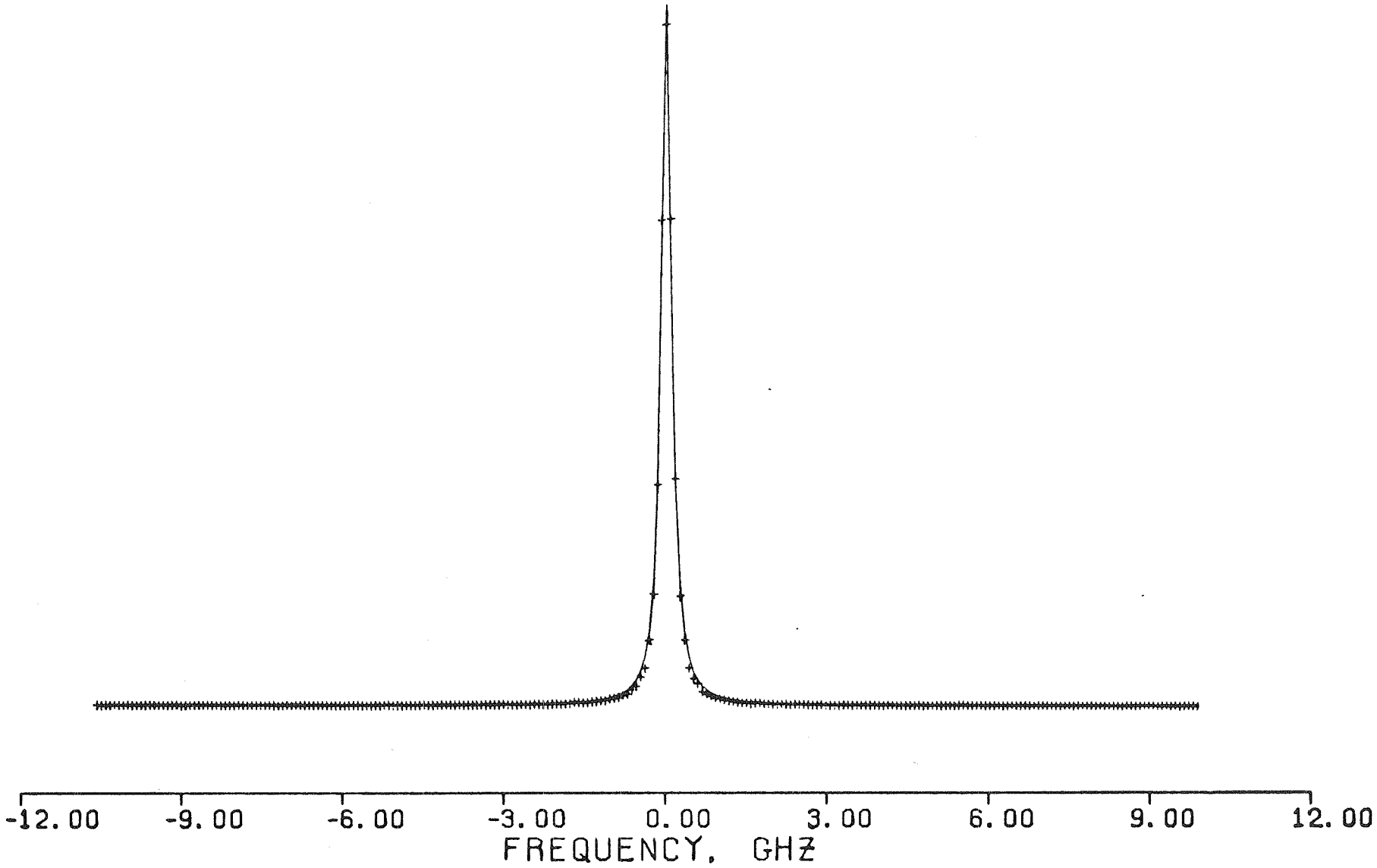

FIGURE 8. Typical instrument function for the Fabry-Perot interferometer used in this study. The HWHH is approximately 150 MHz. The solid line represents a Lorentzian fit.

assuming that the cavity medium is air (n_3). Thus for any d, light will be transmitted at many frequencies corresponding to the order m. The frequency separation of adjacent orders is just the FSR, Δf. The actual observed spectrum is therefore given by

$$O(\vec{\kappa}, \omega) = \sum_{n=-\infty}^{n=\infty} \bar{S}_A(\vec{\kappa}, \omega + n\Delta f)$$

$$= \sum_{n=-N}^{n=N} \bar{S}_A(\vec{\kappa}, \omega + n\Delta f) \qquad (3.6)$$

This effect is referred to as overlapping orders and can produce severe distortions depending on the spectrum being measured and the FSR. The number of adjacent orders needed to adequately describe $O(\vec{\kappa}, \omega)$ depends on the overall frequency range of the true spectrum relative to the FSR. If the overlap is small, i.e. FSR>> spectrum's frequency range, then N=1 is usually adequate. As the overlap increases more orders must be accounted for. For the present polarized scattering studies the FSR was about twice the Brillouin splitting at the highest scattering angle and N was set at two. For the depolarized experiments the FSR was anywhere from 2 to 8 times the HWHH of the rotational line. The value of N used in the data analysis varied from 2 to 6.

Another source of line broadening results from a finite collection aperture. This produces a small spread in the wave vector, κ, actually measured. This effect is expected to be of importance only in the measurement of Brillouin linewidths, since this line is shifted by an amount proportional to κ. Even for the Brillouin lines, this broadening should be small for the aperture and collecting lens used here and thus probably only significant at low scattering angles where the linewidths are narrow. The broadening from the κ^2 dependence of the linewidths produced by hydrodynamic modes is expected to be totally negligible.

For a circular aperture, the intensity of scattered light passing through the aperture for a given κ can be approximated by[43]

$$I(\kappa) \propto \left[1-\frac{(\kappa-\kappa_0)^2}{(\delta\kappa)^2}\right]^{\frac{1}{2}} \qquad |\kappa-\kappa_0| \leq \delta\kappa \tag{3.7}$$

$$= 0 \qquad |\kappa-\kappa_0| > \delta\kappa$$

where $\delta\kappa = \left(\frac{r}{2R}\right)(4\kappa_I^2-\kappa_0^2)^{\frac{1}{2}}$

In the above equations, κ_I is the incident wave vector, κ_0 is the wavevector of the light passing through the center of the aperture, r is the radius of the collection aperture, and R is the focal length of the collection lens. The spread in κ produced by the aperature is $\delta\kappa$. These equations are valid for R>> r. The scattered light spectrum which is measured by the interferometer, $S_A(\kappa,\omega)$, is related to the true liquid spectrum, $S(\kappa,\omega)$, by

$$S_A(\kappa_0,\omega) = \int_{\kappa_0-\delta\kappa}^{\kappa_0+\delta\kappa} S(\kappa',\omega)I(\kappa'-\kappa_0;\delta\kappa)d\kappa' \tag{3.8}$$

Note that this is basically just a convolution in κ-space.

The straightforward procedure for obtaining $S(\kappa,\omega)$ would be to strictly deconvolute the observed spectrum, Fourier transforming equations (3.5) and (3.8), and then fitting the result to a theoretical expression taking into account overlapping orders[40]. However this method was not attempted since it is known to be very sensitive to noise. Instead the following procedure was employed:

(1) The observed spectrum, $O(\kappa,\omega)$, was fit at each scattering angle to the theoretical expression for the true liquid spectrum assuming overlapping orders. This gave a reasonably good fit since the theoretical lineshapes are basically Lorentzian and the major change that occurs in measuring a spectrum is a

convolution with the instrument function which was also closely Lorentzian in shape.

(2) Next a true liquid spectrum, $S(\kappa, \omega)$, was assumed and then aperature broadened according to equation (3.8). The integration was carried out directly using a Simpson's rule algorithm. This gives $S_A(\kappa, \omega)$. A good initial guess was not difficult since the spectrum was, to a fair approximation, just broadened by an amount equal to the HWHH of t function.

(3) The aperture broadened spectrum was then convoluted with the appropriate instrument function and the effect of overlapping orders included. The convolution was carried out using fast Fourier transforms. The accuracy of this numerical convolution was checked by convoluting two Lorentzian lineshapes. One was given a HWHH equal to that of a typical instrument function and the HWHH of the other was varied. The finite frequency range for the calculation was identical to that used in the actual experiments. Results for this calculation are shown in table 2. Note that HWHH's add as expected.

(4) The spectrum resulting from steps (2) and (3) was then once again fitted to the theoretical expression. When the results of this fit agreed with that obtained in step (1) to within the standard error of each parameter, then the $S(\kappa, \omega)$ assummed in (2) was taken to be the correct liquid spectrum.

The above procedure was also done without aperture broadening in order to isolate the magnitude of this effect. The results are given in table 3. As expected the broadening is small and only important at low angles.

Sample Preparation and Characterization

All liquids studied here were obtained in the highest purity grade possible. Still many of the liquids, especially the nitrogen bearing compounds, showed a slight yellow discoloration. These liquids were vaccumed distilled to obtain a

Test of Numerical Convolution		
HWHH of 1st Lorentzian	HWHH of 2nd Lorentzian	HWHH of 1st & 2nd Convolution
3.2	0.1	3.22
3.2	3.0	6.19
3.2	5.0	8.19
3.2	10.0	13.18
3.2	15.0	18.16
3.2	20.0	23.14

TABLE 2. A check on the accuracy of the numerical convolution procedure. All HWHH's are in units of channels with 1 channel = 52.4 MHz.

Aperature Broadening		
	Brillouin Line Broadening	
Angle (Degrees)	p-Anisaldehyde (MHz)	Aniline (MHz)
21.6	12.8	-
26.0	11.5	-
30.0	8.9	11.0
35.0	7.9	-
40.0	7.1	8.9
50.0	6.5	7.4
60.0	6.0	5.3
70.0	5.6	3.2

TABLE 3. Line broadening produced by a 3 mm aperture and 8 cm focal length collecting lens.

clear sample. This was an absolute necessity since small amounts of an absorbing impurity results in heating induced divergence (lensing) of the incident beam. Samples were kept in the dark and under dry nitrogen except when a spectrum was actually being collected.

Elimination of small scattering centers in the liquid ("dust") is essential for depolarized measurements. Even very small amounts of dust can produce enough spurious elastic light to obscure the depolarized fine structure. Thus very careful attention was given to this problem. High purity clear liquids were repeatedly filtered through 0.25 micron Millipore filters directly into the scattering cell. This worked well. However, distillation itself seemed to be an effective method of removing dust, and since most liquids had to be redistilled, this proved to be a convienent technique. In order obtain the cleanest sample possible, the basic vaccuum distillation process was modified slightly. A Vigreaux column was used to help prevent entrainment of dust from the boiler. Samples were collected directly in the scattering cell. The entire system was initially purged with filtered nitrogen to clear it of airborne dust. The scattering cell was fitted with a capillary tube so that as it filled with condensate it could be drained off. This procedure of collecting and draining was repeated many times during the distillation before a sample was taken. In this way the system was throughly cleaned in situ and the light distillation fraction was removed. As a final measure, the entire system was enclosed in a filtered nitrogen filled enclosure.

For the experiments performed here, independent knowledge of the kinematic shear viscosity and refractive index of the liquid was required. Shear viscosity data for several of the liquids could not be found and consequently had to be measured in our own lab. This was done using a Cannon-Fenske Routine viscometer and a P.M. Thompson viscometer bath. The thermostating fluid used

was isopropanol. This allowed for temperatures down to -20°C. Temperature control was better than ± 0.05°C. The viscometer was carefully calibrated with distilled water. Liquid densities, when needed and not available at the desired temperature, were taken to be that at room temperature except for aniline which was measured at the temperature of interest.

Refractive indices for most of the liquids could be obtained from the literature[44,45] but only at one temperature which was generally 20°C. The refractive indices of aniline, benzenethiol, and benzylamine were measured using an Abbe-56 refractometer at several temperatures between 0° and 20°C. The results are shown in figure 9. In all three cases the temperature dependence was linear and $\frac{dn}{dT}$ was approximately the same at -0.0005/°C. Temperature corrections for other liquids than the three above were also based on this. An accurate measurement of the refractive index was only needed for the polarized measurements involving aniline and para-anisaldehyde. Aniline's refractive index was measured at the temperature of interest, and para-anisaldehyde, though not measured, needed only a 12° correction.

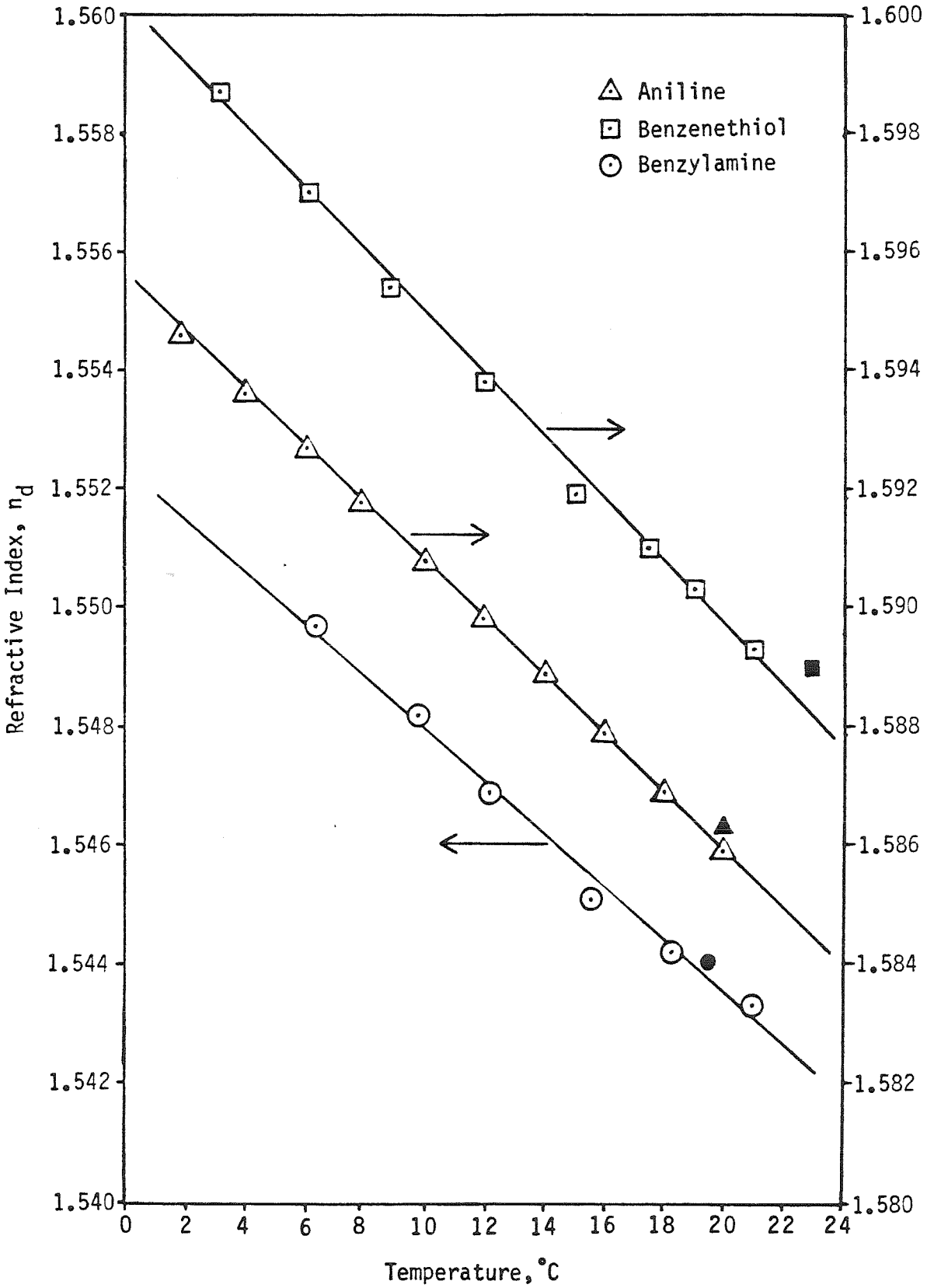

Figure 9. Refractive index as a function of temperature for aniline, benzenethiol, and benzylamine. The solid symbols represent literature values.[44,45]

Chapter 4

THEORY OF DEPOLARIZED LIGHT SCATTERING

Introduction

As stated previously, early experimental results in depolarized light scattering from condensed media were based upon the hydrodynamic theory of Rytov[4]. In this theory fluctuations in the local anisotropic strain are directly related to fluctuations in the dielectric tensor via a photoelastic constant. Therefore fluctuations in the anisotropic strain are the direct source of the depolarized scattering. The dynamics of the strain fluctuations are calculated using viscoelastic theory with stress related to strain through a frequency dependent shear modulus. The depolarized spectrum is then determined by the autocorrelation function of the anisotropic strain. This theory does predict a doublet structure in basic agreement with experimental results. The doublet arises from propagating shear waves whose existence is guaranteed by the introduction of a frequency dependent shear modulus. A broad unshifted Lorentzian is also predicted. The origin of this mode is related to the relaxation process producing the frequency dependent shear modulus and its HWHH is the reciprocal of the relaxation time of the modulus. Rytov's theory is intuitively appealing, and the nature of the relaxation process is completely general. However, it is phenomenological in nature and thus the coupling parameters and relaxation time do not have rigorous molecular definitions. Also the constant viscous flow relation between the high frequency shear modulus, shear viscosity, and relaxation time, $\mu_\infty \tau = \eta_s$, is not found to be satisfied experimentally. Since the hydrodynamic theory has generally been abandoned in favor of the more rigorous and quantitatively correct molecular theories, it will not be discussed further.

Molecular theories of depolarized light scattering from neat liquids have been proposed by several authors. Ailawadi and Berne[46] have reviewed the different theories categorizing them according to which fluctuating quantity is directly coupled to dielectric fluctuations, i.e. the "primary" variable, and the total number of coupled variables. All appear to be qualitatively correct. However, the two variable theories of Keyes and Kivelson[6] and Anderson and Pecora[5] have received by far the most attention both theoretically and experimentally. Keyes's result is based upon linear response theory[9]. He argues that the primary variable should be the polarizability density tensor and couples this to the transverse momentum density or shear modes. Anderson introduces an arbitrary tensor with the correct symmetry as the primary variable and also couples it to shear modes. The Anderson-Pecora theory is based upon the projection operator formalism of Zwanzig[8] and Mori[7]. Both theories yield the same result if Anderson's primary varible is identified with the polarizability tensor. Agreement between the molecular theory and experiment appears to be very good above the freezing point.

In the following, a derivation of the depolarized spectrum based upon the projection operator technique is presented. It is now generally agreed that the polarizability density tensor is the correct primary variable, and it will be used here as such.

Projection Operator Formalism

The projection operator formalism of Zwanzig and Mori is the basis of almost all microscopic theories of collective motion of many particle systems. This theory provides a rigorous statistical mechanical method for generating dynamical equations for a specified set of variables. The basic approach is to transform the classical equation of motion into the form of a generalized

Langevin expression and then show under what conditions a Markov approximation is valid. We follow closely the derivation as given by Berne and Pecora[47].

The state of a mechanical system with N degrees of freedom is specified by a phase space vector, $\Psi(\vec{q},\vec{p})$, whose components are the N generalized coordinates, q_i, and conjugate momenta, p_i. Any mechanical property of the system is by definition a function of the state, $A(\Psi)$, and according to classical mechanics obeys the following equation of motion:

$$\frac{\partial A(\Psi,t)}{\partial t} = iLA(\Psi,t) \tag{4.1}$$

The operator L is called the Liouvillian and is given by

$$iL = \sum_{i=1}^{N}\left[\frac{\partial H}{\partial p_i}\frac{\partial}{\partial q_i} - \frac{\partial H}{\partial q_i}\frac{\partial}{\partial p_i}\right] \tag{4.2}$$

where H is the Hamiltonian of the system. The formal solution of equation (4.1) is

$$A(\Psi,t) = e^{iLt}A(\Psi_0,0) \tag{4.3}$$

The property A varies from an intial state Ψ_0 at t=0 to some future state at time t according to the time evolution operator or propagator e^{iLt}. Thus the exact time dependence of A, though completely specified is a function of an enormous number of varibles. The idea behind the projection operator technique is to try to resolve the propagator in such way as to affect a separation of the terms linear in A. This formalism is discussed next.

First a set of mechanical properties, $\vec{A}$, is chosen and the invariant parts are set equal to zero. Thus averages of these quantities will vanish, $<\vec{A}>=0$. This set defines a subspace of the space spanned by all mechanical properties. A projection operator, P, is now introduced by the following definition:

$$P \equiv (\cdots,\vec{A}^{+})\cdot(\vec{A},\vec{A}^{+})^{-1}\cdot\vec{A} \tag{4.4}$$

where $\vec{A}^{+}$ is the Hermitian conjugate of $\vec{A}$. P, since it is a projection operator, has the following three properties: $P\vec{A}=\vec{A}$, $P^2=P$, and P is Hermitian. The scalar product (,) is defined for any two arbitrary properties F and G as

$$(F,G^{*}) \equiv \int d\Psi\, \rho_0(\Psi) G^{*}(\Psi) F(\Psi) \tag{4.5}$$

where $\rho_0(\Psi)$ is the equilibrium distribution function. The set of all mechanical properties together with the above definition of a scalar product defines a Hilbert space often referred to as Liouville space. Thus the operator P simply projects an arbitrary property in Liouville space onto the subspace of $\vec{A}$. The orthogonal compliment to P is defined by

$$Q = 1-P \tag{4.6}$$

This operator projects onto the subspace orthogonal to $\vec{A}$. The effect of these operators on an arbitrary property B is illustrated geometrically in figure 10 below.

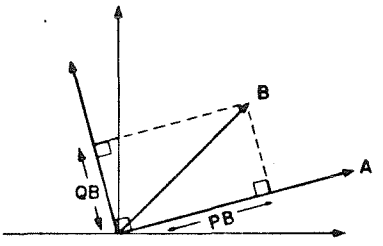

Figure 10. Geometrical interpretaion of the effect of orthogonal projection operators P and Q on an arbitrary property B

Using the identity P+Q=1, equation (4.1) can be rewritten as

$$\frac{\partial \vec{A}(t)}{\partial t} = (P+Q)iLe^{iLt}\vec{A}(0)$$

$$= e^{iLt}PiL\vec{A}(0) + e^{iLt}QiL\vec{A}(0)$$

$$= i\Omega \cdot \vec{A}(t) + e^{iLt}QiL\vec{A}(0) \tag{4.7}$$

Ω is commonly referred to as the frequency matrix and is defined by

$$\Omega = (L\vec{A},\vec{A}^{+})\cdot(\vec{A},\vec{A}^{+})^{-1} \tag{4.8}$$

The term $e^{iLt}QiL\vec{A}(0)$ can also be expanded further by use of the identity

$$e^{iLt} = e^{iO_1Lt} + \int_0^t d\tau\, e^{iL(t-\tau)}iO_2Le^{iO_1L\tau} \tag{4.9}$$

where O_1 and O_2 are any two operators such that $O_1+O_2=1$. This follows from the operator identity $B^{-1}-A^{-1}=A^{-1}(B-A)B^{-1}$. Taking B=s-iL and A=s-iO_1L and then Laplace inverting yields equation (4.9). Letting O_1=Q and O_2 =P, equation (4.7) becomes

$$\frac{\partial \vec{A}(t)}{\partial t} = i\Omega \cdot \vec{A}(t) + \int_0^t d\tau\, e^{iL(t-\tau)}iPLe^{iQL\tau}QiL\vec{A}(0) + e^{iQLt}QiL\vec{A}(0) \tag{4.10}$$

The random forces, $\vec{F}(t)$, are defined as

$$\vec{F}(t) \equiv e^{iQLt}QiL\vec{A}(0) \tag{4.11}$$

Introducing this into equation (4.10) gives

$$\frac{\partial \vec{A}(t)}{\partial t} = i\Omega \cdot \vec{A}(t) + \int_0^t d\tau\, e^{iL(t-\tau)}iPL\vec{F}(\tau) + \vec{F}(t) \tag{4.12}$$

Since both L and Q are Hermitian operators, one can write

$$iPL\vec{F}(\tau) = -(\vec{F}(\tau),\vec{F}^{+}(0))\cdot(\vec{A},\vec{A}^{+})^{-1}\vec{A}(0) \tag{4.13}$$

Defining the memory function matrix, $\mathbf{K}(t)$, by

$$\mathbf{K}(t) = (\vec{F}(t),\vec{F}^{+}(0))\cdot(\vec{A},\vec{A}^{+})^{-1} \tag{4.14}$$

and substituting into equation (4.12) yields

$$\frac{\partial\vec{A}(t)}{\partial t} = i\Omega\cdot\vec{A}(t) - \int_0^t d\tau\, \mathbf{K}(\tau)\cdot\vec{A}(t-\tau) + \vec{F}(t) \tag{4.15}$$

This is the desired result, a generalized Langevin equation. The equation of motion has now been separated into a part containing only linear terms and a random part containing the dependence on other degrees of freedom and non-linear terms in $A(t-\tau)$, $t \geq \tau \geq 0$. Thus extracting the linear part from the basic equation of motion is equivalent to projecting $\vec{A}(t)$ onto the subspace spanned by $\vec{A}$ in a Hilbert space of dynamical variables.

Several aspects of the above derivation with regard to $\vec{F}(t)$ should be mentioned here. The random forces are orthogonal to $\vec{A}$, i.e. $(\vec{F}(t),\vec{A}^{+})=0$. This follows from the identity $e^{iQLt}=Qe^{iQLt}Q$, which in turn implies

$$\vec{F}(t) = Q\vec{F}(t) \tag{4.16}$$

Thus the random forces lie completely within the subspace orthogonal to $\vec{A}$. Also note that the random forces evolve in time according to a modified or projected propogator, e^{iQLt}. Finally, equation (4.14) shows that the memory function matrix is directly proportional to the autocorrelation of the random forces. This relation is called the second fluctuation-dissipation theorem.

Markov Approximation

By making a "good" choice of variables for the set $\vec{A}$, the generalized Langevin equation previously derived can be simplified considerably. Suppose all the possible dynamic variables can be separated into two sets such that the properties in one set relaxes much slower than those in the other. We are thinking in terms of fluctuating quantities here. More specifically, assume that τ_s characterizes

the shortest relaxation time of the variables in the slow set. Then if this set has been chosen correctly,

$$\tau_s >> \tau_f \tag{4.17}$$

where τ_f characterizes the longest relaxation time of the all the other variables. It should be pointed out here that there is no a priori method for choosing the slow set $\vec{A}$ nor is there any guarantee that the separation in time scales can even be made. The selection is basically a matter of intuition. The action of the projection operator in the case where the separation is possible and $\vec{A}$ is chosen correctly is clear. P projects onto the subspace of slowly relaxing variables while Q projects onto the orthogonal or "fast" subspace. As has been previously noted, the random forces will lie entirely in the fast subspace and thus the memory function matrix should decay rapidly. Hence for times $t>>\tau_f$, the memory matrix, $\mathbf{K}(t)$, can be treated as a delta function,

$$\mathbf{K}(t) = 2\mathbf{\Gamma}\delta(t) \tag{4.18}$$

$\mathbf{\Gamma}$ is called the relaxation matrix and from equation (4.18) can be expressed as

$$\mathbf{\Gamma} = \int_0^\infty d\tau\, \mathbf{K}(\tau) \tag{4.19}$$

This treatment is usually referred to as the Markov approximation. Substituting equation (4.18) into the generalized Langevin equation yields

$$\frac{\partial \vec{A}(t)}{\partial t} = i\mathbf{\Omega}\cdot\vec{A}(t) - \mathbf{\Gamma}\cdot\vec{A}(t) + \vec{F}(t) \tag{4.20}$$

Taking the scalar product with $\vec{A}^+(0)$ yields a dynamical expression for the time correlation function matrix, $\mathbf{C}(t)=(\vec{A}(t),\vec{A}^+(0))$

$$\frac{\partial \mathbf{C}(t)}{\partial t} = i\mathbf{\Omega}\cdot\mathbf{C}(t) - \mathbf{\Gamma}\cdot\mathbf{C}(t) \tag{4.21}$$

Laplace transforming this expression gives

$$\tilde{\mathbf{C}}(s) = \mathbf{C}(0)\cdot(s\mathbf{I} - i\boldsymbol{\Omega} + \boldsymbol{\Gamma})^{-1}$$

$$= \mathbf{C}(0)\cdot\mathbf{Z}^{-1}(s) \qquad (4.22)$$

$\mathbf{C}(0)$ is the static correlation matrix and $\mathbf{Z}^{-1}(s)$ is usually referred to as the transport matrix. Note that the components of the relaxation matrix, Γ, cannot be directly calculated and therefore should be thought of as quantities to be deduced through comparison with experiments.

Including all the slow variables in $\vec{A}$ is obviously the critical step in making a Markov approximation. If, for instance, a slow variable is left out of the set, then $\vec{F}(t)$ will not lie entirely in the fast subspace and causal behaviour (memory) will result. This points out the equivalence between including additional variables in the molecular theory and introducing frequency dependence into the transport coefficients in a phenomenological treatment[48]. Since the correct choice of variables is a critical step in applying the Zwanzig-Mori formalism, we digress briefly to discuss this problem and indicate those variables which are certainly candidates for $\vec{A}$.

Slow Variables

In general one takes the variables in $\vec{A}$ to be fluctuations in functions of many particles or i.e. collective variables. This is certainly reasonable since one expects these fluctuations to be relatively slow in relaxing. However this is by no means a guarantee that any collective variable should be included in $\vec{A}$. As previously noted, light scattering theory will always involve fluctuations in collective variables since only long wavelength fluctuations, $o(1000\text{Å})$, are probed. With the above in mind, the components of $\vec{A}$ are normally taken to be the densities of a single particle property $a_j(t)$,

$$A(\vec{r},t) = \sum_j a_j(t)\delta(\vec{r} - \vec{r}_j(t)) \tag{4.23}$$

where $\vec{r}_j(t)$ is the position vector of the j^{th} particle. Since there is no systematic way of picking the slow variables, one must rely on intuition. The densities of conserved variables represent the most obvious choice. For conserved quantities

$$\frac{\partial A(\vec{r},t)}{\partial t} = -\nabla \cdot \mathbf{J}_A(\vec{r},t) \tag{4.24}$$

where $\mathbf{J}_A$ is the flux of A. The spatial Fourier transformation of this expression yields

$$\frac{\partial A(\vec{\kappa},t)}{\partial t} = i\vec{\kappa}\cdot\mathbf{J}_A(\vec{\kappa},t) \tag{4.25}$$

Therefore as $\kappa \to 0$, one expects $\frac{\partial A}{\partial t} \to \infty$ and A should be slowly relaxing. Thus fluctuations in a conserved quantity should be long-lived in the low κ regime, becoming infinite as $\kappa \to 0$. Properties which demonstrate this behaviour are often referred to as hydrodynamic modes. Therefore the number, momentum, and energy densities will always be included in the set $\vec{A}$ unless symmetry prohibited.

Symmetry Considerations

In applying the Mori-Zwanzig theory to a particular system, symmetry properties of the Hamiltonian can be extremely helpful. Symmetry arguments can reduce the number of independent parameters, elucidate wavevector dependencies, and decouple some of the dynamic equations for $\vec{A}(t)$. Some of the more important symmetry properties are discussed next.

Time Reversal Symmetry. If the properties in $\vec{A}$ have definite time reversal symmetry, then under the phase space transformation $(\vec{q},\vec{p}) \to (\vec{q}, -\vec{p})$,

$$A_i = \gamma_i A_i$$

where $\gamma_i = \pm 1$ is the time reversal signature. The elements of the correlation matrix, $\mathbf{C}(t)$, have the following property under time reversal:

$$C_{ij}(t) = \gamma_i \gamma_j C_{ij}(t) = \gamma_i \gamma_j C_{ij}^*(t) \tag{4.26}$$

Thus if $\gamma_i = \gamma_j$ the correlation function is an even function of time and the auto-correlation function, C_{ii}, is a real, even function of time. As a special case of the above transformation property, the static correlation elements, $C_{ij}(t=0)$, will be zero for different time reversal symmetries, i.e. $\gamma_i \neq \gamma_j$. The elements of the frequency matrix, Ω_{ij}, vanish unless the properties A_i and A_j have different time reversal symmetry, i.e.

$$\Omega_{ij} = -\gamma_i \gamma_j \Omega_{ij} \tag{4.27}$$

Thus the frequency matrix couples properties with different time reversal symmetry. The elements of the relaxation matrix, Γ_{ij}, have exactly the same transformation property under time reversal as the time correlation functions. If the static correlation matrix is diagonal, then the elements of the relaxation matrix are related in the following manner:

$$\Gamma_{ij} = \gamma_i \gamma_j \frac{C_{ii}(0)}{C_{jj}(0)} \Gamma_{ji}^* \tag{4.28}$$

This is a very useful relationship since as previously noted the Γ_{ij} are not readily amenable to direct calculation. In choosing a set $\vec{A}$, it is standard practice to construct the set such that the A_i are orthogonal. Thus the static correlation matrix will always be diagonal.

Inversion Symmetry. If the properties of set $\vec{A}$ transform like

$$A_i = \varepsilon_i A_i \quad , \quad \varepsilon_i = \pm 1$$

under phase space inversion, $(\vec{q},\vec{p}) \rightarrow (-\vec{q},-\vec{p})$, then the A_i are said to have definite parity. For properties with definite parity, the time correlation matrix

elements transform like

$$C_{ij}(t) = \varepsilon_i \varepsilon_j C_{ij}(t) \tag{4.29}$$

Thus properties with different parity are uncorrelated for all time. The same is true for the memory function matrix,

$$K_{ij}(t) = \varepsilon_i \varepsilon_j K_{ij}(t) \tag{4.30}$$

Therefore $K_{ij}(t)=0$ if $\varepsilon_i \neq \varepsilon_j$. Obviously this also applies to the relaxation matrix. The elements of the frequency matrix also have the same transformation property. Thus $\Omega_{ij}=0$ for $\varepsilon_i \neq \varepsilon_j$. Finally, for properties which transform like

$$A_i(\vec{\kappa}) = \varepsilon_i A_i(-\vec{\kappa})$$

under inversion, the elements of all the matrices discussed above will be odd functions of κ if the parities are different and even functions of κ if the parities are the same.

Reflection Symmetry. Properties which transform like

$$A_i = \alpha_i A_i \quad , \quad \alpha_i = \pm 1$$

under the phase space transformation

$$(x_j, y_j, z_j, p_{jx}, p_{jy}, p_{jz}) \rightarrow (x_j, -y_j, z_j, p_{jx}, -p_{jy}, p_{jz})$$

are said to possess reflection symmetry in the xz plane. For such properties the elements of $\mathbf{K}(t)$, $\mathbf{C}(t)$, and Ω are zero for $\alpha_i \neq \alpha_j$. Thus for a set $\vec{A}$ with definite reflection symmetry, the properties with $\alpha_i=1$ are totally uncorrelated with those of $\alpha_j=-1$.

Depolarized Spectrum of Scattered Light

In calculating the depolarized spectrum the scattering geometry shown in

figure 11 will be used.

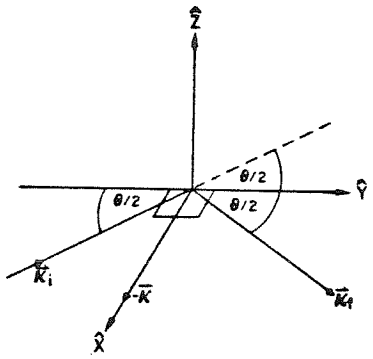

Figure 11. Scattering geometry for depolarized spectrum

From a molecular viewpoint, the depolarized spectrum is given in terms of fluctuating Fourier components of the polarizability density tensor, $\delta\alpha_{VH}$,

$$I_{VH}(\vec{\kappa}, \omega) \propto \int_{-\infty}^{\infty} dt < \delta\alpha^{*}_{VH}(\vec{\kappa}, 0)\ \delta\alpha_{VH}(\vec{\kappa}, t) > e^{-i\omega t} \tag{4.31}$$

Using the geometry in figure 11 and equation (1.7) shows that $\delta\alpha_{VH}$ has two components,

$$\delta\alpha_{VH}(\vec{\kappa}, t) = \delta\alpha_{zy}(\vec{\kappa}, t)\sin\frac{\Theta}{2} - \delta\alpha_{zz}(\vec{\kappa}, t)\cos\frac{\Theta}{2} \tag{4.32}$$

It would be more precise to use equation (1.6) which relates the spectrum to fluctuations in the spatial Fourier components of the dielectric tensor. However one must then directly relate these fluctuations to some other variable(s) with the same symmetry, i.e a primary variable. Since the polarizability density tensor is now generally assumed to be this primary variable, the two approaches are identical.

We begin by restricting attention to rigid, symmetric top molecules since this simplifies the theory considerably and yet still yields all the salient features observed in experimental spectra. A principal axis system in the molecule can always be found such that the molecular polarizability tensor is diagonal. For a

symmetric top the polarizability tensor in the body-fixed axis system is given by

$$\begin{bmatrix} \alpha_\perp & 0 & 0 \\ 0 & \alpha_\perp & 0 \\ 0 & 0 & \alpha_\parallel \end{bmatrix}$$

where $\alpha_\parallel$ is the component parallel to the symmetry axis and $\alpha_\perp$ is the component perpendicular to the symmetry axis. Taking $\hat{u}$ to be the unit vector along the symmetry axis, the polarizability tensor in a lab-fixed coordinate system, $\alpha(t)$, can be expressed by

$$\alpha_{km}(t) = <\alpha> \delta_{km} + \beta\left[u_k(t)u_m(t) - \frac{1}{3}\delta_{km}\right] \tag{4.33}$$

where $u_k(t)$ is the projection of $\hat{u}$ onto the k^{th} axis of the lab-fixed coordinate system and,

$$<\alpha> = \frac{1}{3}(2\alpha_\perp + \alpha_\parallel) \quad \beta = (\alpha_\parallel - \alpha_\perp)$$

The components of the fluctuations in the polarizability density tensor are therefore given by

$$\delta\alpha_{km}(\kappa,t) = <\alpha> \delta_{km} \sum_j e^{i\kappa x_j(t)} + \beta \sum_j \left[u_k^j(t)u_m^j(t) - \frac{1}{3}\delta_{km}\right] e^{i\kappa x_j(t)} \tag{4.34}$$

Note that the first term is an isotropic contribution proportional to the Fourier transform of the number density, $\sum_j \delta(\vec{r} - \vec{r}_j)$. The second term is a symmetric, anisotropic contribution. From equation (4.31) it can be seen that fluctuations in the polarizability density result from both translational and rotational motions. The components which directly contribute to the depolarized spectrum are, in the assumed geometry,

$$\delta\alpha_{zx}(\kappa,t) = \beta\sum_j u_z^j u_x^j e^{i\kappa z_j} \tag{4.35a}$$

$$\delta\alpha_{zy}(\kappa,t) = \beta\sum_j u_z^j u_y^j e^{i\kappa z_j} \tag{4.35b}$$

Thus the depolarized spectrum results from the anisotropic contribution only. Note that $\delta\alpha_{zx}$ and $\delta\alpha_{zy}$ are pure 2nd rank tensorial quantities. The above orientational variables may also be conveniently expressed in terms of an irreducible representation using Wigner rotation functions, $D^J_{KM}(\Psi_i)$, where Ψ_i represents the Euler angles specifying the rotation which transforms the body-axis system of molecule i into the lab frame[49].

$$\delta\alpha_{zx}(\kappa,t) = \beta 6^{-\frac{1}{2}}\sum_j \left[D^2_{0-1}(\Psi_j(t)) - D^2_{01}(\Psi_j(t))\right] e^{i\kappa z_j} \tag{4.36a}$$

$$\delta\alpha_{zy}(\kappa,t) = i\beta 6^{-\frac{1}{2}}\sum_j \left[D^2_{01}(\Psi_j(t)) + D^2_{0-1}(\Psi_j(t))\right] e^{i\kappa z_j} \tag{4.36b}$$

In the theory that follows, equation (4.32) will be used to describe $\delta\alpha_{zx}$ and $\delta\alpha_{zy}$ since it is intuitively appealing and the symmetry properties transparent. However, for completely anisotropic molecules or if more than one orientational variable is involved, the representation in terms of Wigner rotation functions is generally used since the properties of the D^J_{KM}'s are well known.

The first step in applying the Zwanzig-Mori formalism is to examine the symmetry properties of the primary variables and then determine what other "slow" variables can possibly couple to the primary variables to complete the set $\vec{A}$. Since $\delta\alpha_{zy}$ and $\delta\alpha_{zx}$ have respectively odd and even reflection symmetry in the zx plane ($u_y \to -u_y$), they are completely decoupled. Thus the depolarized spectrum reduces to

$$I_{VH}(\kappa,\omega) \propto \int_{-\infty}^{\infty} dt \left\{ < \delta\alpha_{zz}(\kappa,t)\delta\alpha_{zz}^{*}(\kappa) > \sin^2\frac{\Theta}{2} + < \delta\alpha_{zy}(\kappa,t)\delta\alpha_{zy}^{*}(\kappa) > \cos^2\frac{\Theta}{2} \right\} e^{-i\omega t} \quad (4.37)$$

The obvious variables to consider for coupling to $\delta\alpha_{zy}$ and $\delta\alpha_{zz}$ are, of course, the hydrodynamic modes considered earlier. The Fourier transforms of these variables are given below.

$$\text{number density} - \rho(\kappa,t) = \sum_j e^{i\kappa z_j}$$

$$\text{momentum density} - \vec{P}(\kappa,t) = \sum_j \vec{p}_j e^{i\kappa z_j} \quad (4.38)$$

$$\text{energy density} - U(\kappa,t) = \sum_j u_j e^{i\kappa z_j}$$

Consideration of reflection symmetry in the xy and zx planes indicates that $\delta\alpha_{zz}$ can couple to P_z only, while $\delta\alpha_{zy}$ couples to none of the above. Thus the calculation of $< \delta\alpha_{zz}(\kappa,t)\ \delta\alpha_{zz}^{*}(\kappa) >$ will involve a 2-variable theory with $\vec{A}$ given by

$$A_1 = \delta P_z(\kappa,t) \quad (4.39)$$

$$A_2 = \delta\alpha_{zz}(\kappa,t)$$

Now consider the static correlation matrix, $\mathbf{C}(0)$, which shall be denoted $\mathbf{N}$. Since A_1 and A_2 have opposite time reversal symmetry, the off-diagonal terms vanish.

$$\mathbf{N}(\kappa) = \begin{bmatrix} N_{11}(\kappa) & 0 \\ 0 & N_{11}(\kappa) \end{bmatrix} \quad (4.40)$$

The elements of $\mathbf{N}$ have the $\kappa \to 0$ form

$$N_{11}(\kappa) = < |P_z(\kappa)|^2 > = mNkT \qquad (\kappa \to 0) \quad (4.41)$$

$$N_{22}(\kappa) = < |\alpha_{zz}(\kappa)|^2 > = \frac{N}{15} g_2 \qquad (\kappa \to 0) \quad (4.42)$$

where N is the number of particles in the scattering volume, k is the Boltzmann

constant, and m is the mass of the particle. g_2 is a static orientational pair correlation function and is given by

$$g_2 = 1 + (N-1)\left\{\frac{< A_2(1)A_2^*(2)>}{< A_2(1)A_2^*(1)>}\right\} \tag{4.43}$$

Opposite time reversal symmetry also leads to vanishing diagonal elements in the frequency matrix. Explicit consideration of the off-diagonal components also reveals these to be zero. Thus the frequency matrix is null.

$$\Omega = \begin{bmatrix} 0 & 0 \\ 0 & 0 \end{bmatrix} \tag{4.44}$$

The relaxation matrix is impossible to evaluate directly since it involves correlation functions of random forces which have projected time dependences. None of these elements can be eliminated by symmetry considerations either. However inversion symmetry shows that the diagonal elements are even functions of κ, while the off-diagonal elements are odd. Explicit consideration of Γ_{11} shows that the leading term in a κ expansion is quadratic in κ. Thus the relaxation matrix looks like

$$\Gamma(\kappa) = \begin{bmatrix} \kappa^2\Gamma''_{11}(\kappa) & \kappa\Gamma'_{12}(\kappa) \\ \kappa\Gamma'_{21}(\kappa) & \Gamma_{22}(\kappa) \end{bmatrix} \tag{4.45}$$

Note that the low-κ dependence of the elements has been factored out. Thus the primed quantities approach constants in the limit $\kappa \to 0$. Inversion symmetry also relates the off-diagonal elements of Γ in the following manner:

$$\Gamma_{12} = -\frac{N_{11}}{N_{22}}\Gamma_{21}^* \tag{4.46}$$

The transport matrix is found by combining equations (4.22) and (4.41) - (4.46) to give

$$Z^{-1}(\kappa,s) = \begin{bmatrix} \frac{s+\Gamma_{22}}{D} & \frac{\kappa\Gamma'_{21}}{D} \\ \frac{\kappa\Gamma'_{12}}{D} & \frac{s+\kappa^2\Gamma''_{11}}{D} \end{bmatrix} \tag{4.47}$$

D is the discriminant of $Z(\kappa,s)$ and is given by

$$D(\kappa,s) = s^2+(\Gamma_{22}+\kappa^2\Gamma''_{11})s+\kappa^2(\Gamma''_{11}\Gamma_{22}-\Gamma'_{12}\Gamma'_{21}) \tag{4.48}$$

From equation (4.37) it can be seen that the depolarized spectrum is determined in part by

$$I^{zz}(\kappa,\omega) \propto \int_{-\infty}^{\infty} dt e^{-i\omega t} < A_2(\kappa,t)A_2^*(\kappa) > \tag{4.49}$$

Since $A_2(\kappa,t)$ is even under time reversal, its auto-correlation function is also an even function of time. Therefore $I^{zz}(\kappa,\omega)$ can be written as

$$I^{zz}(\kappa,\omega) \propto \mathrm{Re}\left\{ < \tilde{A}_2(\kappa,s=i\omega)A_2^*(\kappa) > \right\} \tag{4.50}$$

where $A_2(\kappa,s)$ is the Laplace transform of $A_2(\kappa,t)$. From equation (4.22) we have

$$\tilde{C}_{22}(\kappa,s) = < \tilde{A}_2(\kappa,s)A_2^*(\kappa) > = N_{22}(\kappa)\left\{ \frac{s+\kappa^2\Gamma_{11}''}{D} \right\} \tag{4.51}$$

Substituting this expression into equation (4.50) yields

$$I^{zz}(\kappa,\omega) \propto N_{22}(\kappa)\left\{ \frac{\omega^2\Gamma_s(\kappa)+\kappa^2\Gamma_{11}''(\kappa^2\omega_s^2-\omega^2)}{(\kappa^2\omega_s^2-\omega^2)^2+\omega^2\Gamma_s^2(\kappa)} \right\} \tag{4.52}$$

In the above equation the following definitions have been introduced: $\Gamma_s(\kappa)=\Gamma_{22}+\kappa^2\Gamma''_{11}$ and $\omega_s^2=\Gamma''_{11}\Gamma_{22}-\Gamma''_{12}\Gamma'_{21}$.

In order to complete the calculation of the depolarized spectrum, the terms involving $\delta\alpha_{zy}$ in equation (4.37) must be accounted for. This contribution is given by

$$I^{zy}(\kappa,\omega)\propto\int_{-\infty}^{\infty}dt e^{-i\omega t}<\delta\alpha_{zy}(\kappa,t)\delta\alpha^{*}_{zy}(\kappa)> \tag{4.53}$$

Once again time reversal symmetry allows $I^{zy}(\kappa,\omega)$ to be calculated by taking the real part of equation (4.53) with s=iω. As has been previously discussed, $\delta\alpha_{zy}$ does not couple to any of the hydrodynamic modes and thus represents the simple case of a single, uncoupled variable. The auto-correlation function of $\delta\alpha_{zy}$, $C_{zy}(\kappa,t)$, therefore obeys the following dynamic equation:

$$\frac{\partial C_{zy}(\kappa,t)}{dt}=-\Gamma_{zy}(\kappa)C_{zy}(\kappa,t) \tag{4.54}$$

The solution of the above equation is

$$C_{zy}(\kappa,t)=C_{zy}(\kappa)e^{-\Gamma_{zy}t} \tag{4.55}$$

Fourier transforming this yields the desired result

$$I_{zy}(\kappa,\omega)\propto C_{zy}(\kappa)\left\{\frac{\Gamma_{zy}}{\Gamma_{zy}^{2}+\omega^{2}}\right\} \tag{4.56}$$

As $\kappa\rightarrow 0$ it is expected that $N_{22}(\kappa)\rightarrow C_{zy}(\kappa)$ and $\Gamma_{22}\rightarrow\Gamma_{zy}$. This is implied by the fact that for isotropic systems the time derivatives of the D^{J}_{KM} involve terms like $J_p D^{J}_{KM'}$, where J_p is the angular momentum about the p^{th} molecular principal axis. Since the subscript K is unchanged, correlation functions of various D^{J}_{KM} with the same K should have the same time dependence. Using this result the depolarized spectrum is dependent upon three unknown quantities: Γ_{22}, Γ''_{11}, and ω_s^2. However, a relation between these parameters and the ordinary shear viscosity can be found by comparing the $\kappa\rightarrow 0$ limit of the auto-correlation function of the tranverse velocity, $<A_1(\kappa,s)A_1^{*}(\kappa)>$, as calculated above with that calculated using hydrodynamic equations[50]. The long time behaviour of $\tilde{C}_{11}(\kappa,s)$ may be determined by examining the pole nearest the origin. For small κ this pole lies at

$$s = \frac{-\kappa^2\omega_s^2}{\Gamma_{22}} \tag{4.57}$$

Thus $\tau = \frac{\Gamma_{22}}{\kappa^2\omega_s^2}$ gives the longest relaxation time, and for long times

$$C_{11}(t) \propto e^{\frac{-t}{\tau}} \tag{4.58}$$

From the linearized Navier-Stokes equations of hydrodynamics the relaxation time is known to be $\tau = \frac{\rho_0}{\eta_s\kappa^2}$, where η_s is the shear viscosity and ρ_0 the equilibrium density. Equating the above two relaxation times yields the desired relation

$$\frac{\eta_s}{\rho_0} = \frac{\omega_s^2}{\Gamma_{22}} \tag{4.59}$$

We now introduce an important quantity in light scattering reflecting the coupling between transverse velocity and orientation. Using the definition of ω_s^2, equation (4.59) can be rewritten as

$$\begin{aligned} \nu_s &= \Gamma''_{11} - \frac{\Gamma'_{12}\Gamma'_{21}}{\Gamma_{22}} \\ &= \Gamma''_{11} + \frac{|\Gamma'_{21}|^2 N_{11}}{\Gamma_{22}N_{22}} \end{aligned} \tag{4.60}$$

where ν_s is the kinematic viscosity. Defining the coupling parameter R by

$$R = \frac{|\Gamma'_{21}|^2 N_{11}}{\nu_s\Gamma_{22}N_{22}} \tag{4.61}$$

yields

$$\Gamma''_{11} = \nu_s(1-R) \tag{4.62}$$

If there is no coupling between orientation and the transverse velocity (R=0), then ν_s will be equivalent to Γ''_{11} as predicted by a single variable theory involv-

ing only the transverse velocity. However, with coupling to an orientational variable, the shear viscosity acquires a new component, $R\nu_s$, related to this coupling. Thus R is often referred to as that fraction of the shear viscosity arising from reorientational motion or rotational degrees of freedom. Obviously 1-R is the fraction due to translational motion.

Substituting equations (4.52) and (4.56) into (4.37) and introducing the definition of R yields the following expression for the depolarized spectrum:

$$I_{VH}(\kappa,\omega)\propto N_{22}\left\{\frac{\Gamma_{22}}{\omega^2+\Gamma_{22}^2}\sin^2\frac{\Theta}{2}+\frac{\Gamma_{22}(\omega^2+(1-R)(\kappa^2\nu_s)^2)\cos^2\frac{\Theta}{2}}{(\omega^2-\kappa^2\nu_s\Gamma_{22})^2+\omega^2(\Gamma_{22}+\kappa^2\nu_s(1-R))^2}\right\} \tag{4.63}$$

In the limit $\frac{\kappa^2\nu_s}{\Gamma_{22}} << 1$ (high T), the equation above reduces to the sum of two Lorentzians

$$I_{VH}(\kappa,\omega)\propto N_{22}\left\{\frac{\Gamma_{22}}{\omega^2+\Gamma_{22}^2}-R\,\frac{\kappa^2\nu_s}{\Gamma_{22}}\,\frac{\kappa^2\nu_s}{\Gamma_{22}+(\kappa^2\nu_s)^2}\cos^2\frac{\Theta}{2}\right\} \tag{4.64}$$

The spectrum predicted by equation (4.64) consists of a broad Lorentzian of HWHH Γ_{22} and a narrow "negative" Lorentzian of HWHH $\kappa^2\nu_s$. It is obviously this narrow Lorentzian which leads to the dip or splitting observed in the spectrum of many liquids. Note that the intensity of the dip is directly proportional to R. The fine structure is a direct consequence of "negative" coupling between orientational motion and shear modes or more simply, rotational-translational coupling.

By considering the microscopic definition of Γ'_{12}, the coupling parameter R can be rewritten in a more enlightening form[12],

$$R=\frac{\left|\int_0^\infty d\tau<\dot{\alpha}_{zz}(\tau)\sigma^*_{zz}>_Q\right|^2}{\nu_s\Gamma_{22}N_{11}N_{22}} \tag{4.65}$$

In the above equation σ_{zx} is a component of the stress tensor, $\dot{\alpha}_{zx}$ is a time derivative, and $< >_Q$ indicates the time dependence results from the modified propagator $e^{iQL\tau}$. Thus R is determined in part by the dynamic coupling between shear stress and the angular momentum of the molecules.

Chapter 5

RESULTS AND DISCUSSION

All depolarized spectra were collected at a scattering angle of 90° and at one temperature except for an initial study of para-anisaldehyde for which spectra were collected at scattering angles of 40° and 90°. At least six spectra were collected for each liquid studied in order to establish reliable error estimates. This was necessary due to the poor signal to noise ratio in many of the spectra. Measurements of the coupling parameter R, the collective reorientation frequency Γ_{22}, and HWHH of the "negative" component, $\kappa^2\nu_s$, are reported. Analysis of the spectra was performed according to the procedure given in chapter 3. This takes into account convolution with the instrumental spectrum and overlapping orders. Both of these effects are very important when studying the depolarized fine structure. Even though R is not a frequency, the convolution effect and overlapping orders tends to fill in the depolarized dip and thus reduce R.

The depolarized spectra were fit to the full two variable theory given in equation (4.63). In addition, the entire expression was multiplied by an adjustable intensity parameter and a baseline was included to account for extremely broad structure produced by collisional scattering. Thus, in general, the fitted parameters were Γ_{22}, R, $\kappa^2\nu_s$, the overall intensity, and a baseline. However, if the fitted shear viscosity was not in agreement with the classically measured value then it was held constant at the appropriate *convoluted* value during the fit. This situation generally occured for weak scatters where the signal to noise ratio was low and has been observed by other investigators[12,15,25].

The para-anisaldehyde study was performed in order to collaborate the earlier results of Alms, et. al.[12]. This was necessary since para-anisaldehyde was

used here in an extensive study of angular dependent polarized scattering. The results of this study are presented in chapter 8. However, it is appropriate to note here that excellent agreement was obtained with Alms' results and, in addition, the predicted κ dependence was verified. This served as a check on both the spectrometer and the data analysis method.

The liquids studied here were aniline, benzylamine, phenol, benzenethiol, bromobenzene, pyridine, picoline, and quinoline. These all represent "small" molecules very similar in size and shape except for quinoline. Quinoline was included due to a recent study[23] indicating R to be independent of density and considerably larger (R=0.64) than any previously reported value. The results for each liquid will now be discussed in turn.

Aniline

Spectra for aniline were obtained at 3° C. Initially parasitic scattering due to dust was evident in the spectra and this was accounted for by including an additional line with the instrumental width. Later, new samples were prepared with much less dust contamination and the spurious scattering was reduced by more than 90%. Typical fits of the observed spectra with high and low parasitic intensities are shown in figures 12 and 13. Note that only every other data point has been plotted. The overall fits to the observed spectra are very good here. This is primarily due to a high signal to noise ratio and relatively large value of $\frac{\kappa^2 \nu_s}{\Gamma_{22}}$ (dip intensity). Results of the spectral analysis are given in table 4 for the high parasitic intensity and table 5 for the low intensity. The ratio $\frac{\kappa^2 \nu_s}{\Gamma_{22}}$ is included in the tabulated results since the intensity of the dip is proportional to this quantity (see eqn. 4.64). The final entry in each column is an average value of the indicated parameter with error estimates based upon the individual measurements above. Note that there was little difference between the results obtained

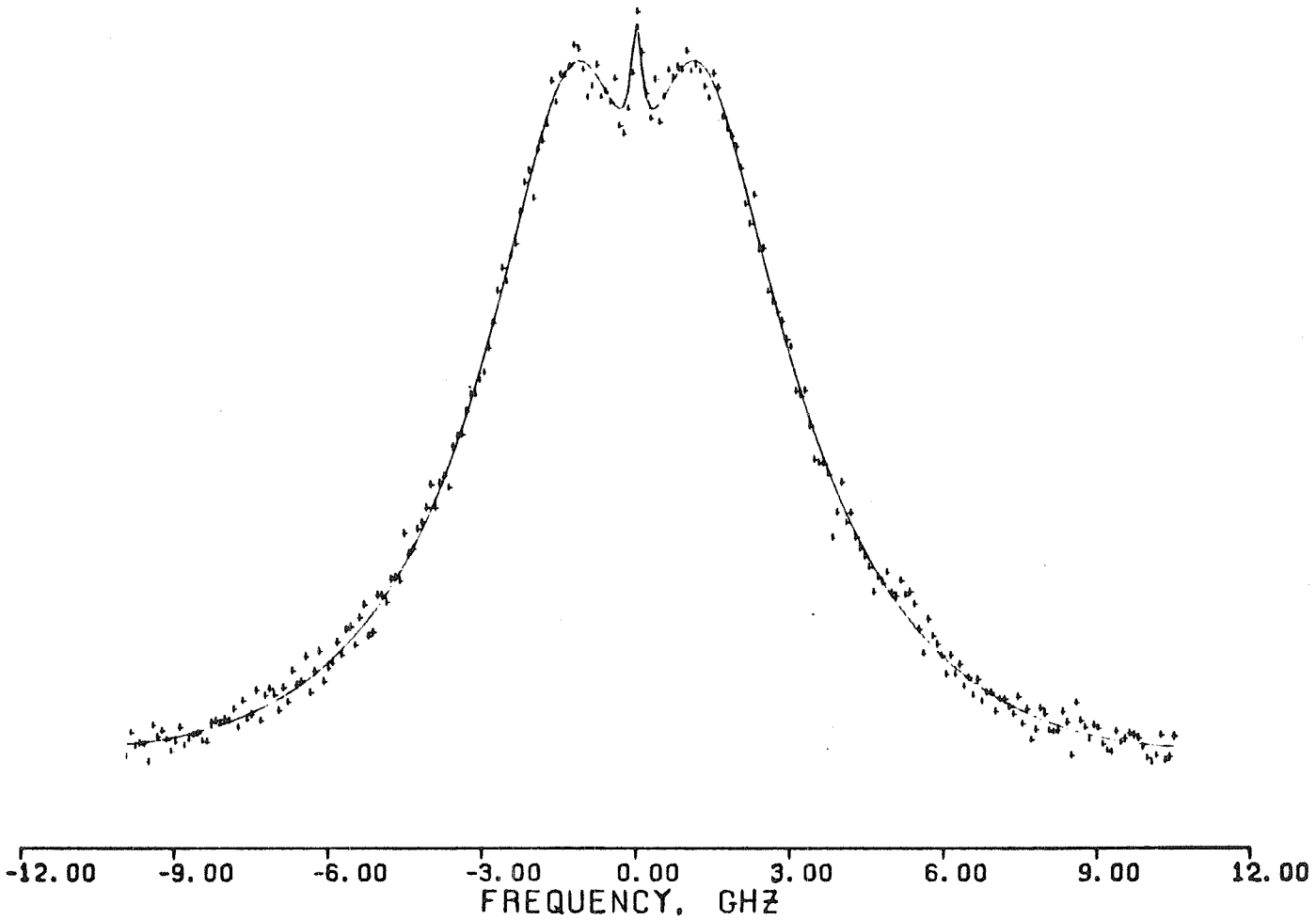

FIGURE 12. Depolarized spectrum of aniline at 3.0°C and a scattering angle of 90°. Note the sharp central peak due to spurious scattering from dust.

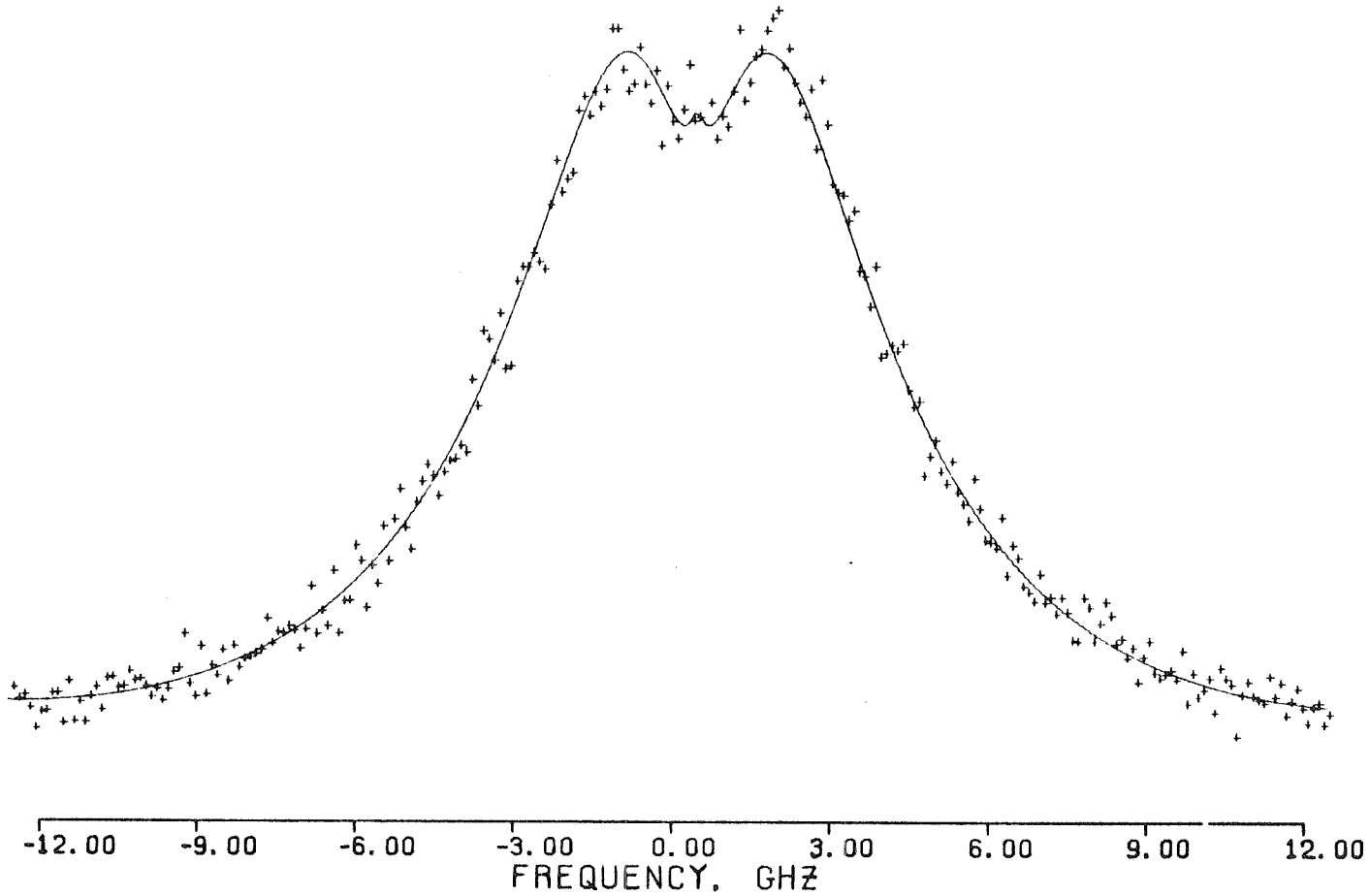

FIGURE 13. Depolarized spectrum of aniline at 3.0°C and a scattering angle of 90° . The spurious peak is much weaker here than in figure 12.

Depolarized Results for Aniline			
Γ_{22} (GHz)	$\kappa^2\nu_s$ (GHz)	R	$\frac{\kappa^2\nu_s}{\Gamma_{22}}$
3.29± .06	1.44± .10	0.52± .02	0.44
3.31± .06	1.24± .10	0.54± .02	0.37
3.34± .06	1.30± .10	0.54± .02	0.39
3.30± .06	1.31± .10	0.55± .02	0.40
3.38± .04	1.15± 06	0.54± .01	0.34
3.39± .04	1.12± 06	0.54± .01	0.33
3.26± .04	1.41± .08	0.53± .01	0.43
3.27± 04	1.36± .06	0.53± .01	0.42
3.32± .06	1.29± .10	0.54± .02	0.39

TABLE 4. Results of analyses for depolarized spectra of aniline at 3° C. These spectra contained a strong parasitic peak.

Depolarized Results for Aniline			
Γ_{22} (GHz)	$\kappa^2\nu_s$ (GHz)	R	$\frac{\kappa^2\nu_s}{\Gamma_{22}}$
3.42± .06	1.18± .09	0.57± .02	0.34
3.40± .06	1.13± .09	0.54± .02	0.33
3.46± .06	1.12± .09	0.54± .02	0.35
3.36± .06	1.16± .09	0.56± .02	0.34
3.41± .06	1.15± .09	0.55± .02	0.34

TABLE 5. Results of analyses for depolarized spectra of aniline at 3° C. These spectra exhibited only a small amount of parasitic scattering

with different parasitic scattering intensities. Γ_{22} became 2.5% larger as the dust level increased, $\kappa^2\nu_s$ dropped by 11%, and R was unchanged to within experimental uncertainty. The Γ_{22}'s obtained, 3.41± .06 GHz and 3.32± .06 GHz, are in good agreement with the early result of Stegeman and Stoicheff[3] where Γ_{22} was found to be 3.34± 0.1 GHz at 3° C. The classically measured value for the shear viscosity is 8.9 cp at 3° C [45] and the density as measured in our lab was 1.037 gm/cc. The refractive index of aniline at 3° C was measured to be 1.612 (figure 9) after a dispersion correction to the 4880Å line of the laser light. Thus the scattering wave vector, κ, was 2.93×10^5 cm^{-1} and $\kappa^2\nu_s$ from classical measurements is 1.18 GHz. This value is in excellent agreement with the present low dust measurement of 1.15± .09 GHz, but approximately 9% lower than the high dust value of 1.29± .1 GHz. The most important result here is the anomalously high value of R found (0.55). A recent measurement of R for nitrobenzene[22] produced an identical result of 0.55± .02 . This is interesting since nitrobenzene and aniline are very similar in size and shape and puzzling since other measurements of R for monosubstituted benzene derivatives have not produced values nearly as large. Our own results to follow lend support to this observation. The implications of this and a possible explanation will be discussed later.

Benzylamine

Although benzylamine represents a molecule slightly larger and more anisotropic than was intended for use in these experiments, it was studied due to the previous result for R in aniline. **Frohlich and Posch**[23] in their investigation of quinoline at elevated pressures found a very large R of 0.64 and observed no pressure dependence. Since other highly anisotropic molecules only gave coupling parameters up to 0.43, they concluded that a non-steric type of interaction must be producing the large coupling in quinoline. This conclusion seemed to be supported by the density independence of R. An interaction between the

lone pair of electrons of the nitrogen and the π-electrons of neighboring molecules was suggested as a possible mechanism. As shall be discussed later, we agree with Frohlich's basic argument that non-steric forces are involved but suggest that resonance interaction with the aromatic ring is the important consideration for aniline. Benzylamine was chosen for study since the amine group is separated from the benzene ring by a $-CH_2$ group and yet the overall size and shape is not changed drastically. This should lessen the resonance interaction and hopefully not alter the steric forces significantly.

Spectra for benzylamine were collected at -10° C and all exhibited parasitic scattering due to dust. The spectra were fit with a central line as was done for aniline to account for this feature. A typical fitted spectrum is shown in figure 14. Since R was unaffected by dust in aniline and both the signal to noise ratio and parasitic intensity were similar to that observed in aniline, no attempts were made to clean the samples further and the results with dust were assumed to be correct. These results are given in table 6.

Depolarized Results for Benzylamine

Γ_{22} (GHz)	$\kappa^2\nu_s$ (GHz)	R	$\frac{\kappa^2\nu_s}{\Gamma_{22}}$
3.77± .04	0.512	0.42± .02	0.14
3.73± .04	↓	0.43± .02	0.14
3.67± .04	↓	0.48± .02	0.14
3.64± .04	↓	0.48± .02	0.14
3.73± .04	↓	0.45± .02	0.14
3.70± .04	↓	0.44± .02	0.14
3.77± .04	↓	0.45± .02	0.14
3.71± .04	↓	0.45± .02	0.14
3.71± .06	0.512	0.45± .03	0.14

TABLE 6. Results of analyses for depolarized spectra of benzylamine at -10° C.

Note that $\kappa^2\nu_s$ has been held constant. This was necessitated since agreement with the classically obtained value was poor. The kinematic viscosity could not be found in the literature at -10° C and thus was measured in our lab. The results are given in figure 15. The kinematic viscosity was found to be 3.93 cs at

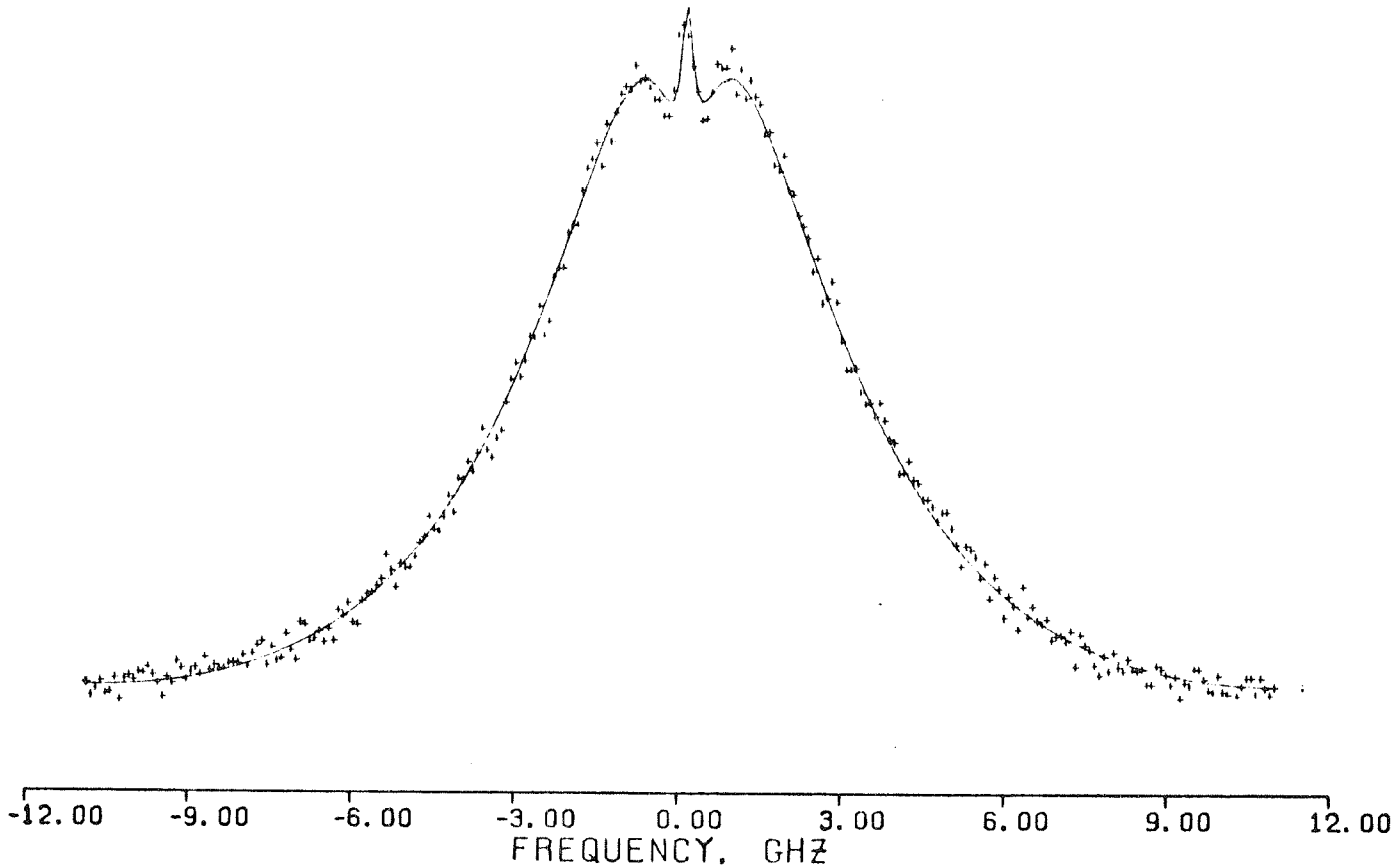

FIGURE 14. Depolarized spectrum of benzylamine at -10°C and a scattering angle of 90°. The sharp central peak is due to parasitic scattering from dust.

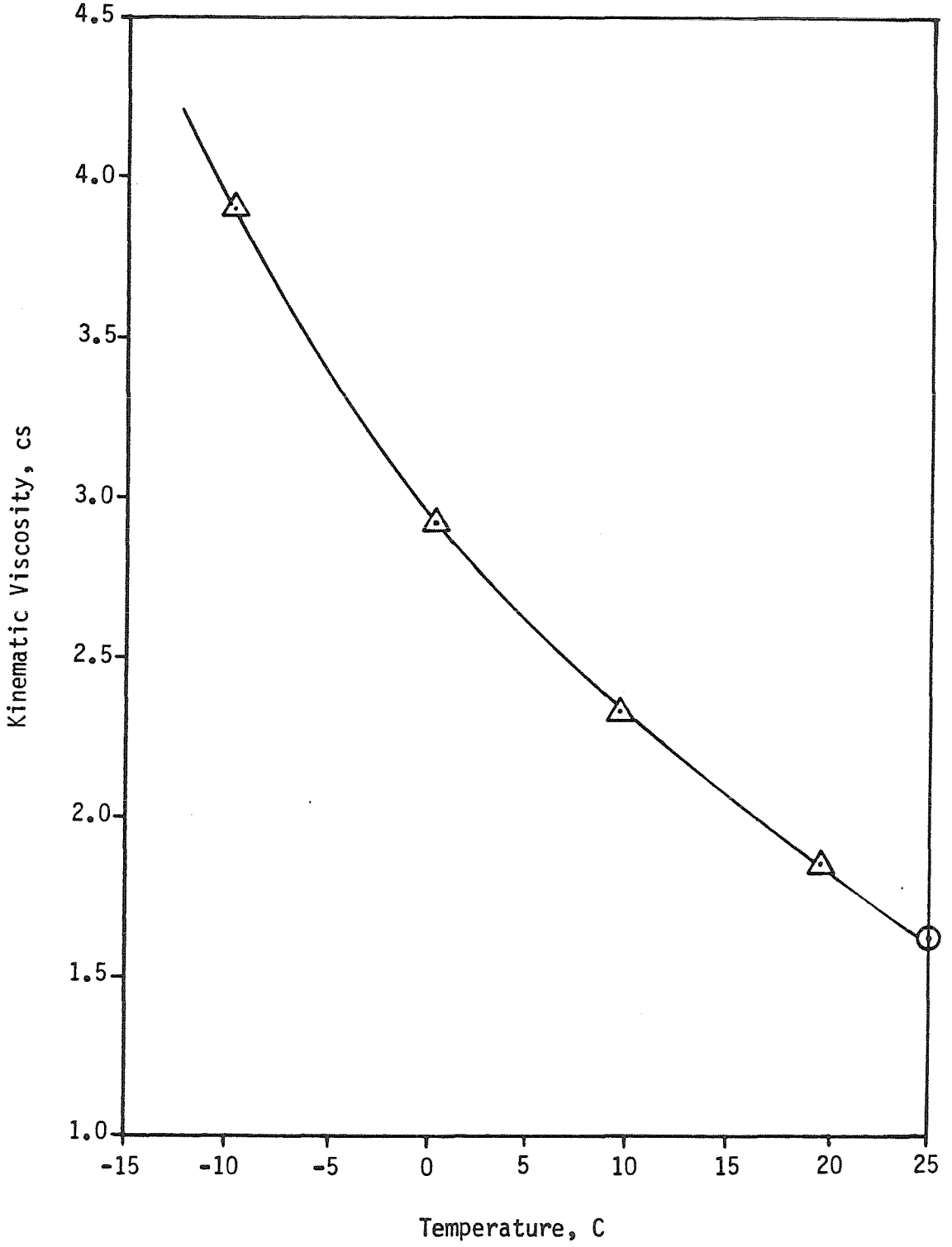

Figure 15. Viscosity of benzylamine as a function of temperature in the range 25°to -10°C. The circle represents a literature value[44].

-10° C. The refractive index was measured to be 1.572 (16° extrapolation) after correction to the 4800Å line. This gave a scattering vector of 2.86×10^5 cm^{-1} and a $\kappa^2\nu_s$ of 0.512 GHz. While fitting the spectra, $\kappa^2\nu_s$ was actually held at its convoluted value of 0.64 GHz. If treated as a free paramater it ranged from 6% to 50% higher than the calculated value, averaging about 0.67 GHz. This is not surprising since a similar problem was observed in aniline with high dust levels. The HWHH of the "negative" Lorentzian, $\kappa^2\nu_s$, was also less than half that of aniline and this is likely to produce more correlation between $\kappa^2\nu_s$ and the parasitic peak (HWHH of 150 MHz). The reorientation frequency for benzylamine was found to be a little larger than in aniline at 3.71 GHz while R dropped to 0.45. If one assumes that the differences in size and shape between benzylamine and aniline did not affect R, then the possibility of resonance interaction influencing the magnitude of R would appear to be supported by this result.

Phenol

Phenol was studied at 43.7° C. This proved to be a very convienent temperature to work at since all the required independent data were available from the literature at approximately the same temperature. The spectra all showed a clearly resolved dip with very little if any parasitic light discernible. Note that the signal to noise ratio was lower here than in benzylamine and aniline. A typical spectrum is shown in figure 16. Results of spectra analyses with no spurious scattering assumed are given in table 7. Once again the collective reorientation frequency was similar to the previous results at 3.61 GHz. The density, 1.0596 gm/cc, and the refractive index, 1.5558, were available from the literature[45] at 40.6° C and assumed to be completely adequate for calculations at 43.7° C. The viscosity is 4.25 cp at this temperature[45]. Therefore the calculated value of $\kappa^2\nu_s$ is 0.512 GHz. Almost all the fitted values of this parameter are in agreement with the calculated value to within experimental error. The average value of $\kappa^2\nu_s$ was

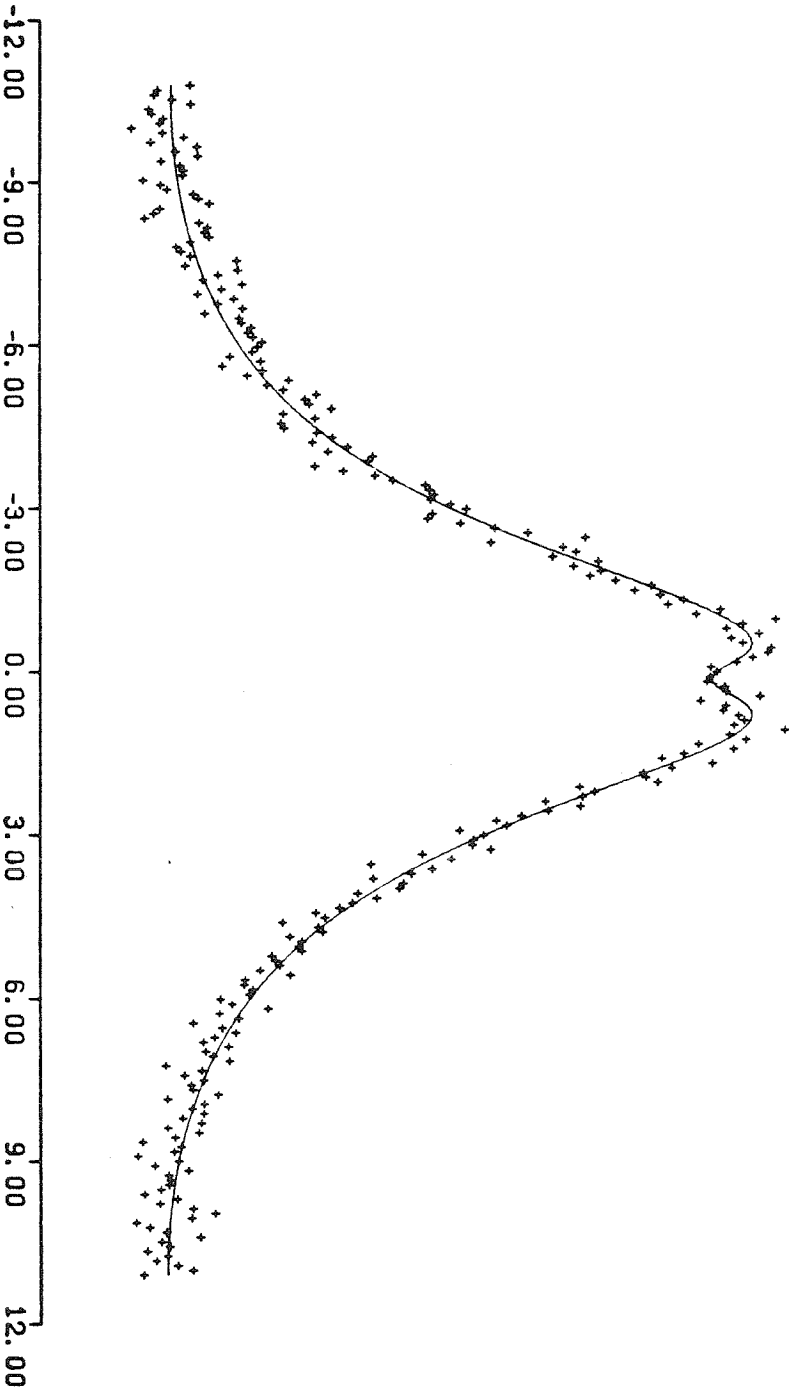

FIGURE 16. Depolarized spectrum of phenol at 43.7°C and a scattering angle of 90°.

Depolarized Results for Phenol			
Γ_{22} (GHz)	$\kappa^2\nu_s$ (GHz)	R	$\frac{\kappa^2\nu_s}{\Gamma_{22}}$
3.73± .05	0.51± .09	0.26± .02	0.14
3.59± .05	0.53± .08	0.28± .02	0.15
3.67± .05	0.44± .08	0.26± .02	0.12
3.59± .06	0.70± .15	0.23± .02	0.19
3.70± .05	0.47± .10	0.28± .02	0.13
3.47± .05	0.57± .08	0.34± .02	0.16
3.67± .05	0.49± .10	0.24± .02	0.13
3.56± .05	0.67± .11	0.26± .02	0.19
3.55± .06	0.67± .12	0.27± .02	0.19
3.58± .05	0.57± .10	0.27± .02	0.16
3.62± .05	0.51± .10	0.30± .02	0.14
3.61± .06	0.56± .10	0.27± .03	0.16

TABLE 7. Results of analyses for depolarized spectra of phenol at 43.7° C.

0.56± .1 GHz . This is once again a little high but well within the error estimate (18%). Thus a fit with $\kappa^2\nu_s$ at its correct convoluted value was not attempted. Since $\kappa^2\nu_s$, Γ_{22}, and scattering intensity are similar for phenol and benzylamine, it would appear that the presence of parasitic light does tend to produce high fitted values and large uncertainties for $\kappa^2\nu_s$.

The coupling parameter, R, was found to be quite small for phenol at 0.27± .03 . This is in complete contrast to the rather large values measured for aniline and benzylamine. Fits were made with a parasitic light peak allowed but the results were inconclusive with parasitic intensities proving to be very small (even negative) and with uncertainties as large as 400%. As would be expected this procedure tended to yield slightly larger R's by about 0.04 with increased uncertainties of ± 0.05 . The overall fits were no better than those with no spurious peak allowed.

Benzenethiol

Benzenethiol spectra were collected at -14° C. In general spurious scattering was not evident. However in two of the experiments an obvious dust peak appeared suddenly during a single scan (1 sec) indicating that dust was present in very small amounts. These spectra were discarded. A representative spectrum is shown in figure 17. The fine structure was adequately resolved but note that the signal to noise ratio was definitely worse than in the previous studies. Spectra fitted with $\kappa^2\nu_s$ as a free parameter produced values that were much too high and thus the analysis was done again with this parameter fixed at the convoluted classical result. Once again the viscosity and refractive index had to be measured in our own lab. See figure 9 for the refractive index results and figure 19 for the viscosity results. The kinematic viscosity was found to be 2.2 cs and the refractive index 1.62 at the laser line. The calculated value of $\kappa^2\nu_s$ is therefore 0.30 GHz. The actual convoluted result used in the fitting procedure was

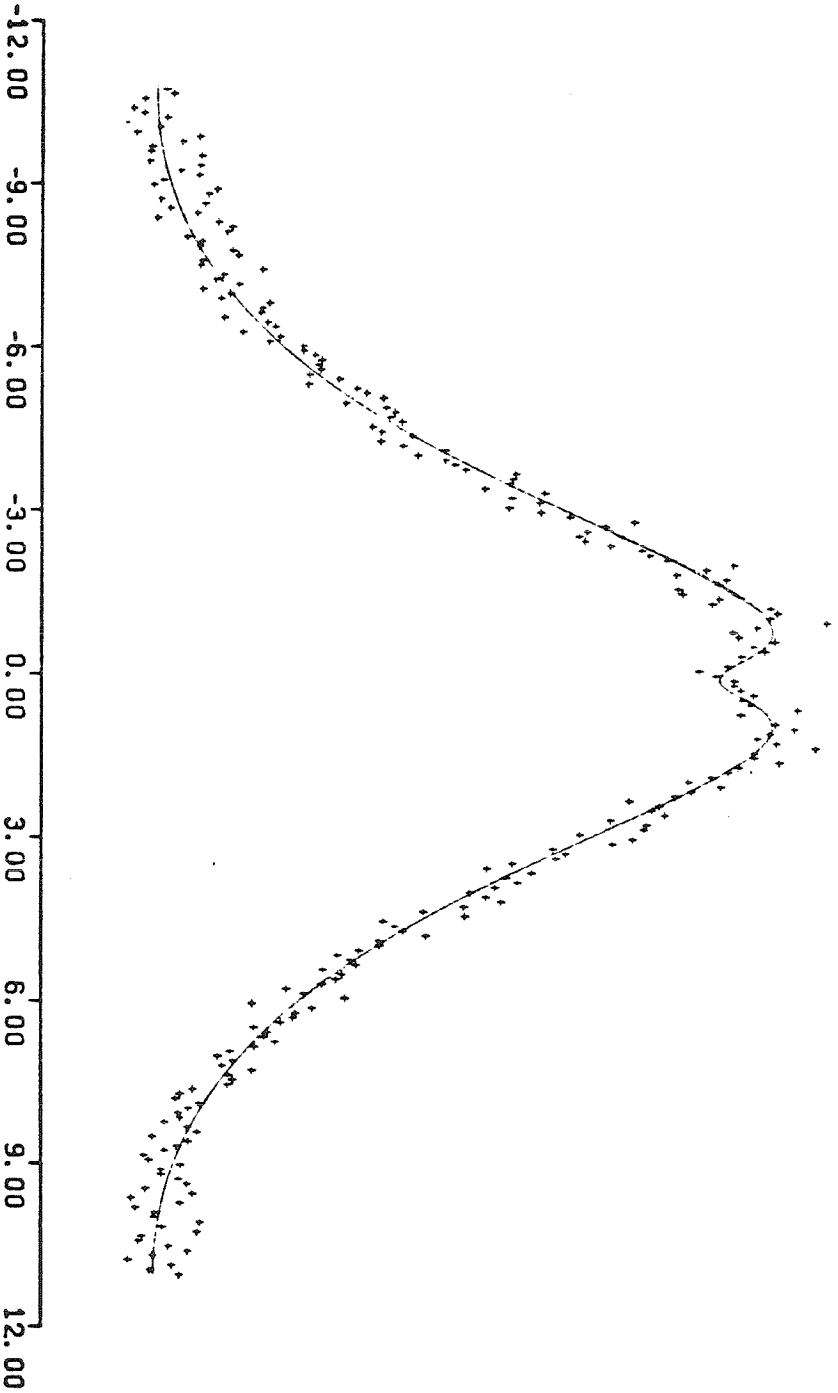

FIGURE 17. Depolarized spectrum of benzenethiol at -14°C and a scattering angle of 90°.

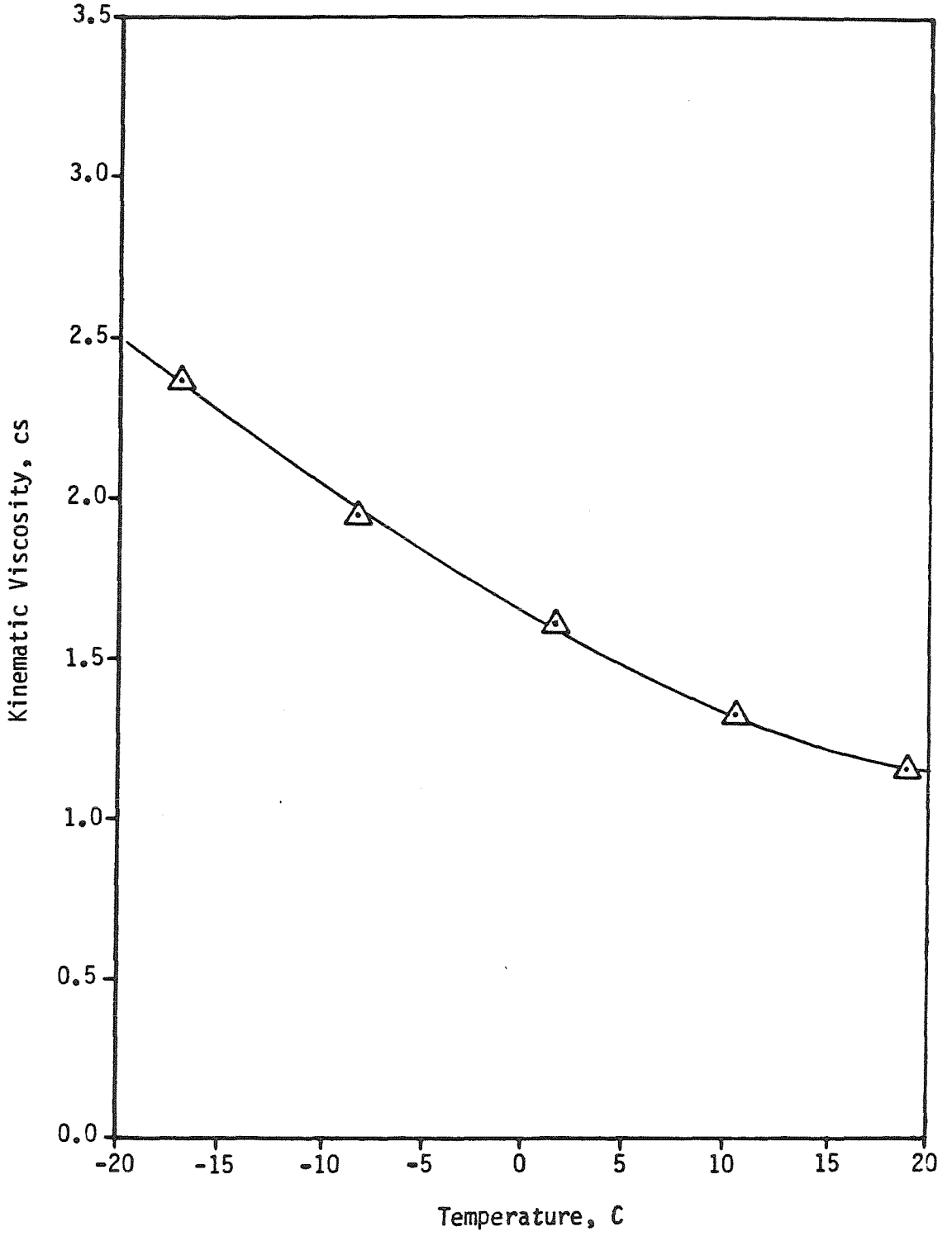

Figure 18. Viscosity of benzenethiol as a function of temperature in the range 20° to -20°C.

0.45 GHz. Results for R and Γ_{22} with no parasitic peak allowed for are given in table 8.

Depolarized Results for Benzenethiol			
Γ_{22} (GHz)	$\kappa^2\nu_s$ (GHz)	R	$\frac{\kappa^2\nu_s}{\Gamma_{22}}$
5.85± .1	0.305	0.37± .02	.052
5.81± .1	↓	0.39± .02	.053
5.67± .1	↓	0.40± .02	.054
5.88± .1	↓	0.42± .02	.052
5.86± .1	↓	0.37± .02	.052
5.73± .1	↓	0.35± .02	.053
6.03± .1	↓	0.29± .02	.051
5.75± .1	↓	0.32± .02	.053
6.06± .1	↓	0.32± .02	.050
5.76± .1	↓	0.35± .02	.053
5.84± .12	0.305	0.36± .04	.052

TABLE 8. Results of analyses for depolarized spectra of benzenethiol at -14° C.

Note that the ratio $\frac{\kappa^2\nu_s}{\Gamma_{22}}$ is quite small here compared with previous results. Obviously this was due to both the low viscosity of benzenethiol and the larger value of Γ_{22} at 5.86 GHz. This low ratio and the weak signal probably are the sources of the poor fits for $\kappa^2\nu_s$. Similar behaviour has been observed in other investigations of depolarized scattering[25]. It should be noted here that holding $\kappa^2\nu_s$ constant at its correct value did not improve the overall fits significantly. The coupling parameter was found to be 0.36± .04 . This value is typical of R's found for many liquids including carbon disulfide, MBBA, and benzonitrile (see table 1).

Bromobenzene

Depolarized spectra for bromobenzene were obtained at -17° C. Once again the signal was weak but the dip was still fairly well resolved. A typical spectrum for bromobenzene is shown in figure 19. Viscosity data could be obtained from the literature[45] but had to be extrapolated 17° for the temperature of interest here. Since a high degree of accuracy was not required, this seemed justified. The viscosity was found to be 2.1 cp . The refractive index was corrected from

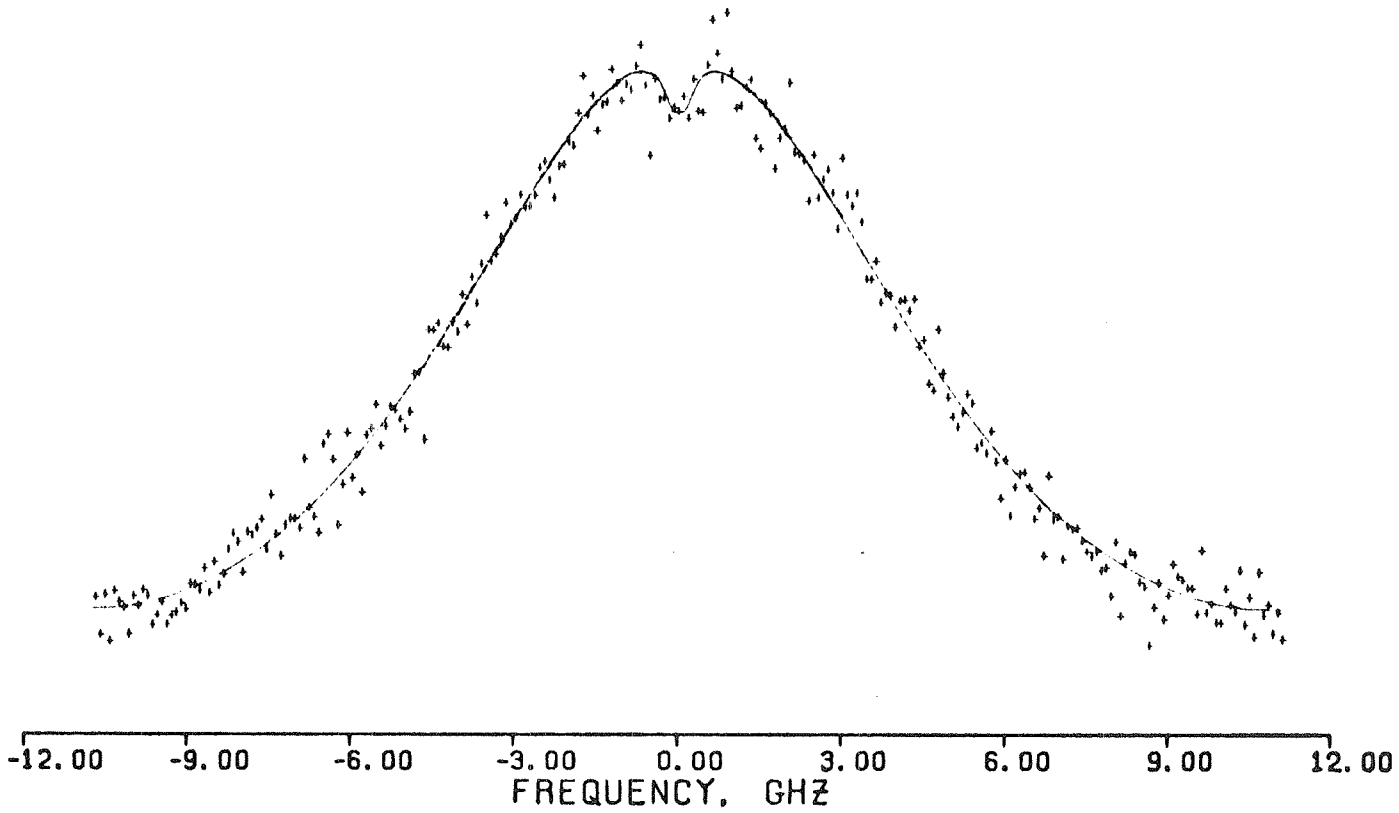

FIGURE 19. Depolarized spectrum of bromobenzene at -17°C and a scattering angle of 90°.

the literature value[44] at 20° C to -17° C using the observed temperature dependence for benzylamine, aniline, and benzenethiol (figure 9) of 0.0005/°C . Again this is justified since the correction is small and high accuracy unnecessary. This procedure yielded a refractive index of 1.592 . The calculated value of $\kappa^2\nu_s$ is therefore 0.18 GHz . As expected from the previous result, $\kappa^2\nu_s$ had to be held constant during the analysis procedure or it would generally be fitted at a value far too large (> 16%). The standard error for $\kappa^2\nu_s$ when treated as a free parameter was about 25%. The results of the spectra analyses are shown in table 9.

Depolarized Results for Bromobenzene

Γ_{22} (GHz)	$\kappa^2\nu_s$ (GHz)	R	$\frac{\kappa^2\nu_s}{\Gamma_{22}}$
7.46± .18	0.180	0.28± .03	.024
7.32± .17	↓	0.34± .03	.024
7.45± .16	↓	0.31± .02	.024
7.21± .16	↓	0.24± .02	.025
7.18± .15	↓	0.29± .02	.025
7.27± .13	↓	0.34± .02	.024
7.32± .2	0.180	0.30± .04	.024

TABLE 9. Results of analyses for depolarized spectra of bromobenzene at -17° C.

The reorientation frequency was found to be 7.32± .2 GHz and the coupling parameter 0.30± .04 . The large uncertainty in R was not unexpected since $\frac{\kappa^2\nu_s}{\Gamma_{22}}$ is very small here. As mentioned in the discussion of the benzenethiol results, this is also the most probable reason for the fitted values of $\kappa^2\nu_s$ being too high.

Pyridine

Pyridine is a good example of a rigid, symmetric top. It has been previously studied by Searby, .et .al[21] and contradictory results for R obtained. In Searby's study the coupling parameter was measured in the conventional I_{VH} geometry and also in the little explored I_{HH} geometry[19] at a scattering angle of 90°. The I_{HH} spectrum is truly depolarized at only 90° and this is why it is rarely used. At

any other scattering angle some of the intense polarized scattering will appear and tend to mask the I_{HH} fine structure containing information on R. Obviously a finite collection aperture will result in some polarized light leakage. Searby found an R of 0.35± .05 from the I_{VH} spectrum and an R of 0.70± .05 from the I_{HH} spectrum. The reason for this discrepancy could not be adequately explained. However since the I_{HH} spectrum is not affected by scattering from dust, they suggested that the large I_{HH} value for R might indeed be correct and spurious scattering from dust producing a low I_{VH} result.

It was decided to include pyridine in the present investigation since it fit the general steric restrictions reasonably well and would provide a check on Searbys' results for R. In addition, picoline (4-methyl pyridine) was to be used in this series of studies and reliable results for pyridine were desired as a base case.

In the present study depolarized pyridine spectra were collected at -41°C. One of the spectra is shown in figure 20. The scattering here was very weak leading to a low signal to noise ratio. The effect of overlapping orders was also apparent here. Data for the analysis of pyridine were taken from Searby's earlier work. The kinematic viscosity at -41° C was measured to be 3.7 cs and the refractive index was 1.55 . The calculated value of $\kappa^2\nu_s$ is 0.48 GHz . All spectra had to be fitted holding $\kappa^2\nu_s$ at its correct convoluted value of 0.61 GHz . The results for R and Γ_{22} are presented in table 10.

Depolarized Results for Pyridine

Γ_{22} (GHz)	$\kappa^2\nu_s$ (GHz)	R	$\frac{\kappa^2\nu_s}{\Gamma_{22}}$
9.4± .5	0.48	0.49± .05	.05
11.1± 1.1	↓	0.30± .06	.04
9.9± .6	↓	0.40± .05	.05
10.2± .8	↓	0.31± .05	.05
10.4± .7	↓	0.35± .05	.05
10.2± .8	0.48	0.35± .05	.05

TABLE 10. Results of analyses for depolarized spectra of pyrdine at -41° C.

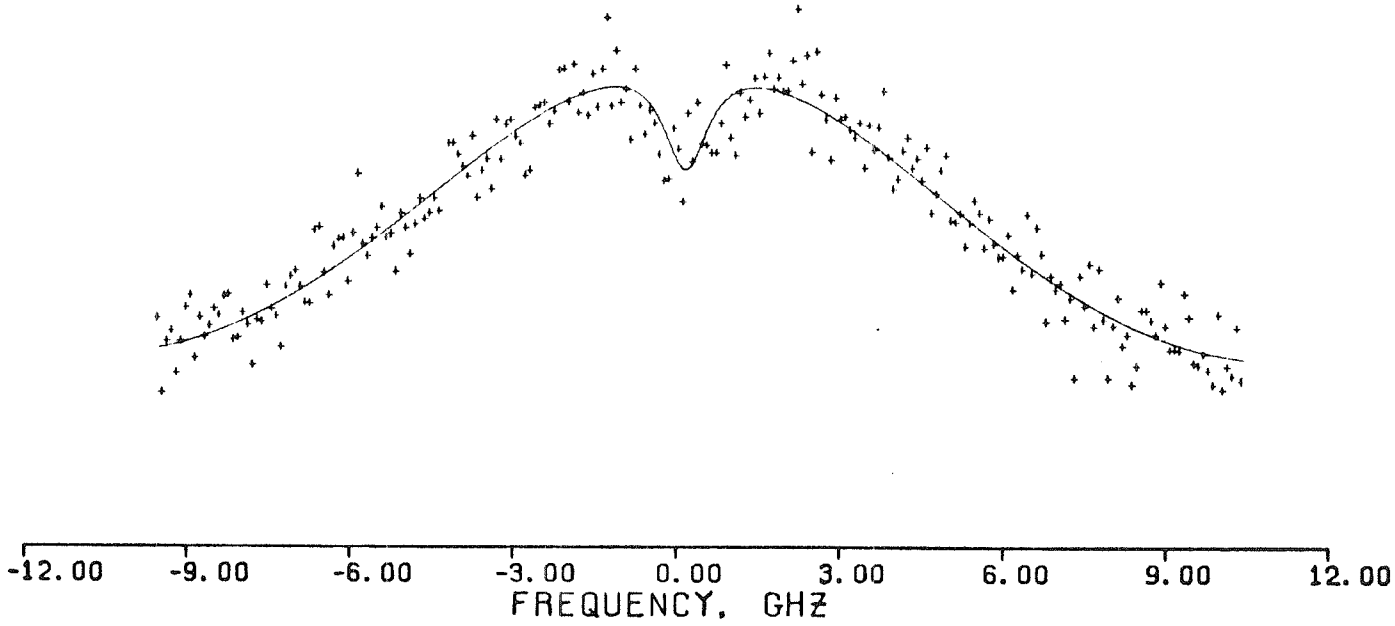

FIGURE 20. Depolarized spectrum of pyridine at -41°C and a scattering angle of 90°.

No parasitic scattering peak was allowed for in the analysis yielding the results in table 10. The reorientation frequency of 10.2± 0.8 GHz found here is in good agreement with Searby's result. The coupling parameter measured here was 0.35± .05 . This agrees with the I_{VH} measurement of Searby in both magnitude and uncertainty. Since the samples used in Searby's study and here were probably prepared in a different manner, it seems unlikely that parasitic scattering from dust could be producing a low result for R. However, fitting the spectra with a dust peak allowed did produce much higher R's with a average coupling of 0.50± .07 . Γ_{22} was not altered to within experimental uncertainty (10.0 GHz). Overall fits of the spectra were not significantly better with a parasitic line but spurious intensity was always found with a typical uncertainty of 30%. Note that an R of 0.5 is still considerably less than Searby's I_{HH} result of 0.7 .

Picoline

The study of picoline or 4-methyl pyridine was undertaken since the spectrum of the simple benzene derivative toluene cannot be resolved adequately enough to observe fine structure at atmospheric pressure. This is a result of the low viscosity and high reorientation frequency of toluene under normal conditions. Picoline however provides a close physical analog to toluene and yet has a freezing point low enough to allow for the observation of a dip and consequently a measurement of R. There is additional interest here since the effect on R of adding a methyl group to the aromatic pyridine ring will be observed.

Picoline was studied at -6° C. No parasitic light was evident in the spectra. The scattering was, as in the case of pyridine, very weak. The dip was resolved but was certainly the poorest resolution of the fine structure in the present investigation. A depolarized spectrum of picoline is shown in figure 21. As has been the case for all the weak scatters here, $\kappa^2\nu_s$ had to be fixed at its theoretical value after suitable adjustment for convolution. Otherwise the fitted results were

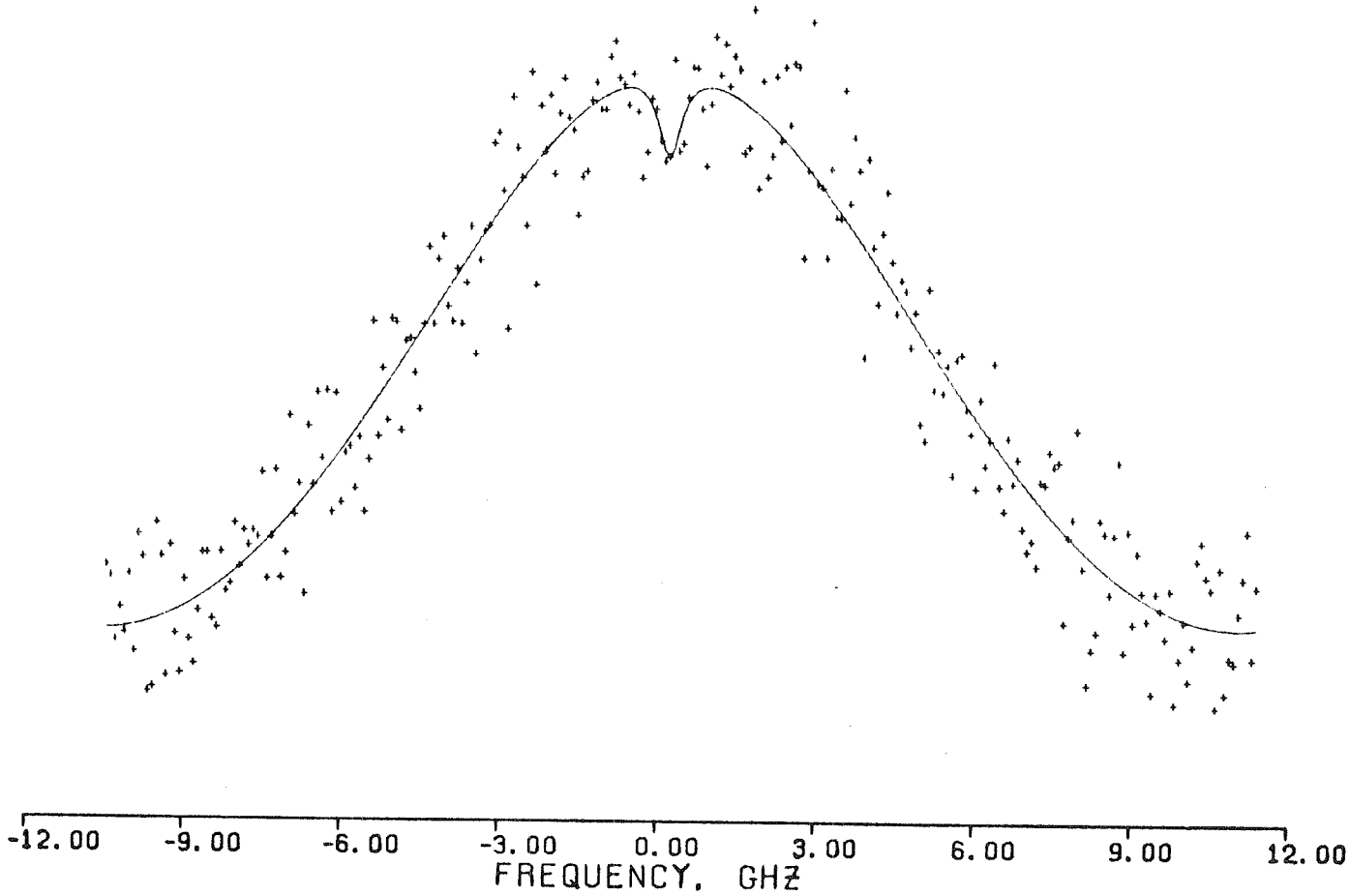

FIGURE 21. Depolarized spectrum of picoline at -6.0°C and a scattering angle of 90°.

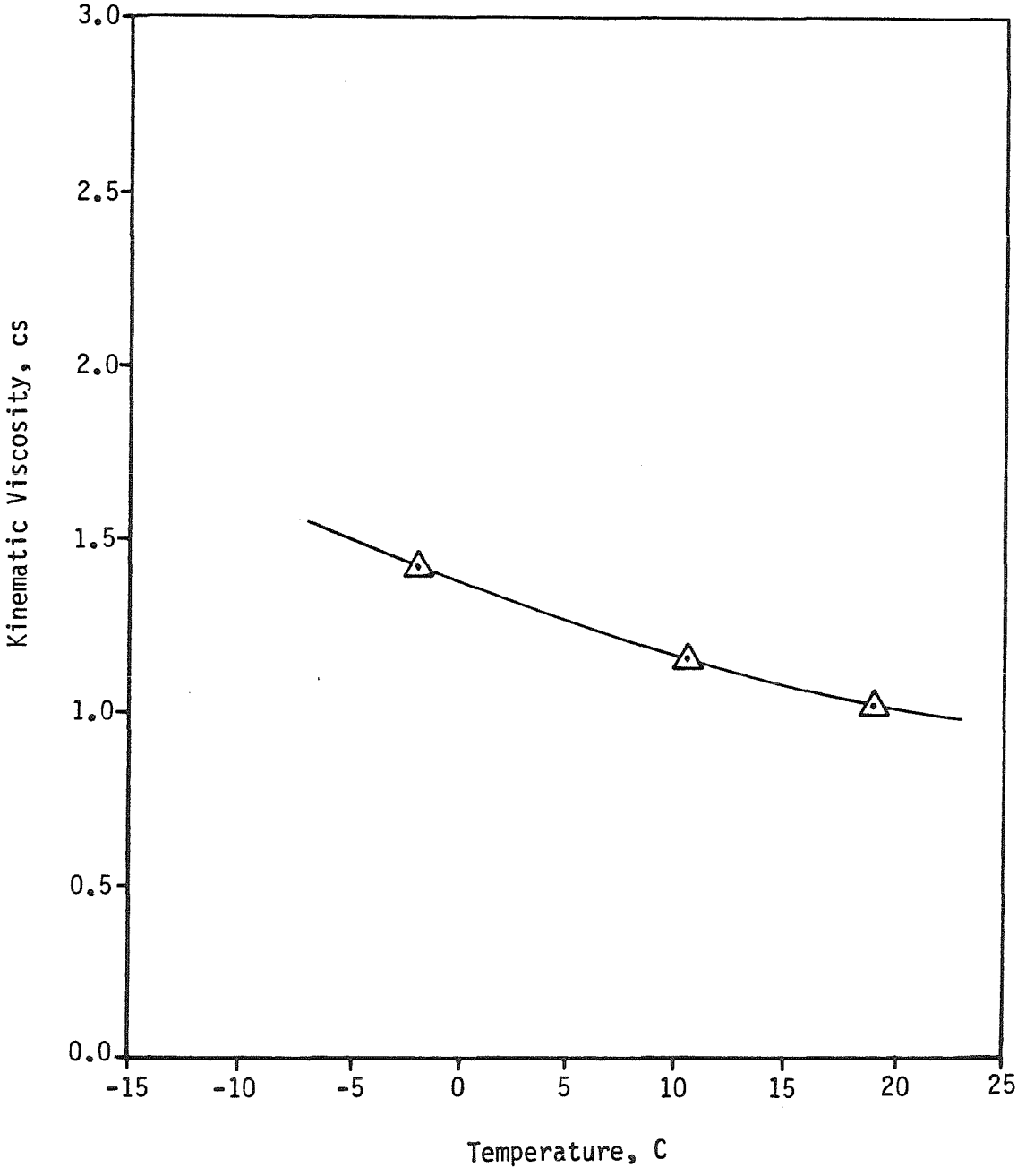

Figure 22. Viscosity of picoline as a function of temperature in the range 20° to -2° C.

much too high as was the standard error for $\kappa^2\nu_s$ (40-70%). The kinematic viscosity of picoline was measured in our own lab with the results given in figure 22. The viscosity at -6° C was 1.52 cs . The refractive index was measured at 20° C (1.5050) and corrected to the temperature of interest using the results in figure 9. At -6° C this was 1.535 . The theoretical value of $\kappa^2\nu_s$ was calculated to be 0.188 GHz, with the convolution adjustment raising it to 0.323 GHz for actual spectrum analysis. The results of the analyses with no dust peak allowed are given in table 11.

Depolarized Results for Picoline

Γ_{22} (GHz)	$\kappa^2\nu_s$ (GHz)	R	$\frac{\kappa^2\nu_s}{\Gamma_{22}}$
9.5± .6	0.19	0.28± .08	.02
10.7± .7		0.24± .04	.02
9.4± .6		0.32± .04	.02
9.3± .5		0.36± .04	.02
10.7± .6		0.19± .03	.02
10.1± .6		0.19± .03	.02
9.8± .5		0.25± .03	.02
10.2± .5		0.22± .03	.02
10.0± .7	0.19	0.24± .05	.02

TABLE 11. Results of analyses for depolarized spectra of picoline at -6° C.

The reorientation frequency was very nearly equal to that of pyridine at 10.0± 0.7 GHz while the coupling parameter was lower at 0.24± .05 . Even though the R's for both pyridine and picoline are subject to a large uncertainty, the drop in R from pyridine to picoline is outside of the error estimates and thus would appear to be real. This indicates that the addition of a methyl group to the aromatic ring results in a lower degree of coupling. However if the analyses are carried out again allowing for a parasitic line, spurious intensity is found (± 50%) and R is increased dramatically to 0.61± .08 . Thus according to the analyses with parasitic scattering allowed, the R for picoline (0.61) is *larger* than that of pyridine (0.5). Finally we note that an R of 0.6 for toulene at high pressure has been reported by Bucaro[51] though a tremendous amount of parasitic

light resulting from birefringence effects was present in the spectra.

Quinoline

Quinoline was the final liquid studied in this series of investigations. Spectra were obtained at 7.9° C. The large size and highly anisotropic shape of this molecule precludes it from being considered in a discussion of the results for the previously studied liquids. The purpose of this study was simply to try an confirm the findings of Frohlich and Posch[23] which indicated an extremely large value of the coupling parameter R. In addition it also serves as a final check on the present results since several independent measurements of the reorientational linewidth are available for comparison. A typical depolarized spectrum for quinoline is shown in figure 23. The large anisotropic polarizability of this molecule make it a strong depolarized scatterer and consequently the spectra are very well defined. This points out one of the reasons why many of the liquids studied to date have been large and highly anisotropic in nature. The spectra were allowed to be fit with a parasitic peak though only in a few cases was such a spurious peak evident. The fits did indicate a small amount of parasitic intensity for these cases while finding only insignificant amounts for the others. Results for R and Γ_{22} are given in table 12.

Depolarized Results for Quinoline

Γ_{22} (GHz)	$\kappa^2\nu_s$ (GHz)	R	$\frac{\kappa^2\nu_s}{\Gamma_{22}}$
2.75± .03	0.69± .05	0.60± .02	0.25
2.75± .03	0.73± .05	0.55± .02	0.26
2.80± .03	0.70± .05	0.56± .02	0.25
2.77± .03	0.66± .05	0.58± .02	0.24
2.76± .04	0.73± .05	0.55± .02	0.26
2.71± .04	0.74± .05	0.57± .02	0.27
2.76± .03	0.70± .05	0.57± .02	0.25
2.76± .04	0.71± .05	0.57± .02	0.25

TABLE 12. Results of analyses for depolarized spectra of quinoline at 7.9° C

Fitted values of $\kappa^2\nu_s$ are all in agreement with the calculated value of 0.68 GHz[45] to within experimental error. The average result of 0.71 is about 4% high. Frohlich

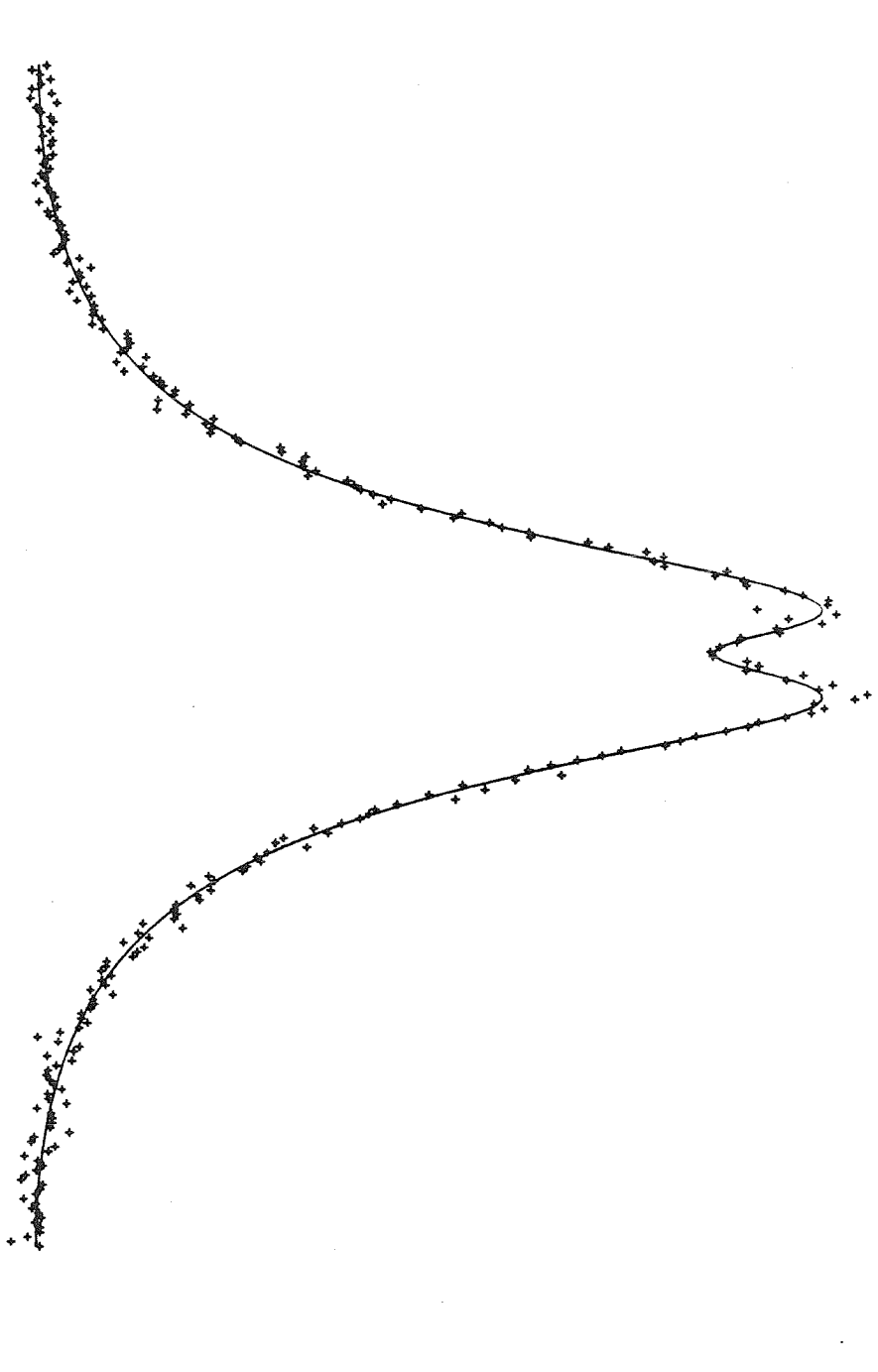

FIGURE 23. Depolarized spectrum of quinoline at 7.9°C and a scattering angle of 90°.

found $\kappa^2\nu_s$ to be anywhere from 2.3% to 32% higher than the calculated result with most being around 6% high. Our Γ_{22} of 2.76± .04 GHz is in substantial agreement with both Frohlich's result of 2.8± 0.1 GHz and Stegeman's[3] result of 2.87± .08 GHz . However our measurement of R gave an average value of 0.57± .02 which is significantly lower than Frohlich's reported result of 0.64± .03 No explanation is offered for this disprepancy but it should be noted that R=0.57 agrees with other high R results (0.55) for aniline and nitrobenzene.

Discussion of Results

In table 13 a compilation of the previous results for R are given along with the number density, molecular volume, and dipole moment for each molecule studied. Results for benzonitile and nitrobenzene are also included here since they are monosubstituted benzene derivatives. For this same reason the results for quinoline have been omitted. The molecular volumes are constructed from a Van der Waals model of transferable atomic radii[81]. The ρV_m product given in table 13 is the ratio of the volume occupied by the molecules to the total volume of the system an hence reflects the the degree of packing. This has been suggested by Alms[20] to be an important factor in determining R. The primary result of this investigation can be understood from table 13.

The size and shape of all the molecules in table 13 are similar and the degree of packing, ρV_m, varies by only about 6%. Yet the variation in R is as large as has been observed for all molecules studied to date (see table 1) if the R=0.64 result for quinoline is ignored. Recall that the results of this investigation indicate an R of 0.57 for quinoline. Note that molecules for which R has been determined include those with such diverse size and shapes as carbon disulfide, pyridine, triphenyl phosphite, and the liquid crystal MBBA. If size and shape considerations alone determined R, then one would certainly expect to see a much more limited

Molecule	Number Density, ρ ($\frac{\text{molecules}}{\text{cm}^3} \times 10^{21}$)	Molecular Volume, V_m[81] (Å^3)	Packing Fraction, ρV_m	Dipole Moment, μ[80] (debyes)	R
Aniline	6.71	93	0.624	1.54	0.55± .02
Benzylamine	5.68	110	0.625	1.3	0.45± .03
Phenol	6.78	87	0.590	1.55	0.27± .03
Benzenethiol	6.05	101	0.611	1.2	0.36± .04
Bromobenzene	5.86	100	0.586	1.75	0.30± .04
Pyridine	7.85	78	0.612	2.2	0.35± .05
Picoline	6.36	96	0.611	2.7	0.24± .05
Benzonitrile	5.90	101	0.596	4.1	0.37± .02
Nitrobenzene	5.89	104	0.613	4.2	0.55± .03

TABLE 13. Comparison of selected molecular parameters for some small aromatic molecules.

range for the liquids in table 13. This suggests that steric forces are not primarily responsible for the observed variation in R. There is also no correlation of R with the limited change in ρV_m in agreement with Frohlich's result indicating a lack of density dependence for R. This reinforces the conclusion that steric forces are not a dominant factor governing the degree of rotational-translational coupling. Thus it appears that nonsteric forces may play an important role in determining the behaviour of this coupling as suggested by Frohlich. This possibility is considered next.

The most obvious nonsteric force would be a dipolar interaction. However, from table 13 it can be seen that there is no clear correlation between μ (or μ^2) and R . Nitrobenzene and aniline both show a high degree of coupling with R=0.55 and yet have widely different dipole moments of 4.2 D and 1.54 D respectively. If electrostatic forces do influence the magnitude of R, then it must be through a different mechanism than the simple dipolar interaction (μ^2). A possible clue as to the seemingly unusual behaviour of R might be found not in the dipole itself, but in the change in dipole moment from the aliphatic compound (CH_3–R) to the phynyl compound (C_6H_5–R). This is referred to as the mesomeric moment[52]. A comparison of dipole moments between the benzene derivatives in table 13 and their aliphatic analogs is given in table 14.

Substituent X	Dipole Moment (debyes) CH_3X	PhX
$-NH_2$	1.3	1.54
$-CH_2NH_2$	1.2	1.3
-OH	1.7	1.55
-SH	1.4	1.2
-Br	1.8	1.75
-CN	4.0	4.1
$-NO_2$	3.5	4.25

TABLE 14. Comparison of dipoles for some monosubstituted benzene derivatives and their aliphatic analogs.

This change in dipole moment has been suggested by Bertucci et. al.[53] as an explanation of orientational pair correlation (see eqn. 4.43) in monosubstituted

benzene derivatives. The notion that interactions which affect the orientational pair correlation (OPC) in a liquid might also influence the degree of rotational-translational as measured by R is certainly reasonable. Consider nitrobenzene which has a very large R and was also found to have a high degree of orientational correlation by Bertucci. The nitro group is a powerful electron-withdrawing substituent and thus nitrobenzene has the following resonance structures:

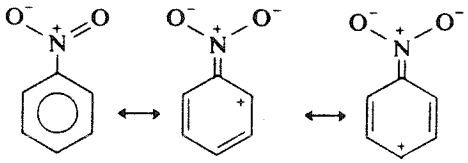

I II III

The increase in dipole moment from CH_3NO_2 to $C_6H_5NO_2$ can be taken as evidence for the strong participation of these formal structures in determining the overall electronic charge distribution in nitrobenzene. Bertucci suggests that structures such as (III) could lead to anti-parallel alignment of neighboring molecules with respect to their C_{2V} axes.

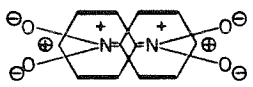

IV

This arrangment puts the formal charges in a favorable position and the electron deficient nitrogen opposite the electron rich π system. The short-range electrostatic interactions leading to (IV) would of course have to compete with short-range steric forces in order to reach an equilibrium liquid structure. Bertucci suggests that structures such as (IV), with charge asymmetry affecting a significant portion of the molecule, produce the large OPC. The physical interpretation of the static OPC is readily understandable and a tendency for parallel or anti-parallel alignment of the molecules is certain to produce a large OPC. A physical interpretation of the dynamic coupling between shear modes

and orientation is not nearly as transparent. However we do suggest that the same structures might also increase the dynamic coupling between shear stress and angular momentum of the molecules and thus lead to a large R. Bertucci also points out that while benzonitrile has a large dipole nearly equal to nitrobenzene, it increases only slightly from its aliphatic analog CH_3CN. The nitrile group is known to be a weaker electron-withdrawing group than $-NO_2$ and the small mesomeric moment reflects this. Thus resonance forms affecting a large portion of the molecule are not expected to be important here. Bertucci's studies indicate an OPC for benzonitrile much less than nitrobenzene in support of the above argument. R has also been determined for benzonitrile and found to be 0.37± .02 . This is significantly less than the R of 0.55 for nitrobenzene and reinforces our contention that orientational-translational coupling is also dependent upon these resonance considerations.

As another example consider aniline. The amine group is a powerful electron-donator as an aromatic substituent. Thus the following resonance structures can be constructed:

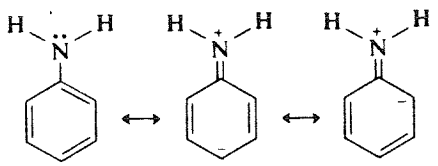

The inductive effect of the amine group is quite weak here since the bonding orbitals of the amino nitrogen are similar in electronegativity to the attached aromatic carbon. The incease in in dipole moment from CH_3NH_2 to $C_6H_5NH_2$ is evidence that the above resonance forms participate very strongly in determining the charge asymmetry. The resonance effects must totally dominate the inductive effect actually reversing the direction of the dipole moment in the aromatic compound from that in the aliphatic compound and increasing its magnitude. Short-range electrostatic interactions could again lead to forms

analogous to (IV) for nitrobenzene. From the preceeding discussion a large R and OPC would be expected for aniline and indeed our results indicate an R of 0.55 . The OPC has not been determined for aniline.

Benzylamine presents a good test of this idea since moving the amine group further from the aromatic ring should diminish the resonance effect. This appears to be correct since the dipole moment drops by .24 D . According to the above arguments the value of R should be lower and this is found to be the case with R=0.45 . The R of 0.30 for bromobenzene is expected since the electron-withrdawing efficacy of bromine is considered to be weak. This is apparent from the insignificant difference in dipole moments between the corresponding aromatic and aliphatic compounds. Benzenethiol's R of 0.36 is also explained by this type of argument. The small decrease in dipole moment from aliphatic to aromatic indicates that the thiol group is a weak electron donator as is generally thought to be the case. Thus resonance forms effective in producing a large R do not contribute strongly in benzenethiol.

An interesting inference can now be made with respect to pyridine and picoline. Pyridine has a dipole moment of 2.2 D due to the following resonance forms:

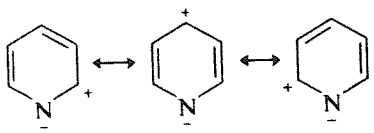

The addition of the electron-donating methyl group in the para position relative to the nitrogen leads to a large increase in dipole moment (2.7) over pyridine. The enhancement is attributed to the presence of the form :

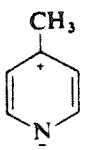

Following the arguments used above, it is reasonable to expect a large R for pyridine and an even larger R for picoline. The analysis, with parasitic light

allowed for, gave exactly this result with an R for pyridine of 0.5 and for picoline 0.61 . Analyses excluding any parasitic light yielded an R of 0.35 for pyridine and 0.24 for picoline. Recall the previous discussion of Searbys' results for pyridine where the I_{HH} measurement of R indicated a value of 0.7± .1 and the I_{VH} result was 0.35± .05 . The possibility of parasitic light producing a low R in the I_{VH} spectrum was suggested. These molecules are both weak scatters with very low signal to noise ratios, small viscosities, and large reorientation frequencies. Is it possible that for such liquids, even weak spurious scattering interferes with the measurement of R? This question is very difficult to answer. There is certainly no system free of this parasitic light since the polarized scattering of the liquid is always present. Perhaps better experimental techniques would help to resolve this question. A careful I_{HH} study of picoline along with a re-examination of the I_{HH} spectrum of pyridine might be beneficial in this regard.

Obviously this type of reasoning with respect to electrostatic forces is heuristic in nature and exceptions can probably be found. While Frohlichs' high pressure findings and our own present results suggest that steric forces are not in general the dominant factor in determining R, they still cannot be totally ignored. It is conceivable that a favorable charge asymmetry might be negated by strong steric hinderance for large molecules or that steric forces due to several substituent groups might even prevent the correct intra-molecular alignment producing favorable resonance structures. However the present study does indicate that the details of the molecular electronic charge distribution are very important in determining the magnitude of collective rotational-translational coupling as measured by depolarized light scattering. The nature of the charge distribution is reflected, in general, by both the dipole moment and the difference in dipole moments between the aromatic and aliphatic analogs of the molecule.

PART II

INVESTIGATION OF THE COUPLING BETWEEN REORIENTATION AND LONGITUDINAL MODES IN THE BRILLOUIN SPECTRA OF LIQUIDS COMPOSED OF ANISOTROPIC MOLECULES

Chapter 6

INTRODUCTION

The nature of polarized scattering from condensed media has actually been understood for quite sometime. Brillouin[54](1914) realized that local density fluctuations could be considered as thermally excited sound waves[55] and reported the first consideration of the spectrum of light scattered by a liquid[56]. The exsistence of shifted Brillouin lines was confirmed experimentally by Gross[57] in 1930. A central or unshifted line was also observed and later attributed to entropy fluctuations by Landau and Placzek[58](1934). Subsequent work in light scattering was quite sparse until the introduction of the laser in the 1960's. Then, based upon an idea suggested by Landau, Mountain[59](1966) presented a complete description of the polarized spectrum of monatomic liquids using the linearized equations of hydrodynamics. The spectrum was assumed to arise from local density fluctuations and the dynamics of these fluctuations were described by hydrodynamic equations.

With the advent of the laser accurate measurements of shifts and linewidths could be made and experimental interest in the polarized spectrum was revived. Fleury and Boon[60] studied liquid argon and found agreement with Mountain's theory to within experimental error. However, for spherically symmetric molecules with structure, differences were noted. Stegeman and Stoicheff[61] investigated the spectrum of CCl_4 and found a new central line and a non-hydrodynamic wave vector dependence for the Brillouin lines. Mountain [62] accounted for these new features by allowing for the weak coupling of internal degrees of freedom to translational modes. This effect was rigorously introduced via a frequency dependent bulk viscosity [48]. The results of this modified theory were confirmed for several liquids, including CCl_4, undergoing apparent vibrational-translational relaxation processes[61,43,63]. The hydrodynamic theory

was also extended to binary solutions by Mountain and Deutch[64]. Lao, et. al.[65] confirmed their results with exacting studies of krypton-argon mixtures, while Gulari, et. al. [66] demonstrated that accurate measurements of binary diffusion coefficients and thermal conductivities could readily be obtained from the polarized spectrum.

Though hydrodynamic theories have proven to be very useful, they are limited to the description of conserved quantities coupled to those variables which can be rigorously included via frequency dependent transport coefficients. The continuum nature of these theories also restrict their validity to the low κ or long wavelength regime. From the point of view of light scattering, the latter restriction is of little concern since light scattering is inherently a low κ experiment. It is the limited ability to describe the dynamics of non-conserved quantities which presents the main liability of the hydrodynamic theory.

The molecular theory described in chapter 4 provides a rigorous method for deriving "generalized hydrodynamic" equations. With this theory it is possible to systematically couple any set of variables (symmetry allowed) which are slowly varying relative to all other variables. Using linear response theory[9], Selwyn and Oppenheim [67] derived the generalized hydrodynamic version of Mountain's orginal work and showed that in the limit of small κ the hydrodynamic result was recovered. Later Weinberg and Oppenheim[68] showed that the same could be done for the case of vibrational-translational relaxation. However, the real success of the microscopic theory came with the description of the depolarized spectrum of anisotropic molecules (see chapter 4). Shear modes were coupled to the orientational density (2-variable theory) to give the depolarized doublet spectrum observed experimentally. Keyes[69] realized that the orientational density could also be coupled to ordinary hydrodynamic variables to better describe the polarized spectrum of anisotropic molecules. Later Lipeles and Kivelson[70]

re-examined Keyes's work and found a slightly different result. In either case the effect of including this variable is to produce orientational relaxation in the shear viscosity. For symmetric tops the strength of this relaxation is just $R\nu_s$, where R is the same coupling parameter as measured in the depolarized spectrum. This is analogous to vibrational-translational relaxation in the bulk viscosity discussed previously, but has not been experimentally investigated.

The objective of the polarized studies conducted here was to investigate orientational relaxation in the Brillioun lines and attempt to confirm the results of the molecular theory. Since the coupling between longitudinal modes and reorientation is theoretically predicted to be the same as that between shear modes and reorientation, these studies should also provide a check on the internal consistency of the 2-variable depolarized theory and orientational relaxation in the Brillouin spectrum. Aniline and para-anisaldehyde were chosen for these studies due to their relatively strong relaxation strength and long relaxation time. In addition the depolarized spectrum of para-anisaldehyde had been previously studied and agreement with the 2-variable theory in the temperature range 6° C to 79° C was found to be excellent. Our own depolarized investigation of aniline also produced good agreement with 2-variable theory at the temperature of interest. This indicates that other relaxation processes manifested through the shear viscosity should not be important here. Thus the orientational theory alone should be adequate to describe shear relaxation in aniline and para-anisaldehyde.

Measurements of Brillioun shifts and linewidths over a wide range of scattering angles are reported for both liquids. From these data, the hypersonic velocity and attenuation of the longitudinal modes or thermal sound waves are calculated. The temporal attenuation of the thermal sound waves is then carefully examined in an attempt to verify the predicted κ dependence of the shear viscosity.

Chapter 7

THEORY OF POLARIZED LIGHT SCATTERING

The main purpose of this chapter will be to present the molecular theory of orientational relaxation in the polarized spectrum of optically anisotropic molecules. However, in presenting this theory, reference is frequently made to the classical hydrodynamic result for polarized scattering from simple fluids. Thus the hydrodynamic theory will also be discussed briefly. Furthermore, since molecular relaxation phenomena can occur via different mechanisms and simultaneously with orientational relaxation, a simple modification of the basic hydrodynamic theory is discussed which accounts for the relaxation of internal degrees of freedom.

Hydrodynamic Theory of Polarized Scattering

The simplest theory for the polarized spectrum of scattered light in a neat liquid is due to Mountain[59]. He calculated the spectrum for a monatomic fluid using the linearized equations of hydrodynamics. From a continuum point of view, the polarized spectrum, $I_{VV}(\kappa, \omega)$, depends upon the autocorrelation function of dielectric fluctuations (eqn. 2.7). For spherically symmetric molecules, the fluctuating part of the dielectric tensor will have no off-diagonal components (isotropic fluctuations) and from equation (2.6),

$$\delta\varepsilon(\vec{r},t) = \varepsilon_0 \mathbf{I} + \delta\varepsilon(\vec{r},t)\,\mathbf{I} \tag{7.1}$$

Thus the polarized spectrum is produced by scalar fluctuations in the dielectric constant, i.e. $\delta\varepsilon_{VV} = \delta\varepsilon(\vec{r},t)$. Assuming small fluctuations and local equilibrium, $\delta\varepsilon(\vec{r},t)$ can be expanded to first order in density and temperature fluctuations

$$\delta\varepsilon(\vec{r},t) = \left[\frac{\partial\varepsilon}{\partial\rho}\right]_T \delta\rho(\vec{r},t) + \left[\frac{\partial\varepsilon}{\partial T}\right]_\rho \delta T(\vec{r},t) \tag{7.2}$$

Ignoring the terms in $\left[\frac{\partial \varepsilon}{\partial T}\right]_\rho$, since this derivative has been found to be very small, the polarized spectrum becomes

$$I_{vv}(\vec{\kappa}, \omega) \propto < \delta\rho^*(\vec{\kappa}), \delta\rho(\vec{\kappa}, \omega)> \tag{7.4}$$

Thus the polarized spectrum is determined by the autocorrelation function of the Fourier components of density fluctuations. Note that one could have taken the polarizability density tensor as the direct source of scattered light, as is done in molecular theories, but it reduces to the number density for spherically symmetric molecules. Hydrodynamic equations, linearized in the fluctuating quantities, are used to describe the time dependence of the density fluctuations in equation (7.4).

$$\frac{\partial \rho_1}{\partial t} + \rho_0 \psi_1 = 0 \tag{7.5a}$$

$$\frac{\partial \psi_1}{\partial t} + \frac{C_0^2}{\gamma \rho_0} \nabla^2 \rho_1 + \frac{\beta C_0^2}{\gamma} \nabla^2 T_1 - \left[\frac{\eta_v + \frac{4}{3}\eta_s}{\rho_0}\right] \nabla^2 \psi_1 = 0 \tag{7.5b}$$

$$\frac{\partial T_1}{\partial t} - \frac{\gamma - 1}{\beta \rho_0} \frac{\partial \rho_1}{\partial t} - \frac{\lambda}{\rho_0 C_v} \nabla^2 T_1 = 0 \tag{7.5c}$$

where : $\psi_1 = \nabla \cdot \vec{v}_1$

$$\gamma = \frac{C_p}{C_v}$$

In the above equations, fluctuating quantities are indicated with a subscript 1 and equilibrium values by subscript 0. The terms η_v and η_s represent the bulk and shear viscosities, respectively; λ and β are the thermal conductivity and expansion coefficient; C_0 is the low frequency (adiabatic) speed of sound. ψ_1 represents a compressional or longitudinal disturbance. Note that once again local equilibrium has been invoked to express pressure and entropy fluctuations in terms of density and temperature. It is apparent from the energy equation

above that even though temperature fluctuations do not directly contribute to the spectrum, they do couple to density fluctuations and thus indirectly affect the spectrum.

In order to obtain the required autocorrelation function of the density, the above equations are Laplace transformed in time and Fourier transformed in space. The transformed fluctuations are defined by

$$\tilde{A}_1(\vec{\kappa},s) = \int_0^\infty dt\ e^{-st} \int_v d\vec{r}\ e^{i\vec{\kappa}\cdot\vec{r}}\, A_1(\vec{r},t) \tag{7.6}$$

This leads to the following transformed set of equations:

$$\begin{bmatrix} s & 0 & 0 \\ \dfrac{C_0\kappa^2}{\gamma\rho_0} & s+b_0\kappa^2 & \dfrac{-\beta C_0\kappa^2}{\gamma} \\ \dfrac{(1-\gamma)s}{\beta\rho_0} & 0 & s+\dfrac{\lambda\kappa^2}{\rho_0 C_V} \end{bmatrix} \begin{bmatrix} \tilde{\rho}_1(\kappa,s) \\ \tilde{\psi}_1(\kappa,s) \\ \tilde{T}_1(\kappa,s) \end{bmatrix} = \begin{bmatrix} 1 & 0 & 0 \\ 0 & 1 & 0 \\ -\dfrac{(1-\gamma)}{\beta\rho_0} & 0 & 1 \end{bmatrix} \begin{bmatrix} \rho_1(\kappa) \\ \psi_1(\kappa) \\ T_1(\kappa) \end{bmatrix} \tag{7.7}$$

where $b_0 = \dfrac{\eta_v + \frac{4}{3}\eta_s}{\rho_0}$.

More concisely we have

$$\tilde{\mathbf{F}}(\kappa,s)\cdot\tilde{\vec{A}}_1(\kappa,s) = \mathbf{N}(\kappa)\cdot\vec{A}_1(\kappa) \tag{7.8}$$

Since correlation functions are of interest here, the ensemble average of equation (7.8) with $\vec{A}^+(\kappa)$ is taken, yielding

$$\langle \tilde{\vec{A}}_1(\kappa,s)\vec{A}_1^+(\kappa)\rangle = \tilde{\mathbf{F}}^{-1}(\kappa,s)\cdot\mathbf{N}(\kappa)\cdot\langle |\vec{A}_1(\kappa)|^2\rangle \tag{7.9}$$

The static correlation matrix, $\langle |\vec{A}_1(\kappa)|^2\rangle$, is diagonal since all cross correlations with ψ_1 vanish due to time reversal symmetry and correlations between $\rho_1(\kappa)$ and $T_1(\kappa)$ are known to be zero from thermodynamic fluctuation theory[71].

The solution for the density autocorrelation function is found to be

$$<\tilde{\rho}_1(\kappa,s)\rho_1^*(\kappa)> = <|\rho_1(\kappa)|^2> \left[\frac{(s+b_0\kappa^2)(s+\frac{\lambda\kappa^2}{\rho_0 C_v})+(1-\frac{1}{\gamma})C_0^2\kappa^2}{|\tilde{\mathbf{F}}(\kappa,s)|}\right] \quad (7.10)$$

where $|\tilde{\mathbf{F}}(\kappa,s)|$ is the discriminant of $\tilde{\mathbf{F}}(\kappa,s)$. Since the autocorrelation function of the number density is a real, even function of time, the polarized spectrum can be calculated as follows

$$I_{vv}(\vec{\kappa},\omega) \propto \mathrm{Re} <\tilde{\rho}_1(\vec{\kappa},s=i\omega)\rho_1^*(\vec{\kappa})> \quad (7.11)$$

Direct evaluation of the above correlation function yields an exact but algebraically complicated spectrum. An approximate and much more enlightening solution can be found by using simple perturbation theory to obtain approximate roots of $|\tilde{\mathbf{F}}(\kappa,s)|$. The perturbation parameters are the small quantities

$$\frac{1}{\rho_0 C_v}\left[\frac{\lambda\kappa^2}{C_0\kappa}\right] \text{ and } \frac{b_0\kappa^2}{C_0\kappa}$$

This is an assumption that all lines in the spectrum are well separated or that the average decay time of any mode is much longer than the period of collective oscillations. Solving for the roots to first order in $\frac{\lambda\kappa^2}{\rho_0 C_v}$ and $b_0\kappa^2$ and then evaluating the spectrum yields

$$I(\kappa,\omega) \propto \left[1-\frac{1}{\gamma}\right]\frac{\frac{\lambda\kappa^2}{\rho_0 C_p}}{\omega^2+\left[\frac{\lambda\kappa^2}{\rho_0 C_p}\right]^2} + \frac{1}{\gamma}\left[\frac{\Gamma_B}{(\omega\pm\omega_B)^2+\Gamma_B^2} \pm \frac{1}{\gamma}A(\kappa)\frac{(\omega\pm\omega_B)}{(\omega\pm\omega_B)^2+\Gamma_B^2}\right] \quad (7.12)$$

where : $\omega_B = C_0\kappa$

$$\Gamma_B(\kappa) = \frac{1}{2}\left[\frac{\eta_v+\frac{4}{3}\eta_s}{\rho_0}+\frac{\lambda(\gamma-1)}{\rho_0 C_p}\right]\kappa^2$$

$$A(\kappa) = \frac{\kappa}{2C_0}\left[\frac{\eta_v+\frac{4}{3}\eta_s}{\rho_0}+\frac{3\lambda(\gamma-1)}{\rho_0 C_p}\right]$$

A typical spectrum as given by equation (7.12) is shown in figure 25 below.

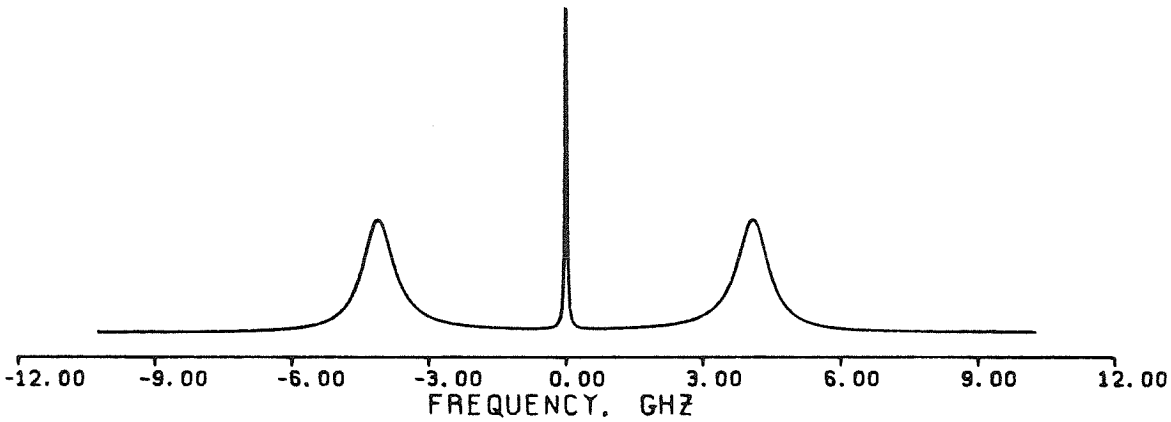

Figure 24. Theoretical polarized spectrum for a simple liquid.

The spectrum basically consists of a sharp central Lorentzian of half- width at half-height (HWHH), $\frac{\lambda\kappa^2}{\rho_0 C_p}$, and two wider Lorentzians shifted by $\pm C_0\kappa$ with HWHH's of Γ_B. The central line, often called the Rayleigh line, represents the decay of entropy fluctuations by thermal conduction. The shifted Lorentzians are called Brillouin lines and result from propagating pressure disturbances or thermal sound waves of frequency $\omega_B = C_0\kappa$ and which are damped in *time*. Thus $\frac{2\Gamma_B}{\kappa^2}$ is the temporal attenuation coefficient of these waves. The decay in time of the Brillouin modes should be contrasted with the *spatial* attenuation of mechanically driven waves in an acoustic experiment[72]. The asymmetric terms in equation (7.12) are also centered at $\pm\omega_B$ but generally do not distort the Brillouin lines significantly since their amplitude, $A(\kappa)$, is first order in the perturbation parameters. These terms arise because the fluctuations probed in a light scattering experiment are randomly driven by a thermal bath as opposed to freely decaying fluctuations[73]. Note the κ^2 dependence of the HWHH's for all the Lorentzians in equation (7.12). This is a general characteristic of the decay of a fluctuation in a conserved quantity.

The validity of equation (7.12) has been demonstrated by Boon and Fleury [60] for liquid argon. However, for spherically symmetric molecules with structure, internal degrees of freedom can couple to translational modes and significantly alter the spectrum. This is the case for CCl_4[61]. Here vibrational modes provide an alternate pathway or relaxation mechanism for the sound wave to dissipate energy. The effect of this additional coupling is to produce a new κ independent central line and alter the the κ dependence of the Brillouin lines. The non-hydrodynamic κ dependence is to be expected since vibrational energy will not be a conserved quantity. In order to take into account the coupling of internal degrees of freedom, Mountain[62] proposed a simple modification of the above theory. He incorporated a relaxing or frequency dependent bulk viscosity into the momentum equation. This was not an ad hoc addition but rather based upon Zwanzig's[48] rigorous statistical mechanical treatment of transport coefficients in the limit of weak coupling between translational and internal degrees of freedom. Zwanzig found for the bulk viscosity

$$\eta_v(\omega) = \eta_v^0 + \left[\frac{(C_p - C_v)C_I}{(C_v - C_I)C_p}\right]\rho_0 C_0^2 \int_0^\infty dt\ e^{-i\omega t}\varphi(t) \tag{7.13}$$

where: $\varphi(t) = \dfrac{<\delta E_I(0)\delta E_I(t)>}{<|\delta E_I(0)|^2>}$

In the above equations, E_I is the energy of internal modes and η_v^0 is the translational part (ω independent) of the bulk viscosity. Zwanzig found no corresponding frequency dependence in the shear viscosity. The correlation function, $\varphi(t)$, contains all the dynamics of the relaxation mechanism. If one assumes this to be a single exponential, $\varphi(t)=e^{\frac{-t}{\tau}}$, then

$$\eta_v(\omega) = \eta_v^0 + \frac{b_1}{1+i\omega\tau} \tag{7.14}$$

where: $b_1 = \left[\frac{(C_p - C_v)C_I}{(C_v - C_I)C_p}\right]\rho_0 C_0^2 \tau$

The generalization to a sum of exponential relaxations is straightforward [42]. Since $\eta_v(\omega)$ as given by equation (7.14) is a Laplace transform with s=iω, it is easily incorporated into the previous theory. The analysis is identical to the previous non-relaxing case except for increased algebraic complexity. Adding frequency dependence to a transport coefficient is analogous to including another coupled equation. Once again perturbation theory can be used to obtain an approximate description of the spectrum. The basic features are the same as given by equation (7.12) for the monatomic case except for a new central Lorentzian. However the detailed κ dependence is different. As observed experimentally, the velocity of the sound waves is no longer found to be constant at C_0 but rather to increase with κ. The velocity, $V(\kappa)$, is approximately given by

$$V(\kappa) = \frac{\omega_B}{\kappa} = \left\{\frac{1}{2}\left[C_\infty^2 - \frac{1}{(\kappa\tau)^2}\right] + \frac{1}{2}\left[\left[\left(\frac{1}{(\kappa\tau)^2} - C_\infty^2\right)^2 + \frac{4C_0^2}{(\kappa\tau)^2}\right]^{\frac{1}{2}}\right]\right\}^{\frac{1}{2}} \qquad (7.15)$$

In the limit $\kappa \to 0$, the velocity approaches the normal low-frequency value C_0. As $\kappa \to \infty$ the velocity increases to a limiting high frequency value of C_∞ defined by

$$b_1 = (C_\infty^2 - C_0^2)\tau$$

The HWHH of the Brillouin line is also no longer simply κ^2 dependent. An approximate expression for Γ_B is found to be

$$\Gamma_B(\kappa) = \frac{1}{2}\left[\frac{\eta_v + \frac{4}{3}\eta_s}{\rho_0} + \frac{\lambda}{\rho_0 C_P}\left[\gamma - \frac{C_0^2}{V^2}\right]\right]\kappa^2 + \frac{1}{2}\left[\frac{b_1\kappa^2}{1+(V\kappa\tau)^2}\right]\left[1 - \frac{\lambda\kappa^2\tau}{\rho_0 C_v}\right] \qquad (7.16)$$

As $\kappa \to 0$ ($\omega \to 0$) the temporal attenuation coefficient, $\frac{2\Gamma_B}{\kappa^2}$, becomes $b_0 + b_1$ and as $\kappa \to \infty$ it approaches b_0. The small thermal terms in these limits have been

ignored. Thus the relaxation strength or decrease in attenuation of the sound wave as ω_B passes through the relaxation region, $\omega_B\tau\sim 1$, is just b_1. The new central line observed experimentally is also predicted. It is a Lorentzian wth HWHH given by

$$\Gamma_R = \left(\frac{C_0^2}{V^2}\right)\tau^{-1} \tag{7.17}$$

The sharp central line due to entropy fluctuations is unchanged from the earlier results. It should also be noted that in the relaxation region the asymmetry in the Brillouin lines can become quite pronounced. For instance, in CCl_4 the amplitude of the asymmetric terms is about 25% of the amplitude of the Brillouin lines for $\omega_B\tau\sim 1$ and the result is an obviously skewed structure.

The above theory has been used to analyze relaxation in a number of molecular liquids. However CCl_4 seems to be the most extensively studied. Here the relaxation appears to be a vibrational-translational mechanism with all vibrational modes participating, i.e. $C_I=C_{vib}$, and a relaxation time of $\tau=6.5\times10^{-11}$sec. The same also appears to be the case for CS_2 with $C_I=C_{vib}$ and $\tau=1.8\times10^{-9}$sec. Weinberg and Oppenheim [68] point out that a single relaxation time vibrational-translational relaxation mechanism is not unrealistic since this would be the case if the vibrational modes equilibrate rapidly with each other relative to vibrational-translational equilibration. Thus if the vibrational-vibrational energy exchange cross section greatly exceeds the vibrational-translational cross section, as it should for many liquids, the relaxation of the complete manifold of vibrational modes can be described by a single vibrational energy density. However, counter examples do exist. Nichols, et.al.[63] examined benzene at 25° C and found that a 2-relaxation mechanism was needed to adequately describe the observed attenuation in the Brillouin lines. All vibrational modes except the lowest appeared to relax with $\tau_1=3.0\times10^{-10}$sec, while the lowest degenerate mode

relaxed with $\tau_2=3.6\times10^{-11}$sec. All the preceeding discussion on molecular relaxation phenomena has been concerned with thermal relaxation or those mechanisms arising from temperature variations induced by the disturbance of the sound wave. Mountain[74] has shown that structural relaxation produced by density variations can also be described by the above results (equ. 7.15 and 7.16) with only a redefinition of b_1 needed. In either case the relaxation in the sound wave attenuation is manifested by a frequency dependence or loss in the *bulk* viscosity only.

Molecular Theory of Polarized Scattering from Anisotropic Molecules

We now want to consider polarized scattering from molecules which are not spherically symmetric, i.e. optically anisotropic molecules. Unfortunately there is no rigorous method of modifying the hydrodynamic equations used previously to account for the anisotropic nature of the molecules. However, from the microscopic theory of depolarized scattering (chapter 4), it should be apparent that anisotropy can be accounted for within the Mori formalism. In depolarized scattering, optical anisotropy directly produces the scattered spectrum. For polarized scattering a different viewpoint is taken. Here orientation will be thought of as an additional variable which provides a more complete description of density fluctuations in a medium composed of anisotropic molecules[69]. In the Mori formalism the orientational density is therefore considered to be a "slow" variable which must be included in the set of other slow variables.

As in the depolarized theory, attention will be restricted to symmetric top molecules. The same scattering geometry will also be employed here (see fig. 11). Internal degrees of freedom will not be considered since these effects seem to be well described by the modified hydrodynamic theory of Mountain. We shall assume that any relaxation occurring in the bulk viscosity can be independently

accounted for using Mountain's results.

From a molecular point of view, the polarized spectrum is given by (see eqn. 2.9)

$$I_{VV}(\vec{\kappa},\omega) \propto \int_{-\infty}^{\infty} dt < \delta\alpha^{*}_{vv}(\vec{\kappa},0)\ \delta\alpha_{vv}(\vec{\kappa},t)> e^{-i\omega t} \tag{7.18}$$

In the scattering geometry of figure 11, $\delta\alpha_{vv}$ is simply

$$\delta\alpha_{vv}(\vec{\kappa},t) = \delta\alpha_{zz}(\vec{\kappa},t) \tag{7.19}$$

For symmetric top molecules $\delta\alpha_{zz}(\kappa,t)$ is given by

$$\delta\alpha_{zz}(\kappa,t) = <\alpha> \sum_j e^{i\kappa z_j(t)} + \beta\sum_j \left[u^j_z(t)u^j_z(t) - \frac{1}{3}\right] e^{i\kappa z_j(t)} \tag{7.20}$$

Or in terms of Wigner rotation functions

$$\delta\alpha_{zz}(\kappa,t) = <\alpha> \sum_j e^{i\kappa z_j(t)} + \frac{2\beta}{3}\sum_j D^2_{00}(\Psi_j(t)) e^{i\kappa z_j(t)} \tag{7.21}$$

Note that for spherically symmetric molecules β=0 and $\delta\alpha_{zz}$ reduces to the Fourier transform of the number density. In general $\delta\alpha_{zz}$ fluctuates due to both density and orientational fluctuations. Substituting equation (7.20) into (7.18) yields for the polarized spectrum

$$I_{VV}(\kappa,\omega) \propto \int_{-\infty}^{\infty} dt e^{-i\omega t}\left\{ <\alpha>^2 <\delta\rho^{*}(\kappa,0)\ \delta\rho(\kappa,t)> \ + \beta^2 <\delta Q^{*}_{zz}(\kappa,0)\delta Q_{zz}(\kappa,t)> \right\} \tag{7.22}$$

where: $\delta Q_{zz}(\kappa,t) = \sum_j \left[u^j_z(t)u^j_z(t) - \frac{1}{3}\right] e^{i\kappa z_j(t)}$

The fact that $\delta\rho$ and δQ_{zz} are orthogonal has been used in obtaining equation (7.22). The polarized spectrum is therefore composed of the normal isotropic contribution from density fluctuations and an anisotropic contribution from the orientational correlation function $<\delta Q^{*}_{zz}(\kappa)\delta Q_{zz}(\kappa,t)>$. This latter contribution will basically be a central Lorentzian with HWHH identical to that which appears

in the depolarized theory, namely Γ_{zz}. Of prime interest here is what effect orientation has on the density fluctuations.

In order to calculate the density-density correlation function using Mori theory, a set of "slow" variables must be chosen which hopefully is complete. Obviously the hydrodynamic quantities of momentum density and energy density should be in this set. Reflection symmetry indicates however that only the x-component of the momentum density can couple to the number density. Since in the assumed scattering geometry the scattering wave vector, κ, lies along the x-axis, this component represents a longitudinal mode. Now the question of orientational coupling must be addressed. Once again reflection symmetry allows the coupling of diagonal components of the polarizability density tensor to the longitudinal momentum. Since these components are not statistically independent but $\alpha_{xx}-\alpha_{yy}$ and $\alpha_{xx}+\alpha_{yy}$ are, the set of slow variables is taken to be

$$\vec{A} = \begin{bmatrix} \delta\rho(\kappa,t) \\ \delta P_x(\kappa,t) \\ \delta U(\kappa,t) \\ \delta\alpha_{xx+yy}(\kappa,t) \\ \delta\alpha_{xx-yy}(\kappa,t) \end{bmatrix} \tag{7.23}$$

Two simplifications are now made. First the energy density will be ignored since it does not couple to orientation for very small κ. Its contribution will be assumed to be the same as given by ordinary hydrodynamics. Secondly, the contribution of $\delta\alpha_{xx+yy}$ is much less than that of $\delta\alpha_{xx-yy}$ and therefore will also be ignored[6]. With these simplifications $\vec{A}$ becomes

$$\vec{A} = \begin{bmatrix} \delta\rho(\kappa,t) \\ \delta P_x(\kappa,t) \\ \delta\alpha_{xx-yy}(\kappa,t) \end{bmatrix} \tag{7.24}$$

The microscopic definitions are as follows:

$$A_1=\delta\rho(\kappa,t)=\sum_j e^{i\kappa x_j} \tag{7.25a}$$

$$A_2=\delta P_x(\kappa,t)=\sum_j p_x e^{i\kappa x_j} \tag{7.25b}$$

$$A_3=\delta\alpha_{xx-yy}(\kappa,t)=2\beta 6^{-\frac{1}{2}}\sum_j\left[D^2_{02}(\Psi_j)+D^2_{0-2}(\Psi_j)\right] e^{i\kappa x_j} \tag{7.25c}$$

The theory of Mori can now be applied and the number density autocorrelation function computed. This procedure has been carried out by Keyes[69] with a slight modification later proposed by Lipeles[70]. Since A_2 has different time reversal symmetry than A_1 and A_3, and as noted earlier, A_1 and A_3 are orthogonal, the static correlation matrix is diagonal

$$\mathbf{N}(\kappa) = \begin{bmatrix} N_{11} & 0 & 0 \\ 0 & N_{22} & 0 \\ 0 & 0 & N_{33} \end{bmatrix} \tag{7.26}$$

The elements of the frequency matrix are zero except for those which involve the coupling of A_1 and A_2 to the momentum density, A_3. This follows from time reversal symmetry. As in the depolarized case, explicit consideration of these elements shows that the coupling of orientation to momentum is zero. The remaining elements are easily evaluated since they represent static correlation functions between conserved quantities and their derivatives. Thus the frequency matrix is given by

$$\Omega(\kappa) = \begin{bmatrix} 0 & \frac{-i\kappa}{m} & 0 \\ -i\kappa m C_0^2 & 0 & 0 \\ 0 & 0 & 0 \end{bmatrix} \tag{7.27}$$

Since Ω_{12} and Ω_{21} must be odd in κ by inversion symmetry, they are evaluated only to first order in κ, higher order terms being neglected.

The relaxation matrix has the form

$$\Gamma = \begin{bmatrix} 0 & 0 & 0 \\ 0 & \kappa^2\Gamma''_{22} & \kappa\Gamma'_{23} \\ 0 & \kappa\Gamma'_{32} & \Gamma_{33} \end{bmatrix} \tag{7.28}$$

where the low-κ dependence has been factored out. The primed quantities are constants as $\kappa \to 0$. Once again inversion symmetry requires that the Γ_{23} and Γ_{32} terms be odd in κ and the diagonal elements be even. The fact that the Γ_{22} term goes as κ^2 in the low κ limit follows from the linear κ dependence of the random force of momentum. The terms involving density vanish because the random force of the density at t=0 is zero.

Combining the above results, the transport matrix is found to be

$$\mathbf{Z}^{-1}(\kappa,s) = \begin{bmatrix} s & \frac{-i\kappa}{m} & 0 \\ -i\kappa m C_0^2 & s+\kappa^2\Gamma''_{22} & i\kappa\Gamma'_{23} \\ 0 & i\kappa\Gamma'_{32} & s+\Gamma_{33} \end{bmatrix}^{-1} \tag{7.29}$$

Lipeles defines a coupling parameter, R_{cp}, between longitudinal waves and orientation by

$$R_{cp} = -\frac{\Gamma'_{23}\Gamma'_{32}}{\nu_s\Gamma_{33}} = \frac{N_{33}|\Gamma'_{23}|^2}{N_{22}\nu_s\Gamma_{33}} \tag{7.30}$$

This is strictly analogous to the coupling of shear modes and orientation in the depolarized theory. He then proceeds to demonstrate that in an isotropic medium $R_{cp}=R_{sh}$ and $\Gamma_{33}=\Gamma_{sh}$ where R_{sh} and Γ_{sh} are the coupling parameter and reorientation frequency found in depolarized theory. Thus the coupling terms between longitudinal momentum and orientation in the relaxation matrix can be rewritten as

$$\Gamma'_{23} = \left[\frac{R\nu_s\Gamma N_{22}}{N_{33}}\right]^{\frac{1}{2}} \tag{7.31a}$$

$$\Gamma'_{32} = \left[\frac{R\nu_s\Gamma N_{33}}{N_{22}}\right]^{\frac{1}{2}} \tag{7.31b}$$

where $R=R_{cp}=R_{sh}$ and $\Gamma=\Gamma_{33}=\Gamma_{sh}$. Lipeles writes the Γ_{22}'' term as $\frac{4}{3}\nu_s(1-R)+\nu_v$. This follows from the observation that Γ_{22}'' can be written as

$$\Gamma''_{22} = <\sigma_{xx}(t)\sigma_{xx}(0)>_Q = \frac{4}{3}<\sigma_{xy}(t)\sigma_{xy}(0)>_Q + <\sigma(t)\sigma(0)>_Q \tag{7.32}$$

where $\boldsymbol{\sigma}$ is the microscopic stress tensor and $\sigma=\frac{1}{3}Tr\ \boldsymbol{\sigma}$. The subscript Q indicates that the time dependence is projected, i.e. e^{iQLt}. The quantity $<\sigma_{xy}(t)\sigma_{xy}(0)>$ is the shear relaxation term in the depolarized theory, i.e. Γ_{11}. This has the form $\nu_s(1-R)$ which was set by the requirement that the lowest eigenvalue of the depolarized transport matrix be the same as predicted be hydrodynamics, namely $\kappa^2\nu_s$. The last term in equation (7.32) is just the bulk viscosity. Thus it follows that Γ''_{22} has the form indicated above.

The transport matrix can now be writtten as

$$\mathbf{Z}^{-1}(\kappa,s) = \begin{bmatrix} s & \frac{-i\kappa}{m} & 0 \\ -i\kappa m C_0^2 & s+\kappa^2\left[\frac{4}{3}\nu_s(1-R)+\nu_v\right] & i\kappa\left[\frac{R\nu_s\Gamma N_{22}}{N_{33}}\right]^{\frac{1}{2}} \\ 0 & i\kappa\left[\frac{R\nu_s\Gamma N_{33}}{N_{22}}\right]^{\frac{1}{2}} & s+\Gamma \end{bmatrix}^{-1} \tag{7.33}$$

The matrix of correlation functions is given by equation (4.22). We of course want the density-density correlation function, C_{11}. This is found to be

$$\tilde{C}_{11}(\kappa,s) = N_{11}(\kappa)\left[\frac{s^2+\left[\Gamma+\kappa^2\left[\frac{4}{3}\nu_s(1-R)+\nu_v\right]\right]s+\Gamma\kappa^2\left[\nu_v+\frac{4}{3}\nu_s\left[1-\frac{R}{4}\right]\right]}{D(s)}\right] \quad (7.34)$$

D(s) is the discriminant of Z(s) and is given by

$$D(s) = s^3+\left[\kappa^2\left[\frac{4}{3}\nu_s(1-R)+\nu_v\right]+\Gamma\right]s^2+\left[\Gamma\kappa^2\left[\nu_v+\frac{4}{3}\nu_s\left[1-\frac{R}{4}\right]\right]+\kappa^2C_0^2\right]s+\kappa^2C_0^2\Gamma \quad (7.35)$$

Assuming $\kappa C_0 \sim \Gamma >> \kappa^2(\nu_v+\frac{4}{3}\nu_s)$, a perturbation solution for the roots of D(κ,s) yields

$$s_1 = \Gamma+\frac{\kappa^2R\nu_s}{1+\left[\frac{\kappa C_0}{\Gamma}\right]^2} \quad (7.36a)$$

$$s_2 = \pm i\kappa C_0\left[1+\frac{1}{2}\frac{\kappa^2R\nu_s\Gamma}{\Gamma^2+(C_0\kappa)^2}\right]-\frac{\kappa^2}{2}\left[\nu_v+\frac{4}{3}\nu_s-\frac{R\nu_s}{3}\left[\frac{\Gamma^2+4(\kappa C_0)^2}{\Gamma^2+(\kappa C_0)^2}\right]\right] \quad (7.36b)$$

The real root, S_1, represents a polarized relaxation line with a HWHH of approximately Γ; the κ-dependent term being very small. This polarized Lorentzian is analogous to the new central line found by Mountain for thermal relaxation (see eqn. 7.17). However here the new polarized line will be superimposed upon a more intense Lorentzian of precisely the same shape resulting from the $<\delta Q_{zz}(\kappa,\omega)\ \delta Q_{zz}^*(\kappa)>$ term in equation 7.22 . Thus it is probably not directly observable.

The complex roots represent the sound waves or Brillouin modes. The imaginary part gives the frequency while the real part gives the temporal attenuation. Thus the velocity and attenuation are

$$V(\kappa) = C_0\left[1+\frac{1}{2}\frac{\kappa^2R\nu_s\Gamma}{\Gamma^2+(C_0\kappa)^2}\right] \quad (7.37)$$

$$\frac{2\Gamma_B}{\kappa^2} = \left[\nu_v+\frac{4}{3}\nu_s-\frac{R\nu_s}{3}\left[\frac{\Gamma^2+4(\kappa C_0)^2}{\Gamma^2+(\kappa C_0)^2}\right]\right] \quad (7.38)$$

Therefore measurements of velocity and attenuation provide an alternate

method of obtaining the coupling parameter R. This also serves as an internal check of the orientational theory. Note the influence of the coupling between orientation and longitudinal momentum on both the velocity and the attenuation of the sound waves. It is strictly additive at this level of approximation and, as expected, non-hydrodynamic in nature. The following limiting conditions are found:

As $\kappa \to 0$ $\frac{\kappa C_0}{\Gamma} << 1$

$$\frac{2\Gamma_B(\kappa)}{\kappa^2} \to \frac{4}{3}\nu_s + \nu_v + \frac{R\nu_s}{3} \tag{7.39a}$$

$$V(\kappa) \to C_0 \tag{7.39b}$$

As $\kappa \to \infty$ $\frac{\kappa C_0}{\Gamma} >> 1$

$$\frac{2\Gamma_B(\kappa)}{\kappa^2} \to \frac{4}{3}\nu_s(1-R) + \nu_v \tag{7.40a}$$

$$V(\kappa) \to C_0\left[1 + \frac{R\nu_s\Gamma}{2C_0^2}\right] \tag{7.40b}$$

This is typical for a molecular relaxation process. As the frequency of the sound increases, passing through the relaxation region ($\kappa C_0 \sim \Gamma$), the velocity increases while the attenuation decreases. Here the loss in attenuation or relaxation strength is simply $R\nu_s$. Thus it is the orientational part of the shear viscosity that is relaxing. Recall that in the case of internal mode coupling the relaxation occurred through the bulk viscosity and the strength, b_1, involved the heat capacity of the internal modes.

Keyes also calculated the polarized spectrum for symmetric top molecules. However he required the lowest eigenvalue of the transport matrix, as $\kappa \to 0$, to be the same as that found from hydrodynamics, namely $\frac{\kappa^2}{2}\left[\frac{4}{3}\nu_s + \nu_v\right]$. This alters

the Γ''_{22} element of the transport matrix. Keyes finds this term to be

$$\Gamma_{22} = \frac{\kappa^2}{2}\left[\frac{4}{3}\nu_s - \nu_v - R\nu_s\right] \tag{7.41}$$

The only effect this has on the previous result for the spectrum is a small change in the form of $\Gamma_B(\kappa)$. The attenuation is now given by

$$\frac{2\Gamma_B}{\kappa^2} = \frac{4}{3}\nu_s + \nu_v - R\nu_s\left[\frac{(\kappa C_0)^2}{\Gamma^2 + (\kappa C_0)^2}\right] \tag{7.42}$$

Note that Keyes's and Lipeles' results differ only by a constant $\frac{R\nu_s}{3}$. The small κ limit of the attenuation is just the hydrodynamic result as required. The $\kappa \to 0$ limit is

$$\frac{2\Gamma_B(\kappa)}{\kappa^2} = \frac{4}{3}\nu_s - \nu_v - R\nu_s \tag{7.43}$$

Thus the relaxation strength is still $R\nu_s$.

In this chapter we have discussed two different relaxation processes. The first resulted from the coupling of internal degrees of freedom to longitudinal sound modes and was introduced via a frequency dependence in the bulk viscosity. The second process was much more specific in nature, resulting from the coupling of orientational motion to longitudinal sound modes. This mechanism was introduced using the rigorous microscopic theory of Mori and led to frequency or κ dependence in the shear viscosity. Other relaxation processes are also possible and can produce additional frequency dependence in the velocity and attenuation of the sound waves. The effect on sound propagation of any relaxation process will be qualitatively similar. Thus there is often a problem in attempting to separate the effects of the various possible mechanisms. This is especially true when the relaxation times are close. In the following chapter this is a very important consideration since experimental results are presented from which

we try to isolate orientational relaxation. Therefore a brief digression will be made here in order to discuss relaxation phenomena in general. Exhaustive treatments of molecular relaxation can be found in several texts on ultrasonics[75,76].

The Brillouin linewidth is given by the sum of contributions from the bulk and shear viscosities. The effect of a particular relaxation process is normally attributed to one of these transport coefficients via a frequency dependent contribution. Thus the viscosity coefficients are assumed to be a sum of frequency dependent terms representing various relaxation processes. In the theory discussed previously, the shear viscosity was partitioned into a a rotational component, $R\nu_s$, and a non-rotational component, $(1\text{-}R)\nu_s$. The rotational part is predicted to relax with a characteristic frequency given by Γ. The non-rotational contribution is assumed to relax at a much higher frequency. This assumption seems justified since the 2-variable theory of depolarized scattering (see chapter 4) gives a good description of the I_{VH} spectrum at moderate viscosities. Problems with the depolarized theory do occur at high viscosity (supercooled liquids) and this is an indication that non- rotational relaxation in the shear viscosity might be important.

We now turn our attention to the bulk viscosity. This transport coefficient can also be taken as the sum of two contributions: (1) a structural or translational relaxation, and (2) a thermal or specific heat relaxation. The first contribution is common in hydrogen bonded systems. In ultrasonic experiments it is characterized by $\frac{\partial \alpha}{\partial T} < 0$ and $\frac{\alpha_{exp}}{\alpha_{cl}}$ independent of temperature. Here α is the *spatial* attenuation coefficient and $\alpha_{exp}, \alpha_{cl}$ represent the experimental and classical (viscous) values. The second contribution was discussed earlier in the section on the relaxation of internal degrees of freedom. In thermal relaxation $\frac{\partial \alpha}{\partial T} > 0$ and

$\frac{\alpha_{exp}}{\alpha_{cl}}$ will be temperature dependent. A specific example of this is relaxation in the heat capacity of vibrational modes. This is a very common high frequency mechanism.

From the above discussion it would appear that orientational relaxation might be an observable process since it occurs as a more or less isolated mechanism in the shear viscosity. Of course interference by a strong relaxation in the bulk viscosity would present a problem in the analysis. Low frequency ultrasonic information might be useful in this case.

In chapter 8 the results of an angular dependent study of the polarized spectra of p-anisaldehyde and aniline are reported. For both liquids the coupling parameter, R, the shear viscosity, and the reorientation frequency, Γ, are such that the effect of orientational relaxation should be observable if the theory discussed above is correct and the effect not obscured by another much stronger relaxation process.

Chapter 8

RESULTS AND DISCUSSION

In this chapter the results of angular dependent studies of the polarized spectra of scattered light from para-anisaldehyde and aniline are reported. The primary goal of these investigations was to try and confirm the predictions of molecular theory in which the orientation of anisotropic molecules is coupled to longitudinal momentum. The principal effect of this orientational coupling is to produce a relaxation in the propagation of longitudinal modes. Thus attention will focus on measurements of velocity and attenuation in the thermal sound waves or Brillouin modes.

Para-Anisaldehyde

Para-anisaldehyde (p-A) was chosen as the subject of an initial polarized scattering study for the following reasons:

(1) The depolarized spectrum of p-A at $\Theta=90°$ had been carefully investigated earlier by Alms, et.al.[12] . The 2-variable theory of Anderson and Pecora[5] was shown to provide an excellent fit to the observed spectra for temperatures between 6° and 79°C . Thus it was expected that the only contribution to relaxation in the shear viscostiy should result from orientational coupling.

(2) The reorientation frequency, Γ, could easily be varied from 0.5 GHz to 4 GHz by changing the temperature from the melting point at 0°C to 79°C . Therefore the relaxation condition $\omega_B\tau \gtrsim 1$ could be satisfied in an angular study. This was a also a convenient temperature range to operate within.

(3) The measured value of the coupling parameter, R, was 0.42 . Examination of other values reported in the literature (see table 1) indicates that this is quite large. An R of 0.33 is about average.

(4) The viscosity was between approximately 6 cp and 10 cp for temperatures

under 15°C . Thus the orientational relaxation strength, $R\nu_s$, could be made large enough to be easily observed if not obscured by another relaxation process.

All spectra for p-A were obtained at T=8.5°C . At this temperature the shear viscosity was 7.6 cp and the density 1.134 gm/cc[12] . Depolarized spectra were also obtained at 8.5°C as both a check on Alms' results and our own spectrometer and data analysis procedure. Spectra were measured at scattering angles of 40° and 90° in order to check the κ dependence of th 2-variable theory. The spectrum and fit for Θ=40° is shown in figure 25. The reorientation frequency was determined to be 0.65± .02 GHz and 0.66± .02 GHz at Θ=40° and Θ=90° respectively, while R was measured to be 0.41± .02 and 0.43± .02 . These results are in good agreement with Alms, and the κ-independence is as predicted by theory. The fitted value of viscosity for both scattering angles was 7.7± 0.2 cp. This is in close agreement with the classically measured result of 7.6 cp .

The orientational relaxation strength as predicted by the theory in chapter 7 is 3.3 cp. Since the predicted relaxation frequency is Γ or 0.66 GHz, it was expected that the frequency range of the sound waves probed in an angular dependent study, normally about 1 to 10 GHz, should be strictly greater than Γ. Therefore the relaxation process should be very nearly complete at the higher Brillouin frequencies, i.e. $\frac{\kappa C_0}{\Gamma} > 1$. At every angle the experiment was repeated at least twice with two complete spectra (orders) obtained each time. The uncertainty in all measured quantities was estimated in this manner. The free spectral range for all spectra was 25.85 GHz and the finesse was normally about 90. Typical fitted spectra for aniline at 3 different scattering angles are shown in figures 26, 27, and 28 . All spectra were fit to two central Lorentzians and two shifted Lorentzians along with their respective asymmetry terms. One of the central Lorentzians represented the thermal Rayleigh line and parasitic scatter-

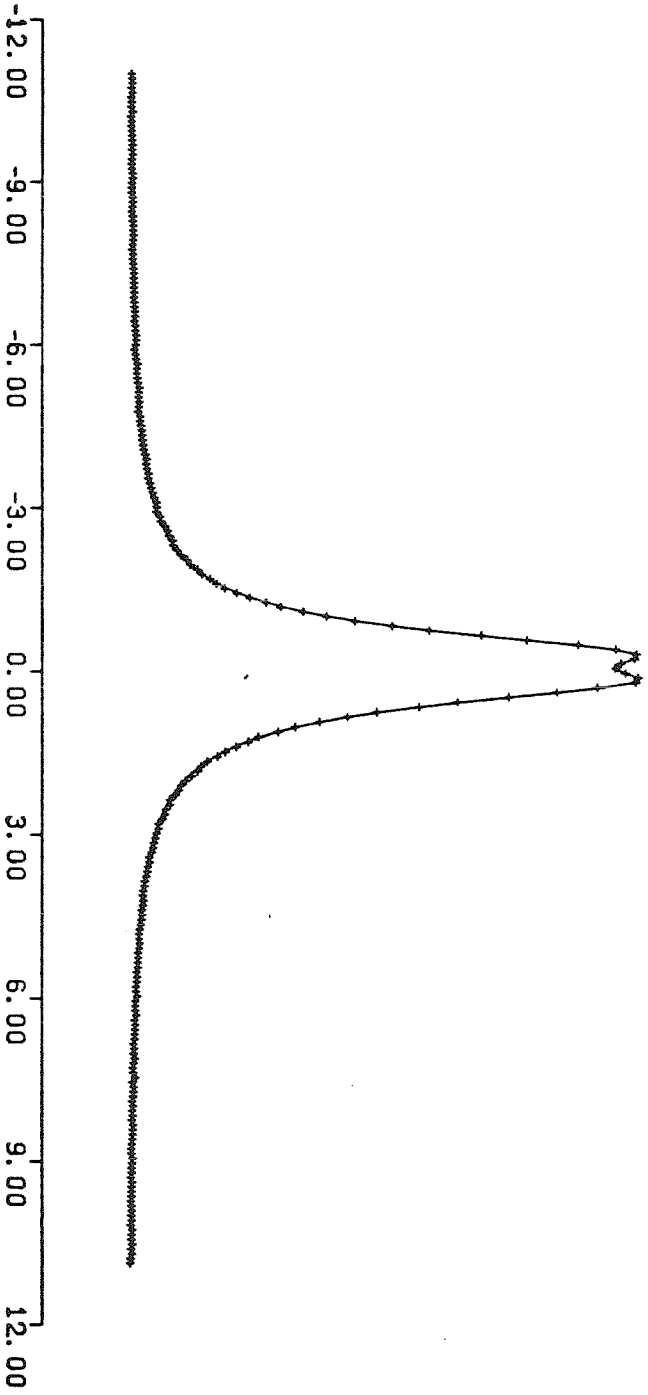

FIGURE 25. Depolarized spectrum of p-anisaldehyde at 8.5°C and a scattering angle of 40°.

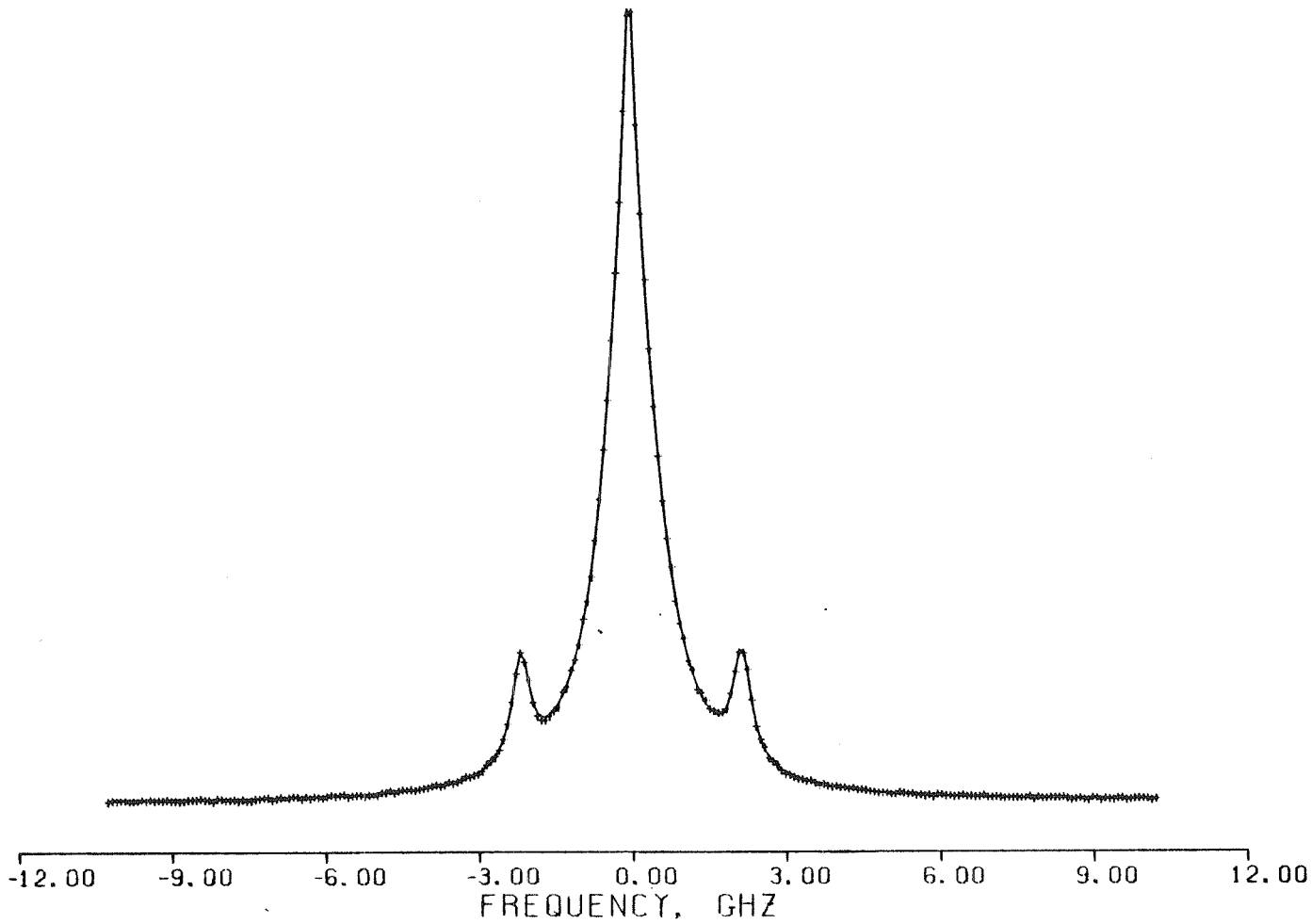

FIGURE 26. Polarized spectrum of p-anisaldehyde at 8.5°C and a scattering angle of 30°.

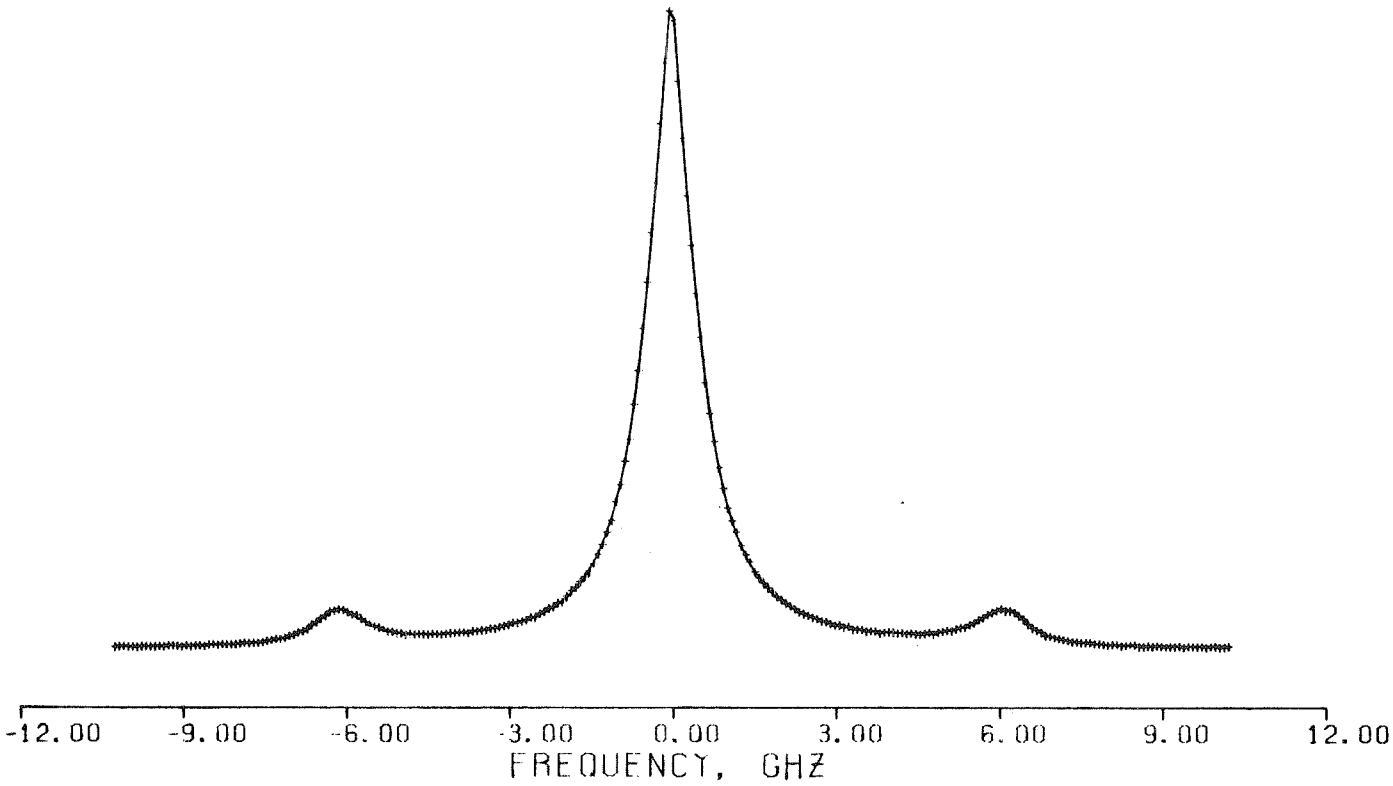

FIGURE 27. Polarized spectrum of p-anisaldehyde at 8.5°C and a scattering angle of 90°.

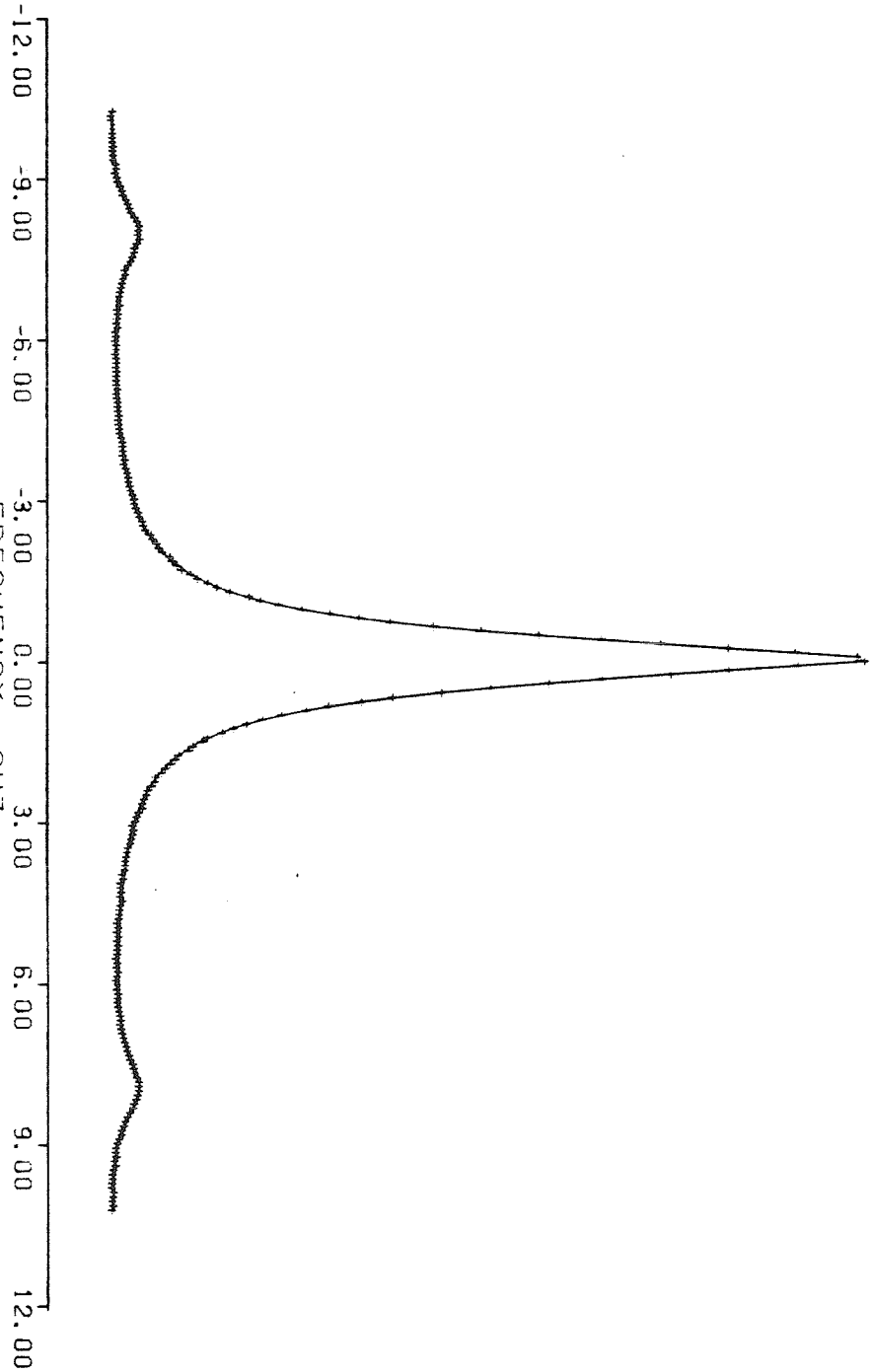

FIGURE 28. Polarized spectrum of p-anisaldehyde at 8.5°C and a scattering angle of 130°.

ing. The linewidth here was resolution limited and thus approximately the same as the instrument function linewidth (150 MHz). The other central component was used to account for the intense rotational line and weak polarized orientational relaxation line. The HWHH of this Lorentzian was found to be 0.65± .01 GHz and independent of scattering angle. This is in good agreement with Γ as measured in the depolarized spectra. As can seen from figures 26 through 28, the fits obtained in this manner are extremely good.

Analysis of the Brillouin lines is given in table 15. As the scattering angle was varied from 21.6° to 148°, the sound wave frequency, ω_B, increased from approximately 2 GHz to 11 GHz . The sound velocity rose from approximately 1616 m/s to 1733 m/s in this frequency or κ range. This is about a 7% dispersion in the velocity. A plot of sound velocity versus κ is shown in figure 29. Note that at the highest scattering angles the velocity appears to be leveling off at roughly 1733 m/s . The coupling of orientation to the sound modes theoretically should produce a velocity dispersion of less than 1% (see eqn. 7.37). The low frequency speed of sound, C_0, in equation (7.37) was assumed to be 1560 m/s since no ultrasonic data are available for p-A. Little justification can be offered for this assumption other than the fact that it is less than 1616 m/s as it certainly must be. It is clear that the observed velocity dispersion is much greater than that which could be attributed to orientational relaxation alone. This suggests the presence of another relaxation process.

We now turn our attention to the observed attentuation. A significant decrease with frequency or κ is seen here, with $\frac{2\Gamma_B}{\kappa^2}$ falling from approximately 13.5 cs to 6.2 cs . A plot of $\frac{2\Gamma_B}{\kappa^2}$ versus κ is shown in figure 30. The observed decrease in attenuation is much greater than that predicted to result from orientational relaxation (2.9 cs). In fact, for the frequency range probed here,

Brillouin Line Analysis for p-Anisaldehyde					
Angle (degrees)	Wave Vector ,κ (10^5 cm^{-1})	Frequency Shift, ω_B (GHz)	Velocity, V (m/sec)	Brillouin Half- width, Γ_B (MHz)	$\frac{2\Gamma_B}{\kappa^2}$ (cs)
21.6	0.77	1.98± .01	1616± 10	77± 8	16.4± 1.5
26.0	0.93	2.40± .01	1627± 9	101± 5	14.8± 1.0
30.0	1.07	2.77± .01	1632± 9	136± 7	15.0± 0.7
35.0	1.24	3.24± .01	1645± 8	176± 5	14.4± 0.4
40.0	1.41	3.70± .01	1650± 7	210± 5	13.3± 0.3
45.0	1.58	4.16± .01	1659± 7	249± 5	12.6± 0.2
50.0	1.74	4.60± .01	1660± 7	292± 6	12.2± 0.3
60.0	2.06	5.50± .01	1676± 6	376± 8	11.1± 0.3
70.0	2.36	6.35± .01	1689± 6	459± 7	10.3± 0.2
80.0	2.65	7.18± .02	1704± 8	541± 10	9.7± 0.2
90.0	2.91	7.94± .02	1713± 7	599± 12	8.9± 0.2
100.0	3.16	8.63± .02	1717± 5	681± 13	8.6± 0.2
105.0	3.27	8.96± .02	1722± 6	692± 14	8.1± 0.2
115.0	3.47	9.57± .02	1731± 7	704± 15	7.3± 0.1
130.0	3.73	10.30± .02	1734± 6	759± 16	6.8± 0.1
148.0	3.96	10.92± .02	1733± 6	770± 16	6.2± 0.1

TABLE 15. Analyses of the Brillouin lines of para-anisaldehyde at 8.5°C and over a wide range of scattering angles.

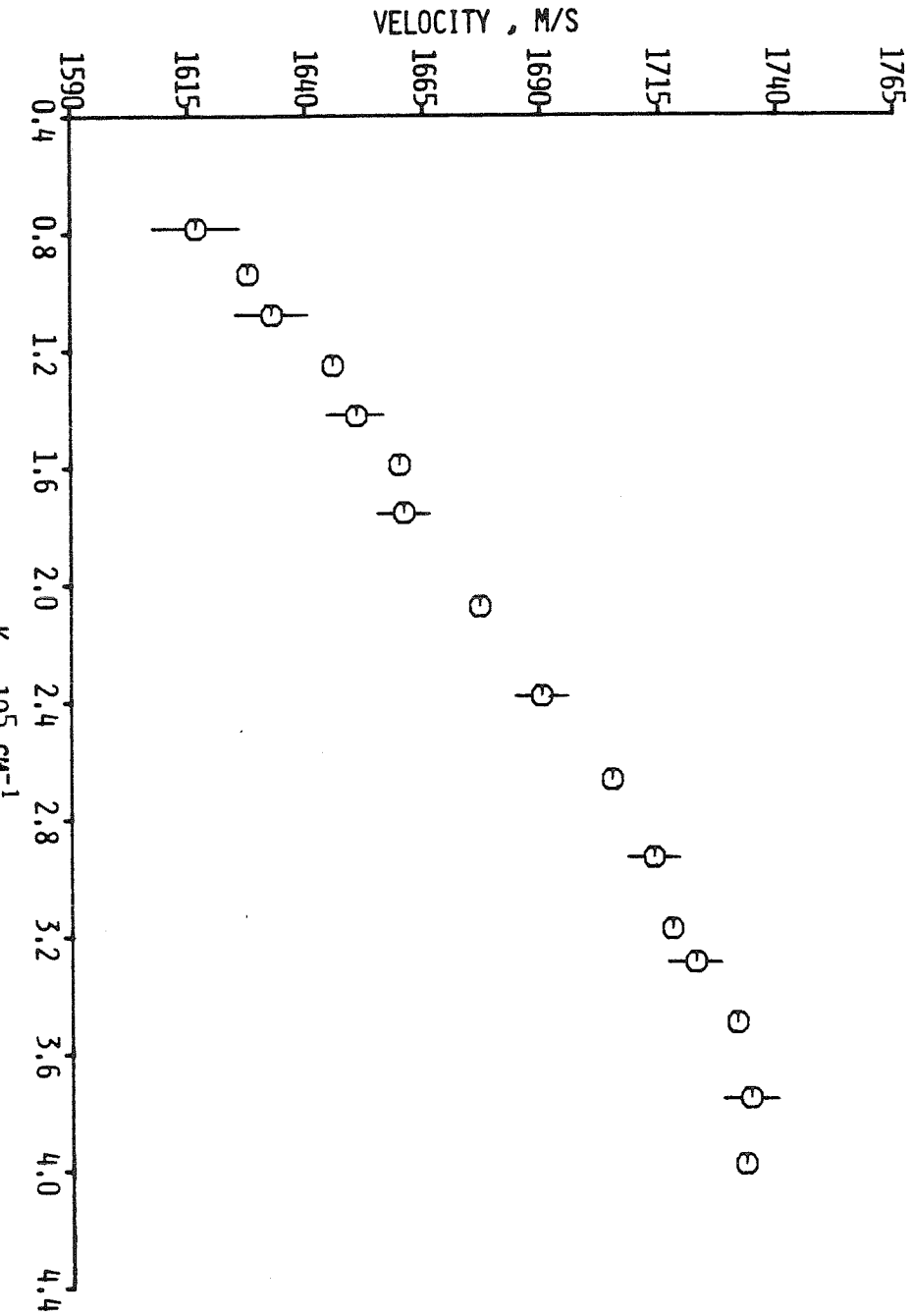

FIGURE 29. HYPERSONIC VELOCITY IN P-ANISALDEHYDE AT 8.5°C

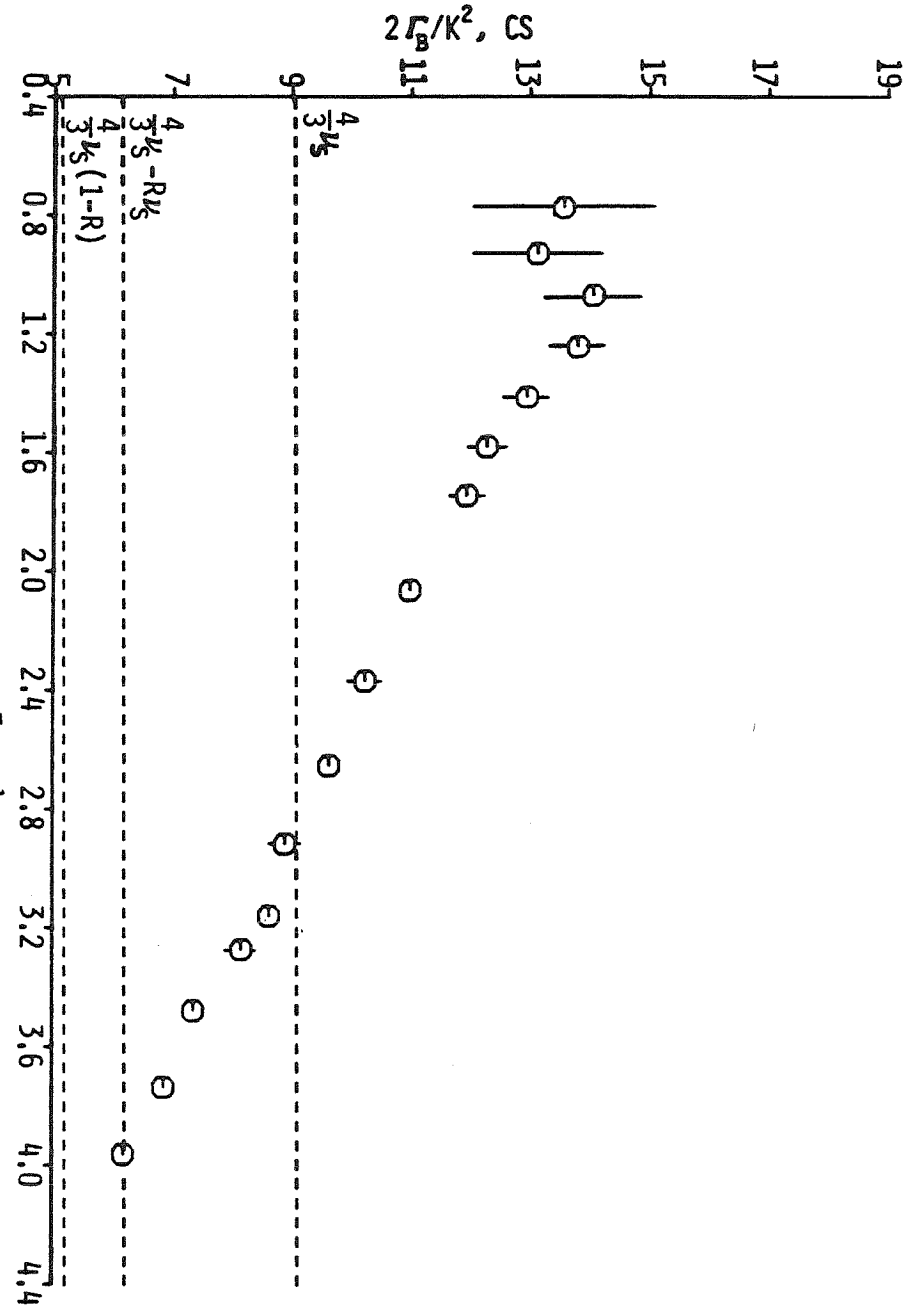

FIGURE 30. HYPERSONIC ATTENUATION IN P-ANISALDEHYDE AT 8.5°C

the drop in attenuation due to orientational coupling should be nearly complete. Thus the κ dependence of the attentuation appears to be almost totally due to another relaxation mechanism(s). This agrees with the velocity results. However, again referring to figure 31, it is clear that a relaxation in the shear viscosity has occurred or is occurring. All measurements of attenuation above a scattering angle of 90° are less than $\frac{4}{3}\nu_s$ and thus some contribution to the shear viscosity has been lost. It is interesting to note that the high frequency limit of the shear viscosity contribution to the attenuation as given by Keyes ($\frac{4}{3}\nu_s - R\nu_s$) is reached at the highest scattering angle and, based on the slope at this point, lower values seem likely. Thus Keyes's high frequency result appears to be in trouble here. Lipeles' high frequency limit of $\frac{4}{3}\nu_s(1-R)$ is about 1 cs lower and thus its validity remains an open question. However, if Lipeles theory is to be correct, then clearly the bulk viscosity must be almost completely relaxing. Both thermal and structural contributions to the bulk viscosity must be frozen out or lost from the overall attenuation above approximately 13 GHz.

As was previously noted, there are no available ultrasonic data for p-A. Thus the results presented here represent the only data on sound propagation in para-anisaldehyde of any kind or at any frequency. Without low frequency information on attenuation and velocity, any attempt to quantitatively analyze the present high frequency results will be extremely difficult and the results of such an exercise questionable. However, in an attempt to gain some qualitative insight into the possible high frequency relaxation mechanisms in p-A, a fit of the attenuation data was performed. The shear viscosity was assumed to be undergoing an orientational relaxation according to Lipeles, while a single relaxation time process was assumed for the bulk viscosity. Mountain's hydrodynamic theory for the bulk viscosity relaxation was utilized here (eqn. 7.16).

Once again 1560 m/s was taken as the low frequency speed of sound. Another assumption must be made with respect to ν_v^0. There is actually no way to determine this non-relaxing contribution to the bulk viscosity though it is often assumed to be roughly equivalent to the shear viscosity. Considering the nature of the analysis here, ignoring ν_v^0 altogether seems justified at this stage. With these assumptions for C_0 and ν_v^0, the number of fitted parameters is reduced to two: (1) the strength of the bulk viscosity relaxation and (2) its relaxation time. The result of this fitting procedure is shown in figure 31. The relaxation strength was found to be 10 cs and the relaxation time 2.8×10^{-11}sec. In general the fit is poor throughout the entire frequency range probed and becomes totally unsatisfactory at the higher frequencies. The main problem appears to be the high frequency limit. With this in mind the attenuation data were refit allowing ν_v^0 to be a free parameter. The result of this fit is given in figure 32. Note the vast improvement, especially at the higher frequencies. For this fit the relaxation strength was 16.4 cs with a relaxation time of 1.4×10^{-11}sec. However ν_v^0 was found to have an unrealistic negative value. In fact the high frequency contribution from the shear viscosity, $\frac{4}{3}\nu_s(1-R)$, was less than $|\nu_v^0|$ and thus the high frequency limit of the attenuation was found to be -2.3 cs . While the negative result for ν_v^0 is not realistic, the enormous improvement over the $\nu_v^0=0$ fit cannot be ignored. If the basic theory is correct then ν_v^0 must be greater than or equal to zero. The negative result indicates that the imposed high frequency limit of the attenuation is too large. This suggests that more than just the orientational contribution to the shear viscosity should be relaxing. In fact the negative attenuation predicted by the fit as $\omega\to\infty$ might possibly be construed as evidence that the shear viscosity is completely relaxing. Recall that non-orientational relaxation of the shear viscosity was initially ruled out on the basis of the success of the 2-variable theory in depolarized studies. The present

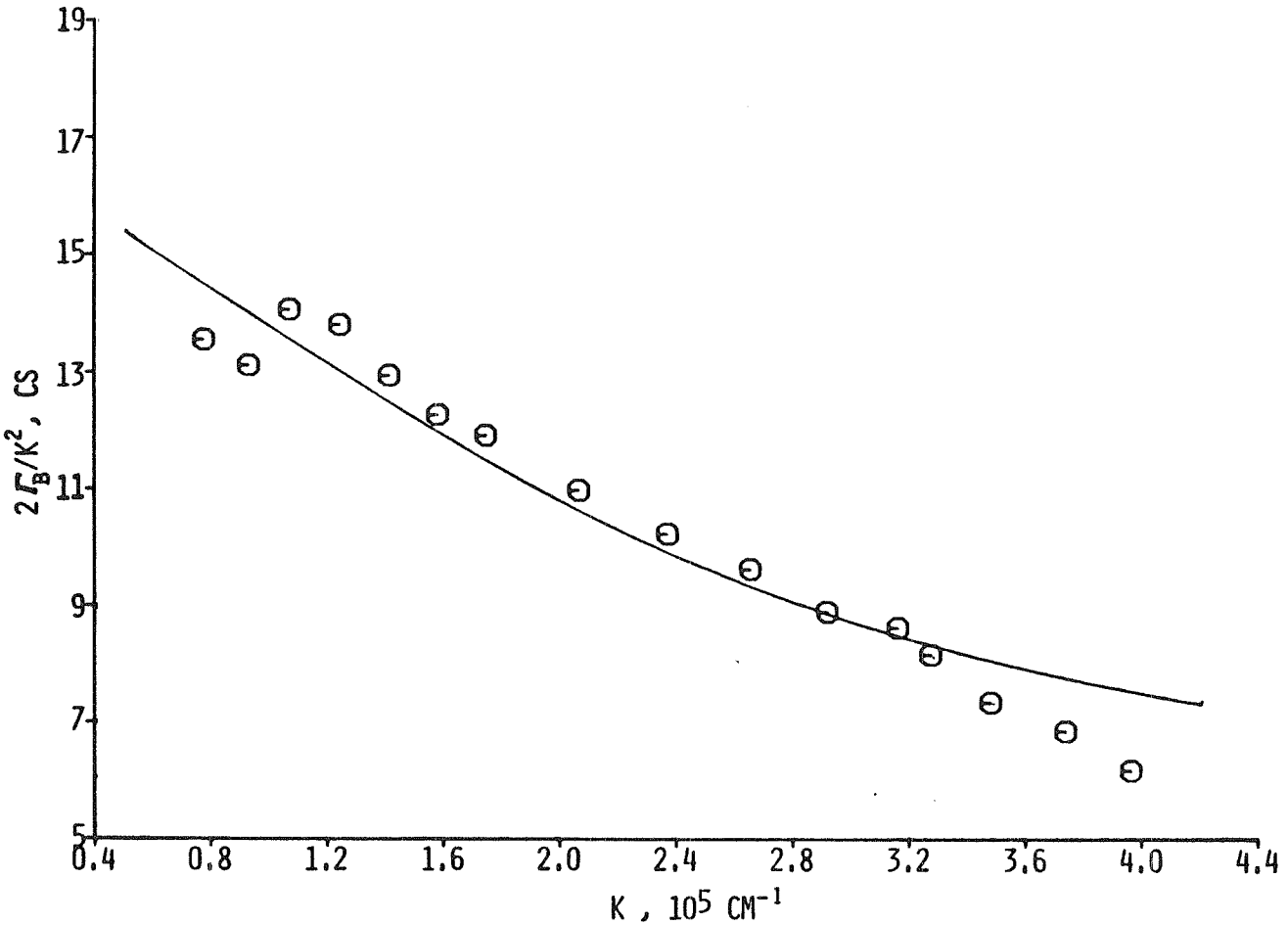

FIGURE 31. Fit of the attenuation results for p-anisaldehyde assuming orientational relaxation of the shear viscosity. The bulk viscosity is also taken to be relaxing with a single relaxation time and $\eta_V^0=0$.

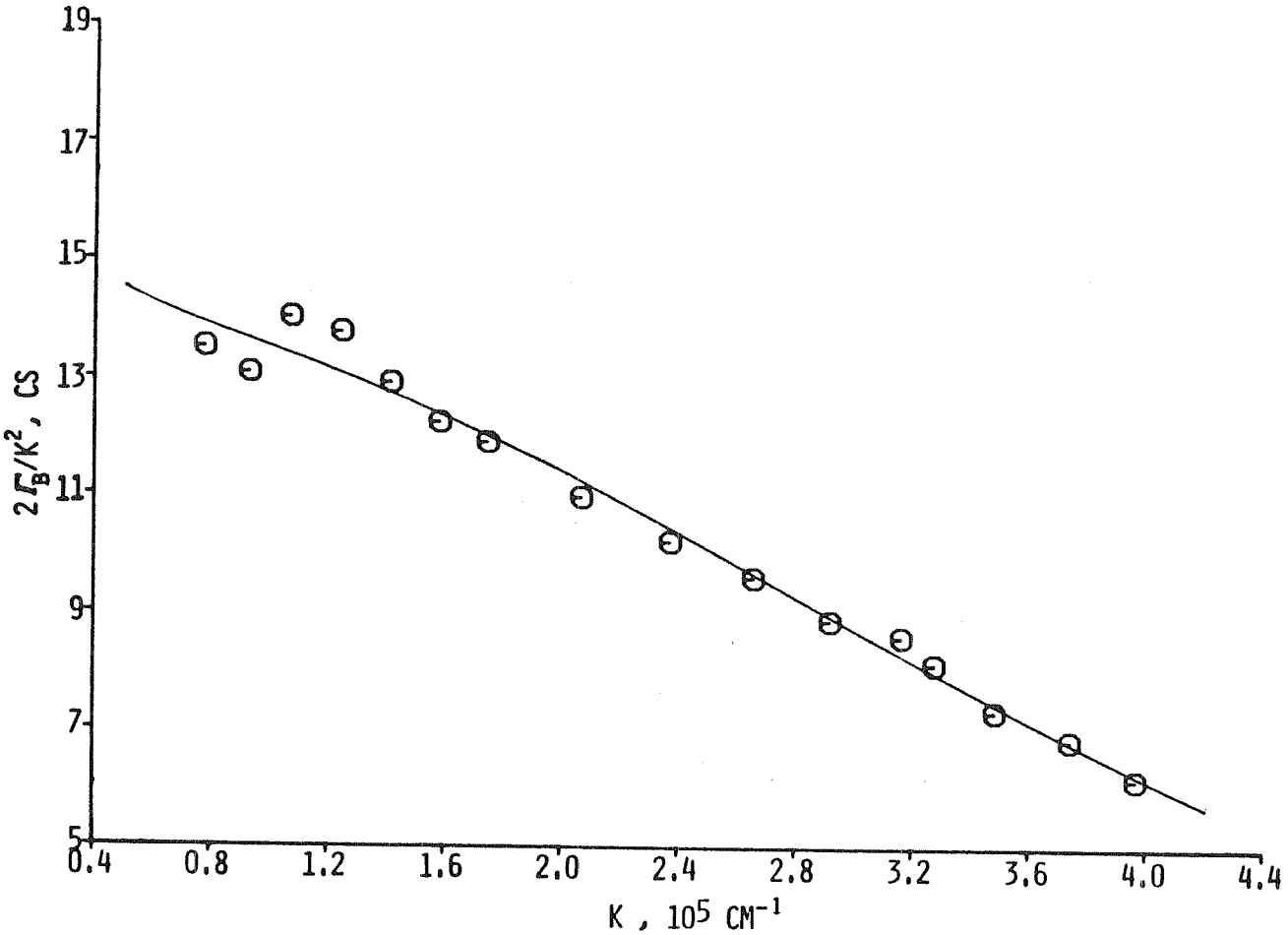

FIGURE 32. Fit of the attenuation results for p-anisaldehyde assuming orientational relaxation of the shear viscosity. The bulk viscosity is taken to be relaxing with a single relaxation time and η_V^0 treated as a free parameter.

results appear to contradict this idea . No explanation of this contradiction can be offered at this time. It should be emphasized that results of the above attenuation fits are not quantitatively meaningful and only serve as a qualitative indication of additional relaxation in the shear viscosity. Unfortunately, this additional shear relaxation precludes any possibility of an unambiguous assignment of an orientational relaxation mechanism.

Aniline

While the effects of orientational relaxation in para-anisaldehyde could not be adequately resolved from an analysis of the Brillouin lines, there certainly appeared to be a strong relaxation in the shear viscosity. There was also evidence that this shear relaxation resulted from more than just orientational coupling. Thus an additional study seemed justified. Aniline was chosen for this study since it exhibited many of the same properties which made p-A attractive. In addition, some ultrasonic data were available. Early studies of the depolarized spectra of aniline indicated that reorientation frequencies of less than 5 GHz could be obtained at temperatures under 10° C . The melting point is -6.3° C . Shear viscosities of 5 cp to 10 cp are also produced in this temperature range. Since these early depolarized studies failed to clearly resolve a dip and molecular theories were not available for data analysis, the spectrum was reexamined here. Both polarized and depolarized spectra were obtained at 3° C . At this temperature the shear viscosity was 8.9 cp and the density 1.037 gm/cc . The depolarized spectra exhibited a well defined dip structure and good fits were obtained using the 2-variable theory of Anderson and Pecora. See chapter 5 for the results of the depolarized study and a representative spectrum. The reorientation frequency, Γ, was found to be 3.41 GHz at 3° C. This is considerably higher than the Γ in the p-A study. Thus the range of Brillouin frequencies should

include the orientational relaxation frequency, i.e. $\frac{\kappa C_0}{\Gamma} \sim 1$, and the sound wave attenuation should exhibit a κ dependence due to orientational relaxation. The coupling parameter, R, proved to be anomalously large at 0.55 and thus the relaxation strength, $R\nu_s$, was 4.8 cp . This is significantly greater than that in p-A and should certainly make the orientational relaxation observable if interference from another process is not too severe.

The polarized spectra of aniline were collected over an angular range of 30° to 150°. Typical spectra at 3 different scattering angles are shown in figures 33, 34, and 35. The spectra were fitted in exactly the same manner as described for p-A except that the HWHH of the central line arising from reorientational motion was held constant at the convoluted value determined from the depolarized studies. This was necessitated by the large uncertainty which resulted if this parameter was fitted. The extremely weak intensity and broad linewidth of the orientational line lead to this uncertainty. A comparison of the polarized spectra of p-A, where the orientational line was easily fit, and aniline graphically illustrates this point. An analysis of the Brillouin components is given in table 16. The frequency range probed in this study was approximately 3 GHz to 12 GHz. Therefore the orientational relaxation should occur under the condition $\frac{\kappa C_0}{\Gamma} > 1$ as expected. The sound velocity in the above frequency range showed a dispersion of about 6%. This is far greater than the 1.5% predicted from the orientational effect alone, and as in p-A suggests the presence of an additional relaxation process. A plot of sound velocity versus κ is shown in figure 36. The velocity increases from approximately 1765 m/s to 1855 m/s with a leveling off occurring at the higher frequencies. The low frequency speed of sound, C_0, is 1730± 8 m/s as determined from ultrasonic experiments[77,78]. Thus if the velocity is indeed approaching its maximum of C_∞ at the higher scattering angles,

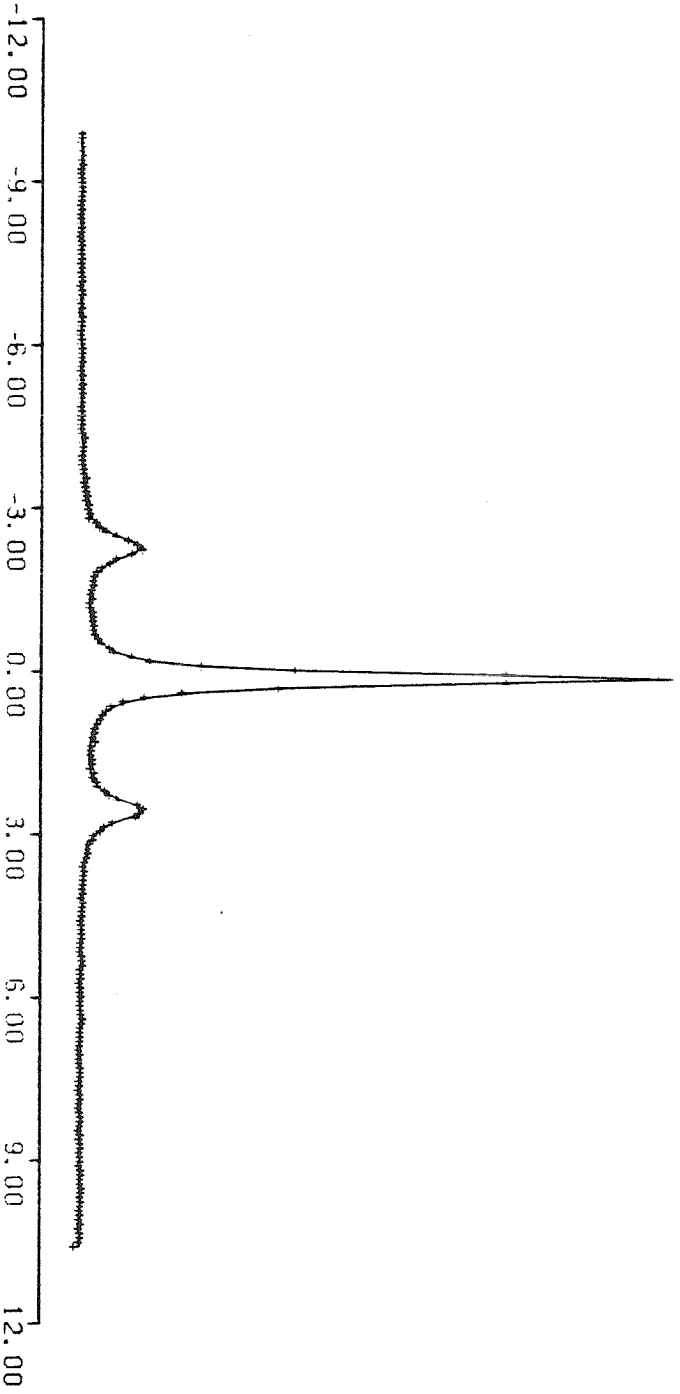

FIGURE 33. Polarized spectrum of aniline at 3.0°C and a scattering angle of 30°.

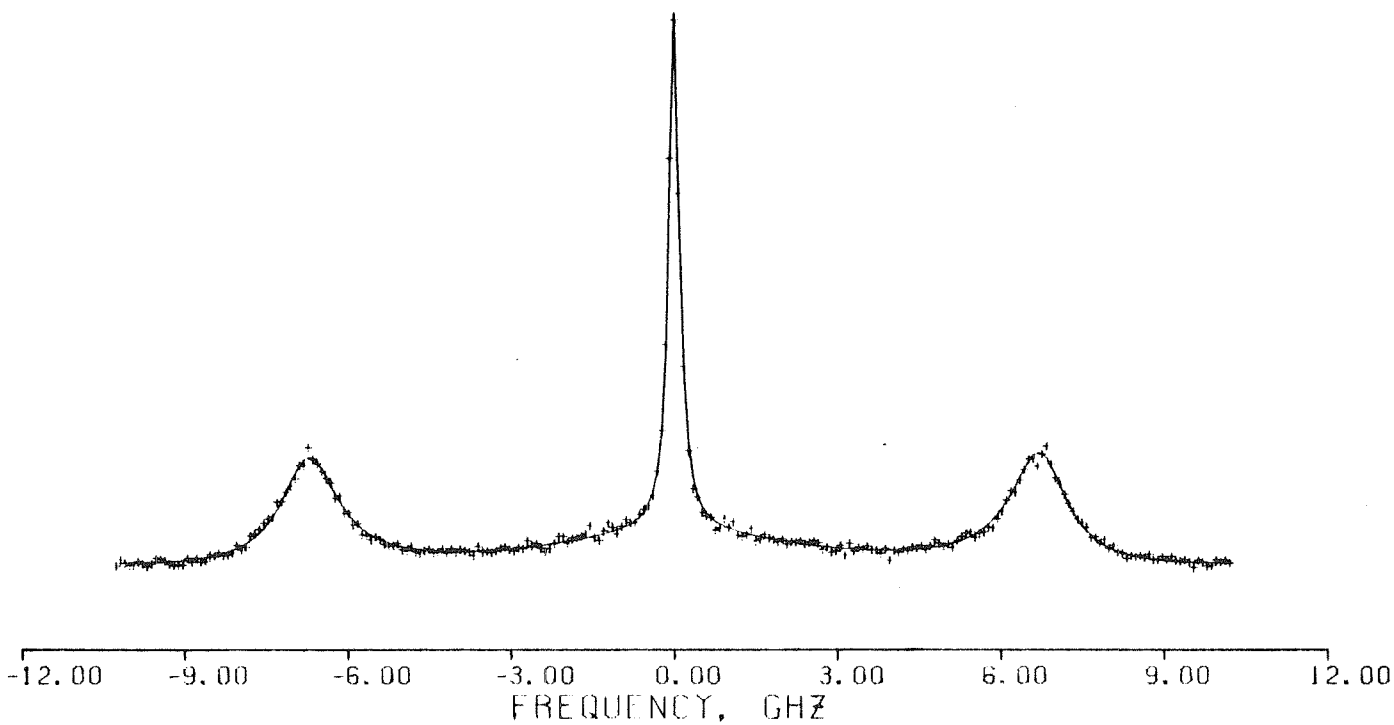

FIGURE 34. Polarized spectrum of aniline at 3.0°C and a scattering angle of 90°.

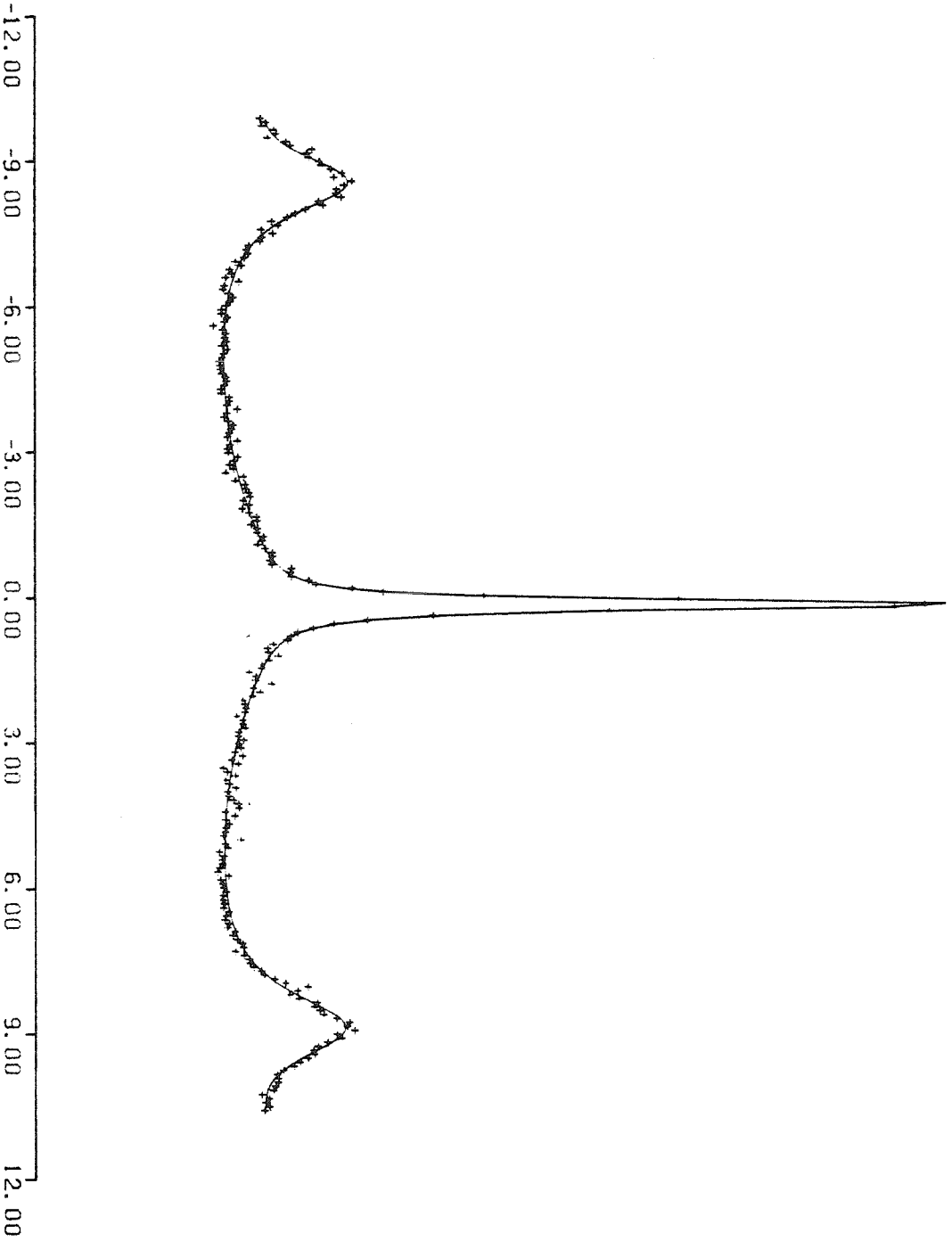

FIGURE 35. Polarized spectrum of aniline at 3.0°C and a scattering angle of 130°.

Brillouin Line Analyses for Aniline					
Angle (degrees)	Wave Vector, κ (10^5 cm^{-1})	Frequency Shift, ω_B (GHz)	Velocity, V (m/sec)	Brillouin Half- width, Γ_B (MHz)	$\frac{2\Gamma_B}{\kappa^2}$ (cs)
30.0	1.07	2.99± .04	1765 ± 25	153± 11	16.7± 1.2
40.0	1.42	3.98± .03	1761± 13	242± 17	15.1± 1.0
50.0	1.75	4.97± .03	1784± 9	337± 10	13.8± 0.4
60.0	2.07	5.93± .02	1794± 8	439± 10	12.8± 0.3
70.0	2.38	6.81± .01	1798± 6	530± 13	11.8± 0.3
80.0	2.67	7.73± .02	1821± 7	642± 13	11.3± 0.2
90.0	2.93	8.56± .02	1835± 5	723± 15	10.6± 0.2
100.0	3.18	9.32± .03	1841± 7	843± 13	10.5± 0.2
110.0	3.40	10.00± .02	1848± 7	883± 15	9.6± 0.2
120.0	3.59	10.62± .03	1859± 8	919± 15	8.9± 0.2
130.0	3.76	11.08± .03	1852± 8	957± 20	8.5± 0.2
150.0	4.01	11.83± .02	1854± 7	1067± 26	8.3± 0.2

TABLE 16. Analyses of the Brillouin lines of aniline at 3°C and over a wide range of scattering angles.

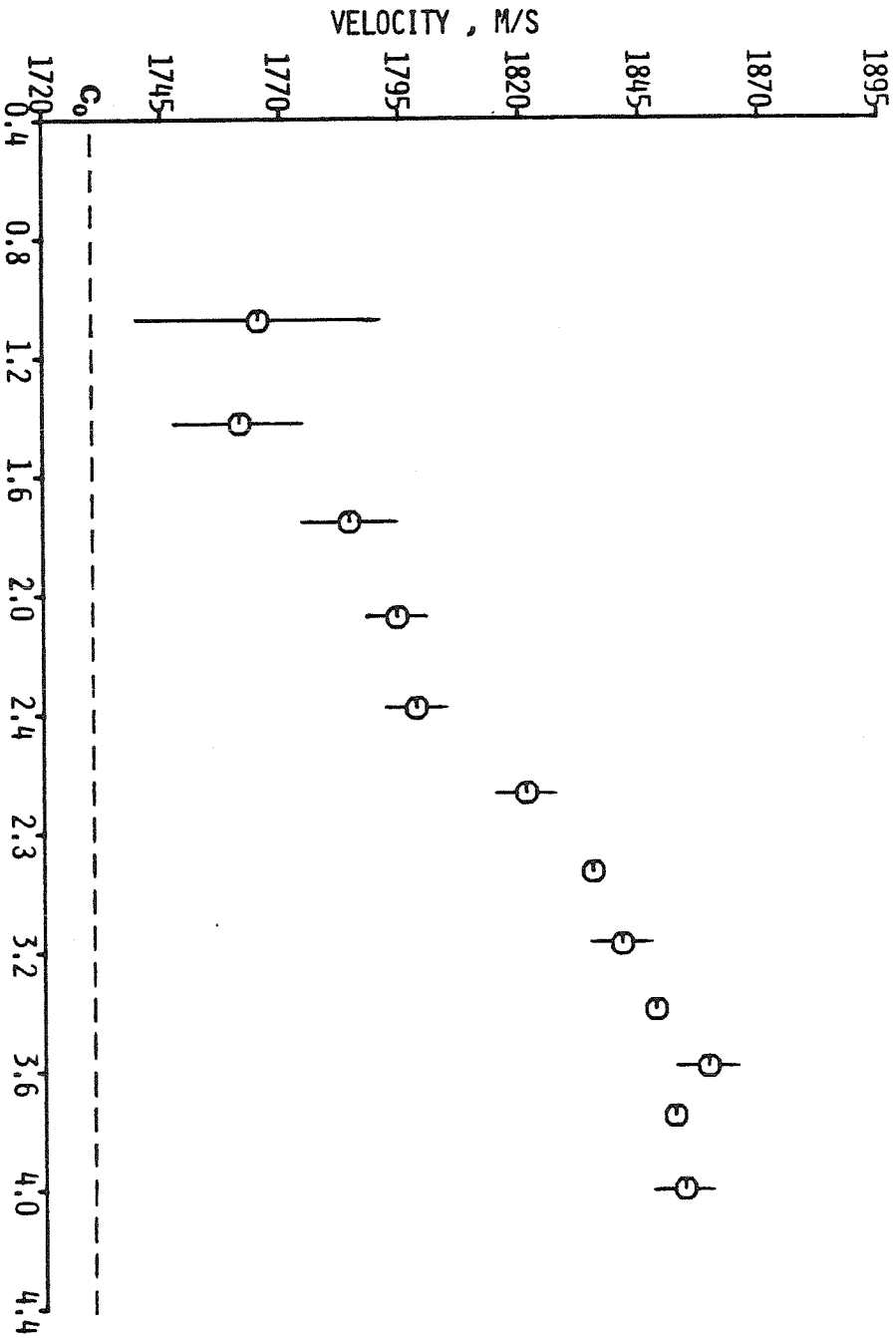

FIGURE 36. HYPERSONIC VELOCITY IN ANILINE AT T=3°C

the total dispersion is about 8%.

The observed wave attenuation in aniline as a function of κ or ω is actually very similar to that seen in p-A, decreasing from 15.5 to 8.3 cs . In fact the shape of these curves is almost identical. A plot of $\frac{2\Gamma_B}{\kappa^2}$ versus κ is shown in figure 37. This should be compared with the corresponding curve for p-A in figure 30. There appears to be an almost constant difference of about 1.7 cs . As in p-A the observed decrease in attenuation (7.2 cs) cannot be explained by orientational relaxation alone and indicates the presence of another process. This is in agreement with the velocity results. However, once again, there is clearly relaxation in the shear viscosity. At frequencies above 7.7 GHz the attenuation is less than $\frac{4}{3}\nu_s$. Recall that the orientational relaxation frequency is 3.41 Ghz . According to Keyes about 70% of the full relaxation strength is observed and about 30% if Lipeles' high frequency result is correct. In contrast to the p-A study, the attenuation results here do not immediately cast doubt upon either high frequency limit. Note that Lipeles' high frequency limits of the shear viscosity for p-A and aniline are nearly identical at 5.1 cs and 5.2 cs respectively.

An attempt was made at fitting the observed attenuation in aniline using the method employed in the p-A study. The result for $\nu_v^0=0$ is shown in figure 38. More credibility can be attributed to this result since C_0 is known. The relaxation strength of the bulk viscosity was 8.9 cs and the relaxation time 7.3×10^{-10}sec . The fit obtained here is much better than the corresponding result for p-A. However it does appear to suffer from the same problem at the higher frequencies as p-A though to a lesser extent. Thus a fit was also attempted with ν_v^0 treated as a free parameter. The result obtained in this manner is shown in figure 39. Note that the improvement is significant at the high frequency end and slightly better almost everywhere else. The relaxation

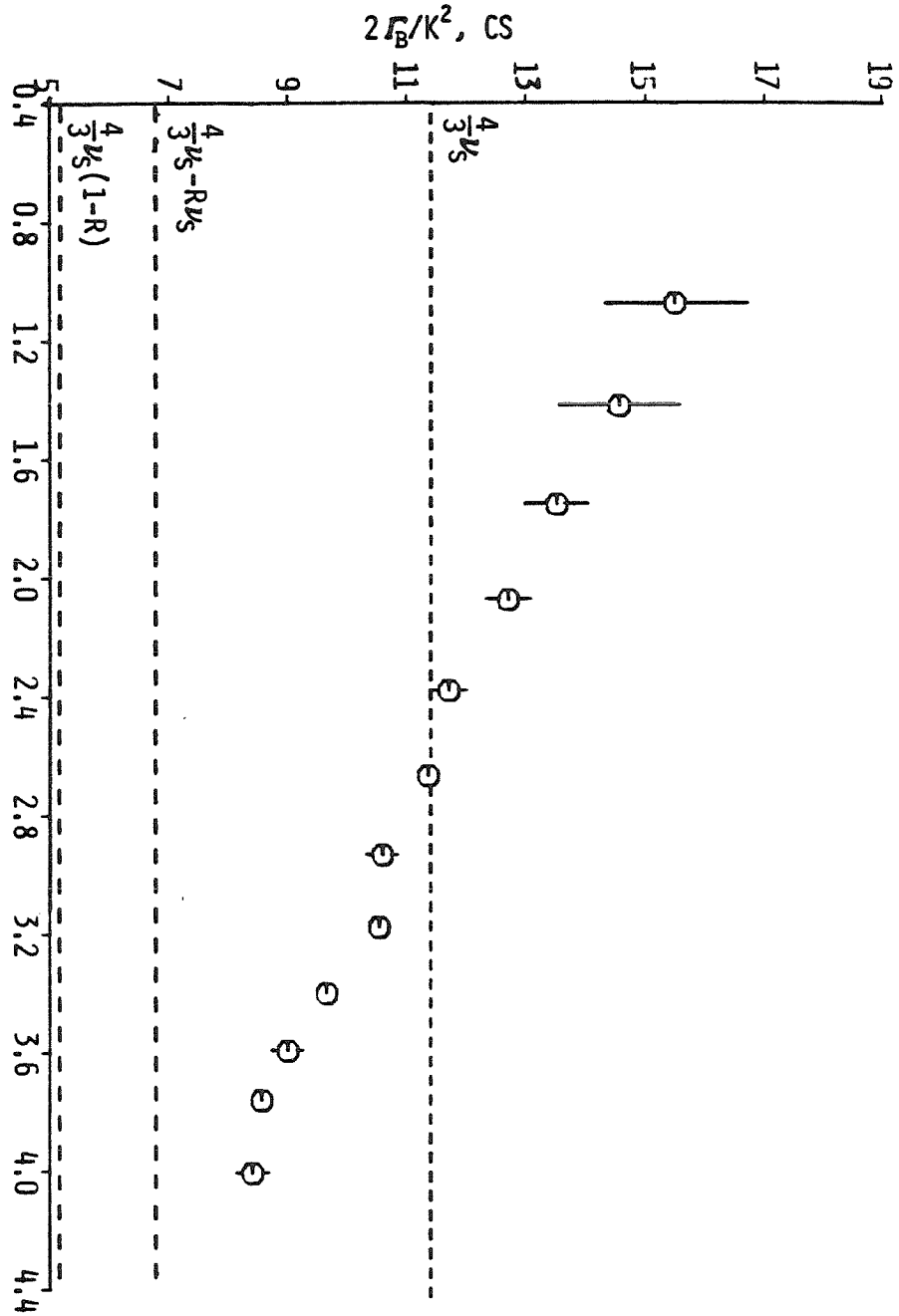

FIGURE 37. HYPERSONIC ATTENUATION IN ANILINE AT T=3°C

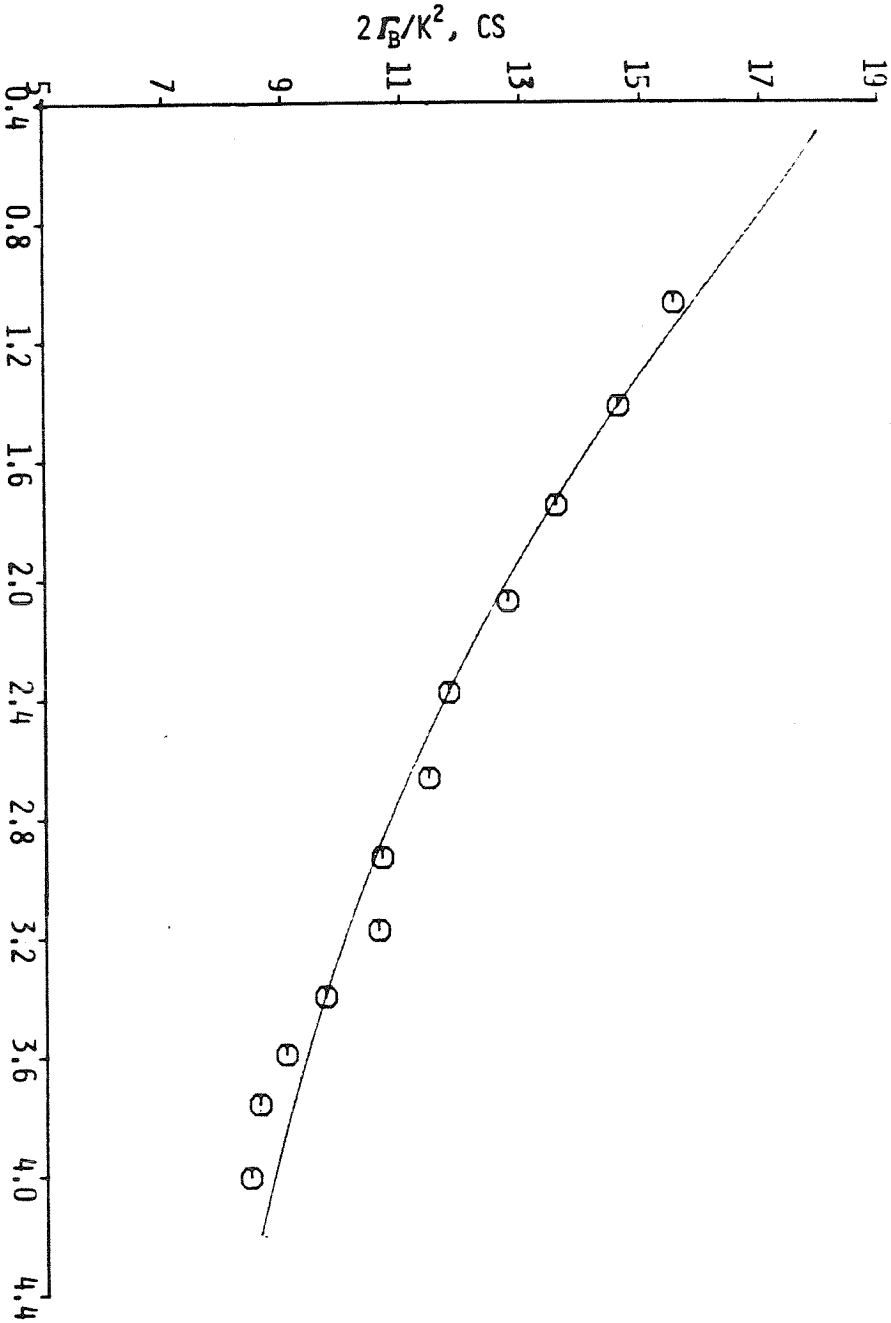

FIGURE 38. Fit of the attenuation results for aniline assuming orientational relaxation of the shear viscosity. The bulk viscosity is also taken to be relaxing with a single relaxation time and $\eta_V^0=0$.

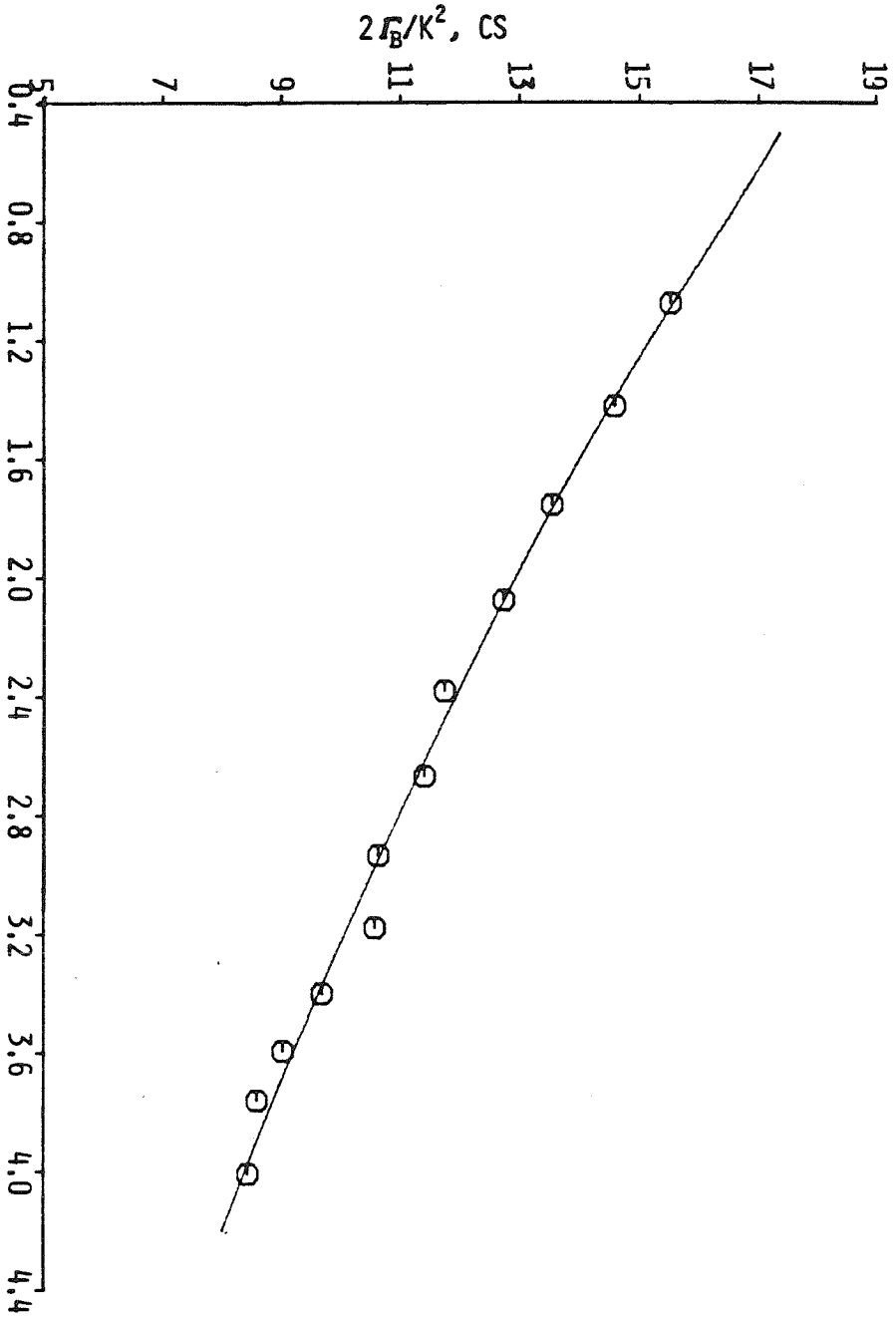

FIGURE 39. Fit of the attenuation results for aniline assuming orientational relaxation of the shear viscosity. The bulk viscosity is also taken to be relaxing with a single relaxation time and η_V^0 treated as a free parameter.

strength here was 13.5 cs with a relaxation time of 1.1×10^{-11} sec . These values are similar to those found for p-A (16.4 cs and 1.4×10^{-11} sec). Once again the improvement was achieved at the expense of an unrealistic negative value for ν_v^0 of -5.21 cs . This time however the high frequency contribution to the shear viscosity, $\frac{4}{3}\nu_s(1-R)=5.13$ cs, is nearly identical to the fitted magnitude of ν_v^0. Thus the high frequency limit of the attenuation is almost zero. The fact that ν_v^0 is being used to cancel the high frequency contribution of the shear viscosity indicates that this contribution should be relaxing as was suggested in the p-A study. The close similarity between the attenuation versus κ curves in p-A and aniline might also be taken as evidence for identical relaxation mechanisms. The existence of non- orientational relaxation in the shear viscosity of aniline under these conditions once again appears to contradict the results of our own depolarized studies which indicate that the coupling of a single orientational variable should be quite adequate. The nature of this apparent non-orientational mechanism and its appearance under the present conditions is an interesting and an open question.

Since a definite relaxation in the shear viscosity was observed at frequencies approximately twice the predicted reorientation relaxation frequency, the existence of orientational relaxation is much more plausible here than in para-anisaldehyde. Ultrasonic studies [79] also indicate that the tail end of a relaxation in the bulk viscosity should be observable in the low gigahertz range. This supports our low frequency results showing the attenuation to be greater than $\frac{4}{3}\nu_s$ and would explain why the attenuation does not fall below $\frac{4}{3}\nu_s$ until 7.7 GHz. However a detailed confirmation of the orientational relaxation theory cannot be concluded here since its κ dependence cannot be unambiguously separated from the other contributions which appear to be present.

LITERATURE CITED

[1] Stegeman, G.I.A and B.P. Stoicheff, *Phys. Rev. Lett.* **21**, 202 (1968).

[2] Starunov, V.S., E.V. Tiganov and I.L. Fabelinskii, *Zh. Eksp. Teor. Fiz. Pis'ma Red.* **5**, 317 (1967) [JETP Lett. **5**, 260 (1967)].

[3] Stegeman, G.I.A. and B.P. Stoicheff, *Phys. Rev. A* **7** (3), 1160 (1973).

[4] Rytov, S.M., *Zh. Eksp. Teor. Fiz.* **33**, 514 (1957) [Sov. Phys. - JETP **6**., 401 (1958)].

[5] Anderson, H.C. and R. Pecora, *J. Chem. Phys.* **54** (6), 2584 (1974).

[6] Keyes, T. and D. Kivelson, *J. Chem. Phys.* **54** (4), 1786 (1974).

[7] Mori, H., *Prog. of Theo. Phys.* **33** (3), 423 (1965).

[8] Zwanzig, R., *Phys. Rev.* **124** (4), 983 (1961).

[9] Kubo, R., *J. Phys. Soc. Japan* **12**, 570 (1957).

[10] Felderhof, B.U. and I. Oppenheim, *Physica* **31**, 1441 (1965).

[11] Tsay, S.J. and D. Kivelson, *Mol. Phys.* **29** (1), 1 (1975).

[12] Alms, G.R., D.R. Bauer, J.I. Brauman, and R. Pecora, *J. Chem. Phys.* **59** (10), 5304 (1975).

[13] Bezot P., G.M. Searby and P. Sixou, *J. Chem. Phys.* **62** (9), 3813 (1975).

[14] Sixou, P., P. Bezot and G.M. Searby, *Mol. Phys.* **30** (4), 1149 (1975).

[15] Enright, G.D. and B.P. Stochieff, *J. Chem. Phys.* **60**, 2536 (1974).

[16] Quentrec, B., *Phys. Rev. A* **15**, 1304 (1977).

[17] Quentrec, B. and P. Bezot, *Mol. Phys.* **39** (3), 427 (1980).

[18] Bezot, P., C. Hesse-Bezot, N. Ostrowsky and B. Quentrec, *Mol. Phys.* **39** (3), 549 (1980).

[19] Searby, G.M., P. Bezot and P. Sixou, *Faraday Symposia of the Chem. Soc.* **11**, 63 (1977).

[20] Alms, G.R., T.D. Gierke and G.D. Patterson, *J. Chem. Phys.* **67** (12), 5779 (1977).

[21] Searby, G.M., P. Bezot and P. Sixou, *J. Chem. Phys.* **64** (4), 1485 (1976).

[22] Lempert, W. and C.H. Wang, *J. Chem. Phys.* **72** (6), 3490 (1980).

[23] Frohlich, P. and H.A. Posch, *Mol. Phys.* **36** (5), 1421 (1978).

[24] Enright, G. and B.P. Stoicheff, *J. Chem. Phys.* **60** (6), 2536 (1974).

[25] Alms, G.R. and G.D. Patterson, *J. Chem. Phys.* **68** (8), 3440 (1978).

[26] Cavanaugh, D.B. and C.H. Wang, *J. Chem. Phys.* **73** (2), 636 (1980).

[27] Patterson, G.D. and G.R. Alms, *Macromolecules* **10** (6), 1237 (1977).

[28] De Gennes, P.G., *Mol. Cryst. Liq. Cryst.* **12**, 193 (1971).

[29] Gierke, T.D., private communication.

[30] Gierke, T.D., *J. Chem. Phys.* **65** (10), 3873 (1976).

[31] Landau, L.D. and E.M. Lifshitz, **Electrodynamics of Continuous Media**, Addison Wesley, Reading, Mass. (1960).

[32] Chu, B., **Laser Light Scattering**, Academic Press, New York (1974).

[33] Jackson, J.D., **Classical Electrodynamics**, Wiley, New York (1965).

[34] McTauge, J.P. and G. Birnbaum, *Phys. Rev. A* **7**, 1376 (1971).

[35] Gelbart, W., *Adv. Chem. Phys.* **26**, 1 (1974).

[36] Fleury, P.A. and J.P. Boon, *Adv. Chem. Phys.* **24**, 1 (1974).

[37] Chiao, R.Y. and B.P. Stoicheff, *J. Opt. Soc. Amer.* **54**, 1286 (1964).

[38] Born, M. and E. Wolf, **Principles of Optics**, 3rd ed., Pergamon, Oxford (1970).

[39] Klein, M., **Optics**, Wiley, N.Y. (1970).

[40] Leidecker, H.W. and J.T. LaMacchia, *J. Acous. Soc. Amer.* **43**, 143 (1967).

[41] Danielmeyer, H.G., *J. Acous. Soc. Amer.* **47**, 151 (1969).

[42] Nichols, W.H. and E.F. Carome, *J. Chem. Phys.* **49** (3), 1000 (1968).

[43] Gewurtz, S., W.S. Gornall and B.P. Stoicheff, *J. Acous. Soc. Amer.* **49** (3), 994 (1971).

[44] **Handbook of Chemistry and Physics**, R.C. Weast, Ed., The Chemical Rubber Co., Cleveland, OH. (1964), 52nd ed.

[45] **International Critical Tables**, Vol. 9, E.W. Washburn, Ed., McGraw-Hill, N.Y. (1930).

[46] Ailawadi, N. and B.J. Berne, *J. Physique, Colloque C1* **33**, 221 (1972).

[47] Berne, B.J. and R. Pecora, **Dynamic Light Scattering**, Wiley-Interscience, N.Y. (1976).

[48] Zwanzig, R., *J. Chem. Phys.* **43** (2), 714 (1965).

[49] Rose, M.E., **Elementary Theory of Angular Momentum**, Wiley, N.Y. (1957).

[50] Kadanoff, L.P. and P.C. Martin, *Ann. Phys.* **24**, 419 (1963).

[51] Bucaro, J.A., H.D. Dardy and R.F. Horton, *J. Chem. Phys.* **60** (4), 1671 (1974).

[52] Branch, G.E.K. and M. Galvin, **The Theory of Organic Chemistry**, Prentice-Hall, N.Y. (1941).

[53] Bertucci, S.J., A.K. Burnham, G.R. Alms and W.H. Flygare, *J. Chem. Phys.* **66** (2), 605 (1977).

[54] Brillouin, L., *Compt. Rend.* **158**, 1331 (1914).

[55] Debye, P., *Ann. Phys. (Leipzig)* **39**, 789 (1912).

[56] Brillouin, L., *Ann. Phys. (Paris)* **17**, 88 (1922).

[57] Gross, E.F., *Nature* **126**, 201; **126**, 400; **126**, 603 (1930).

[58] Landau, L. and G. Placzek, *Phys. Z. Sovjetunion* **5**, 172 (1934).

[59] Mountain, R.D., *Rev. Mod. Phys.* **38** (1), 205 (1966).

[60] Fleury, R.A. and J.P. Boon, *Phys. Rev.* **186**, 244 (1969).

[61] Stegeman, G.I.A., W.S. Gornall, V. Volterra and B.P. Stoicheff, *J. Acous. Soc. Amer.* **49** (3), 979 (1970).

[62] Mountain, R.D., *J. Res. N.B.S.* **70A**, 207 (1966).

[63] Nichols, W.H., C.R. Kunsitis-Swyt and S.P. Singal, *J. Chem. Phys.* **51** (12), 5659 (1969).

[64] Mountain, R.D. and J. Deutch, *J. Chem. Phys.* **50** (3), 1103 (1969).

[65] Lao, Q.H., P.E. Schoen, B. Chu and D.A. Jackson, *J. Chem. Phys.* **64** (12), 5013 (1976).

[66] Gulari, E., R.J. Brown and C.J. Pings, *A.I.Ch.E. Journal* **19** (6), 1196 (1973).

[67] Selwyn, P. and I. Oppenheim, *Physica* **54**, 161 (1971).

[68] Weinberg, M. and I. Oppenheim, *Physica* **61**, 1 (1972).

[69] Keyes, T., PhD Dissertation, UCLA (1972).

[70] Lipeles, R. and D. Kivelson, *J. Chem. Phys.* **67** (10), 4564 (1977).

[71] Landau, L.D. and E.M. Lifshitz, **Statistical Physics**, Addison-Wesley, Reading, Mass. (1960).

[72] Markam, J.L., R.T. Beyer and R.B. Lindsey, *Rev. Mod. Phys.* **23**, 353 (1951).

[73] Montrose, C.J., V.A. Solovyev and T.A. Litovitz, *J. Acous. Soc. Amer.* **43** (1), 117 (1968).

[74] Mountain, R.D., *J. Res. N.B.S.* **72A**, 75 (1968).

[75] Herzfeld, K.F. and T.A. Litovitz, **Absorption and Dispersion of Ultrasonic Waves**, Academic Press, N.Y. (1959).

[76] **Physical Acoustics**, W.P. Mason, Ed., Academic Press, N.Y. (1964).

[77] Eastman, D.P., A. Hollinger, J. Kenemuth and D.H. Rank, *J. Chem. Phys.* **50** (4), 1567 (1969).

[78] Parzyan, V.A. and E.O. Rabichev, *Vestnik Moskovskogo Universiteta. Khimiya* **30** (3), 370 (1975).

[79] Pulatova, D.F., *Akademiia Nauk Uzbekskoi, Tashkent. Doklady* **75** (9), (1975).

[80] McClellon, A.L., **Tables of Experimental Dipole Moments**, Freeman, San Fransisco (1963).

[81] Bondi, A., *J. Phys. Chem.* **68**, 441 (1964).